SPECTRAL ANALYSIS AND INTERPRETATION OF AEROMAGNETIC ANOMALIES OVER THE UPPER BENUE TROUGH, NIGERIA

By

Prince Obiora NWOGBO B.Sc. (Hons) Unilag.

A thesis submitted to the Postgraduate School, Ahmadu Bello University, Zaria in partial fulfilment of the requirements for the award of the degree of Master of Science in Applied Geophysics.

Department of Physics
Faculty of Science
Ahmadu Bello University
Zaria

AUGUST, 1987

DEDICATION

This work is dedicated to my brothers

Kanayochukwu, Samuel and Ositadimma,

and to my sister

Nkechinyelu.

DECLARATION

The report presented in this thesis is not a published, or an unpublished work of another author. It is the result of an original study carried out by this author. To the best of my knowledge, it has not been submitted in whatever form to any other institution, organisation or body other than the Ahmadu Bello University for the award of a degree. Where the work of others are made use of, such sources are appropriately acknowledged and referenced.

P. O. Nwogbo

CERTIFICATION

This thesis entitled 'Spectral Analysis and Interpretation of Aeromagnetic anomalies over the Upper Benue Trough, Nigeria' by Prince Obiora NWOGBO meets the regulations governing the award of the degree of Master of Science of Ahmadu Bello University, and is approved for its contribution to knowledge and literary presentation.

..... Date: 16/10/87

(Name and Signature)
Dr. S. B. Ojo
Chairman, Supervisory Committee

..... Date: 16/10/87

(Name and Signature)
Dr. I. B. Osazuwa
Member, Supervisory Committee

..... Date: 16-12-87

(Name and Signature)
Dr. J. Adetunji
Head of Department

..... Date: .....

(Name and Signature)
Prof. G. Osuide
Dean, Postgraduate School

ACKNOWLEDGEMENT

I wish to take this opportunity to thank all those who have helped in the preparation of this work. In particular I wish to express my gratitude to my Supervisor Dr.S. B. Ojo for his many valuable contributions to this work, and for a leadership that was at times wearing but at the end most appreciated. An equally invaluable contribution has been made by Dr. I. B. Osazuwa, who at various stages of the programme provided guidance and useful advice which helped in the successful completion of this work. It is a pleasure to acknowledge with thanks the assistance of Professor D.E. Ajakaiye now of the University of Jos, who conceived the subject and supplied the gridded aeromagnetic data for the entire project area; Dr. C.D. Okujeni of the Geology Department and Dr. C.O. Ofoegbu of the University of Port Harcourt for providing some useful materials on the geology of the project area. I am gratefully indebted to Messrs Law Dim and M. Umego both of the Physics Department; Tim Ekwueme, Ken Nwogbo, George Aniemena, Eddie Nwagu, Uche Okafor and Miss Titi Arize for the interest shown in this work but even more for their hospitality during the course of this programme.

Many people have helped in numerous ways during the development of this work. I would like to acknowledge such assistance and participation from Basil Nwosu, Abayomi Fagbemi and Mary Momoh all of

the Physics Department, for helping in preparing and assembling some of the materials needed for this work; and Kingsley Amabie-Nimigha, of the University of Port Harcourt for sorting out the problems I had with computer programming at the beginning of this work. I also wish to make special mention of the following who were especially helpful: Matthew Onoh and Ifeanyi Nwadialor, both of Surveying Department; Jude Oha, of the Geology Department; Tyna and Mabel of Chemistry and Library Science Departments respectively.

Much thanks and sincere appreciation go to Mike Oladosu and Alex Akpa for providing me with comfortable accommodation during the extra year I had to stay in Zaria. Much thanks are also due to my other colleagues in the Geophysics programme; Sikiru Ayinde, Sam Alkali, Sylva Aneke, Sani Ali, Mohammed Hassan and Segun Adeniyi for their friendly cooperation and positive attitudes.

This work would not have been possible without the unfailing cooperation and friendly assistance of the entire staff of the Ahmadu Bello University Computer Centre. I thank all for their help even though I do not mention their names specifically.

I must also express my appreciation and sympathy for my parents Mr. and Mrs. G.N. Nwogbo, and other members of my family for their many sacrifices during the course of this programme,

when my activities appeared to be far removed from the traditional duties of a senior member of the family.

Finally special recognision is due to my younger brothers Kanayochukwu and Kodilichukwu, and my elder sisters Gladys and Nkechi for financing this programme in spite of their obvious financial limitations.

ABSTRACT

Aeromagnetic data of the Upper Benue Trough have been analysed by one- and two-dimensional spectral analysis to determine the lateral variation in sedimentary thickness and structure under the basin. A two-dimensional standard model interpretation of an aeromagnetic profile was also presented as a supplementary technique. The area investigated covers the portion of the trough from 09° 00' - 12° 60'N and 009° 30' - 012° 30'E.

Spectral depth determinations to magnetic sources in the region give four depth ranges namely: 9.40km to 31.52km, 4.37km to 5.10km, 2.0km to 2.83km, and 0.04km to 0.96km. Deep source depths occuring at 9.40km and 31.52km refer respectively to some layer of intra-crustal source structures, and to the lithologic interface corresponding to the crust-mantle boundary. The intermediate mean depths varying between 4.37km and 5.10km may represent the top of some intrusive material occuring within the basement. Some of these intrusions as indicated by the two-dimensional model interpretation occur at depths of up to 6.0km. Mean depth values in **the** range of 2.0km to 2.83km agree with previous estimates from gravity data and may relate to the magnetic level corresponding to the true basement surface. This depth range indicate clearly the magnitude of the undulation of the basement topography in the study area. Variations in the depth

values also reveal a general trend in the basement surface, from shallow in the North-west and North-east to deep in the South central area. Mean depths to shallower sources in the region vary between 0.12km and 0.96km, and may be attributed to shallow intrusive materials or some near-surface basement rocks.

Sediment thickness in the study area therefore varies between mean values ranging from 0.12km to 2.83km, and the numerous intrusions in the valley may occur either within the basement or within the sediments or both.

TABLE OF CONTENTS

		Page
	Title page	i
	Dedication	ii
	Declaration	iii
	Certification	iv
	Acknowledgements	v
	Abstract	viii
	Table of Contents	x
	List of Tables	xiii
	List of Figures	xiv
	List of Appendices	xvii
CHAPTER 1:	GENERAL INTRODUCTION	1
1.1	Aeromagnetic Survey of the Study Area	1
1.2	Spectral Analysis of Potential fields	4
1.3	The Benue Trough	5
1.4	Review of Previous geophysical Studies in the Upper Benue Trough	10
1.5	Scope and Objectives of study	14
CHAPTER 2;	GEOLOGY OF THE UPPER BENUE TROUGH	16
2.1	Introduction	16
2.2	The Basement Complex	16
2.3	Cretaceous Stratigraphy of the Upper Benue Trough	18
2.4	Structures in the Upper Benue Trough	23
2.5	Igneous Intrusions and Volcanic activity	25
2.6	Tectonic Evolution and Origin of the Benue Trough	26
2.7	Economic Geology of the Upper Benue Trough	27

		Page
CHAPTER 3:	SPECTRAL ANALYSIS OF AEROMAGNETIC FIELDS	32
3.1	Fourier Analysis of two-dimensional Aeromagnetic data	32
3.2	Data Organisation and Treatment	34
3.2.1	Regional Field Separation	36
3.3	Choice of Map Windows	38
3.4	Procedure for Spectral depth Estimation in Magnetics	42
3.5	Slope-Depth Relation for Power Spectrum Analysis	44
3.6	Spectral Prediction of Source Depths from theoretical Models	46
CHAPTER 4:	GENERAL DESCRIPTION AND QUALITATIVE INTERPRETATION OF THE FIELD ANOMALIES	51
4.1	Description of the anomalies and discussion of trends	51
4.2	Correlation of the field anomalies with the spectrum plots	53
4.3	Correlation of the Magnetic anomalies with surface geological information	57
CHAPTER 5:	POWER SPECTRUM ANALYSIS AND INTERPRETATION	61
5.1	Map Sizes and Target Depths	61
5.2	Spectral Magnetic Depth Determinations	62
5.2.1	Power Spectrum Analysis for $\frac{1}{2}^{o}$ x $\frac{1}{2}^{o}$ Grid	64
5.2.2	Power Spectrum Analysis for 1^{o} x 1^{o} Grid	79
5.2.3	Power Spectrum Analysis for $1\frac{1}{2}^{o}$x$1\frac{1}{2}^{o}$ Grid	85
5.2.4	Power Spectrum Analysis for a North-South Profile	92

Page

5.3 Two-Dimensional Model Interpretation 98

5.4 Structural Implications of the Interpreted Results 101

CHAPTER 6: REVIEW AND CONCLUSIONS 104

6.1 Review and Discussions 104

6.2 Summary and Conclusions 107

References 111

Appendices 118

LIST OF TABLES

	Page
TABLE 2.1: General Stratigraphical Succession in the Upper Benue Trough	21
TABLE 5.1: Crustal thickness in the Benue Valley	96

LIST OF FIGURES

		PAGE
Figure 1.1:	Location map of the study area	3
Figure 1.2:	African Phanerozoic Sedimentary Basins	6
Figure 1.3:	Location map of the Benue Valley	7
Figure 1.4:	Divisions of the Benue Valley	11
Figure 2.1:	Simplified Geological map of Nigeria	17
Figure 2.2:	General geology map of the Study area	19
Figure 2.3:	Economic Mineral Occurences in the Benue Trough	29
Figure 3.1:	Rectangular data window and the corresponding spectral window	40
Figure 3.2:	A Cosine-bell data window and the corresponding spectral window	40
Figure 3.3:	An extended cosine-bell data window	40
Figure 3.4:	Computation of Radial Spectrum from the Spectrum matrix	43
Figure 3.5:	Single layer Model	48
Figure 3.6:	Regular Step Model	48
Figure 3.7:	Power Spectrum Analysis for the Single layer model	49
Figure 3.8:	Power Spectrum Analysis for the Regular step model	50
Figure 4.1 :	Total field anomaly map of the study area	52
Figure 4.2:	Spectrum Plots for $1\frac{1}{2}^{o}x1\frac{1}{2}^{o}$ map sizes	55

		Page
Figure 4.3:	Combined geology and Total field anomaly map	58
Figure 5.1:	Grid locations for $\frac{1}{2}^{O}x\frac{1}{2}^{O}$ Blocks	65
Figure 5.2:	Spectral depths for $\frac{1}{2}^{O}$ x $\frac{1}{2}^{O}$ Blocks	66
Figure 5.3:	Power Spectrum Analysis for Block 83	67
Figure 5.4:	Power Spectrum Analysis for Block 191	68
Figure 5.5:	Power Spectrum Analysis for Block 106	71
Figure 5.6:	Power Spectrum Analysis for Block 128	72
Figure 5.7:	Power Spectrum Analysis for Block 149	73
Figure 5.8:	Power Spectrum Analysis for Block 170	74
Figure 5.9:	Power Spectrum Analysis for Block 107	76
Figure 5.10:	Power Spectrum Analysis for Block 133	77
Figure 5.11	Power Spectrum Analysis for Block 174	78
Figure 5.12:	Grid locations and Spectral depths for $1^{O}x\ 1^{O}$ Blocks	80
Figure 5.13:	Power Spectrum Analysis for Block 1	81
Figure 5 .14:	Power Spectrum Analysis for Block 2	82
Figure 5.15:	Power Spectrum Analysis for Block 3	83
Figure 5.16:	Power Spectrum Analysis for Block 4	84
Figure 5.17:	Grid locations and Spectral depths for $1\frac{1}{2}^{O}$ x $1\frac{1}{2}^{O}$ Blocks	86

Figure 5.18: Power Spectrum Analysis for Block 1 87

Figure 5.19: Power Spectrum Analysis for Block 2 88

Figure 5.20: Power Spectrum Analysis for Block 3 89

Figure 5.21 Power Spectrum Analysis for Block 4 90

Figure 5.22 Combined geology and total field map with locations of interpreted profiles 94

Figure 5.23: Spectral Analysis of a North-South profile along longitude 11^{o} 15' 95

Figure 5.24: Two-Dimensional model interpretation of profile BB' 100

LIST OF APPENDICES

		Page
Appendix A;	Spectral Plots for the $\frac{1}{2}^{o}x\frac{1}{2}^{o}$ Blocks	118
Appendix B:	Spectral Plots for the $1^{o}x1^{o}$ Blocks	146
Appendix C:	Total field anomaly maps of the 4 Blocks of $1\frac{1}{2}^{o}$ x $1\frac{1}{2}^{o}$ map window	152

CHAPTER 1

GENERAL INTRODUCTION

1.1 Aeromagnetic Survey of the Study Area.

Owing to radical technical improvements in instrumentation, field methods, and modern interpretation techniques resulting mainly from the emergence of large digital computers and their application to geophysics, the use of airborne measurements of the magnetic field has become widespread in several fields of the earth sciences. Of particular importance is its various applications in the investigation of the structure of the earth, and in the search for metallic ores, industrial minerals and the raw materials of energy such as oil and gas.

The planning and execution of a national programme of aeromagnetic surveying is an important activity in all countries. It is now customary for government departments to finance and promote aeromagnetic surveys of their countries. The Geological Surveys of Nigeria (GSN) has responsibility for airborne magnetic surveying of the country and the publication of the airborne geophysical map

series. The entire Nigeria's land mass has been effectively covered by airborne magnetic surveys carried out in the early- and mid- 1970s. The resulting maps were compiled from information recorded along pre-determined flight lines spaced at intervals of 2km on a mean flying altitude of 150m above the terrain. The aeromagnetic maps have since been published by the GSN and are now available in half-degree sheets mostly on a scale of 1:100,000, with contours of total magnetic field intensities in gammas. The contours are spaced at intervals of 10 gammas and sometimes 5 gammas. The anomalies expressed by the magnetic contours are dependent on the variable magnetic intensities of the underlying rocks and may be due to conditions near or at unknown depths below the surface.

The aeromagnetic maps used in this study extend from latitudes 09^{o} 00'N to 12^{o} 00' N and from longitudes 009' 30'E to 012^{o} 30'E in the North-Eastern part of Nigeria - covering what is known as the Upper Benue Trough and overlapping small portions of the Chad basin and the bordering crystalline basement complex (Figure 1.1).

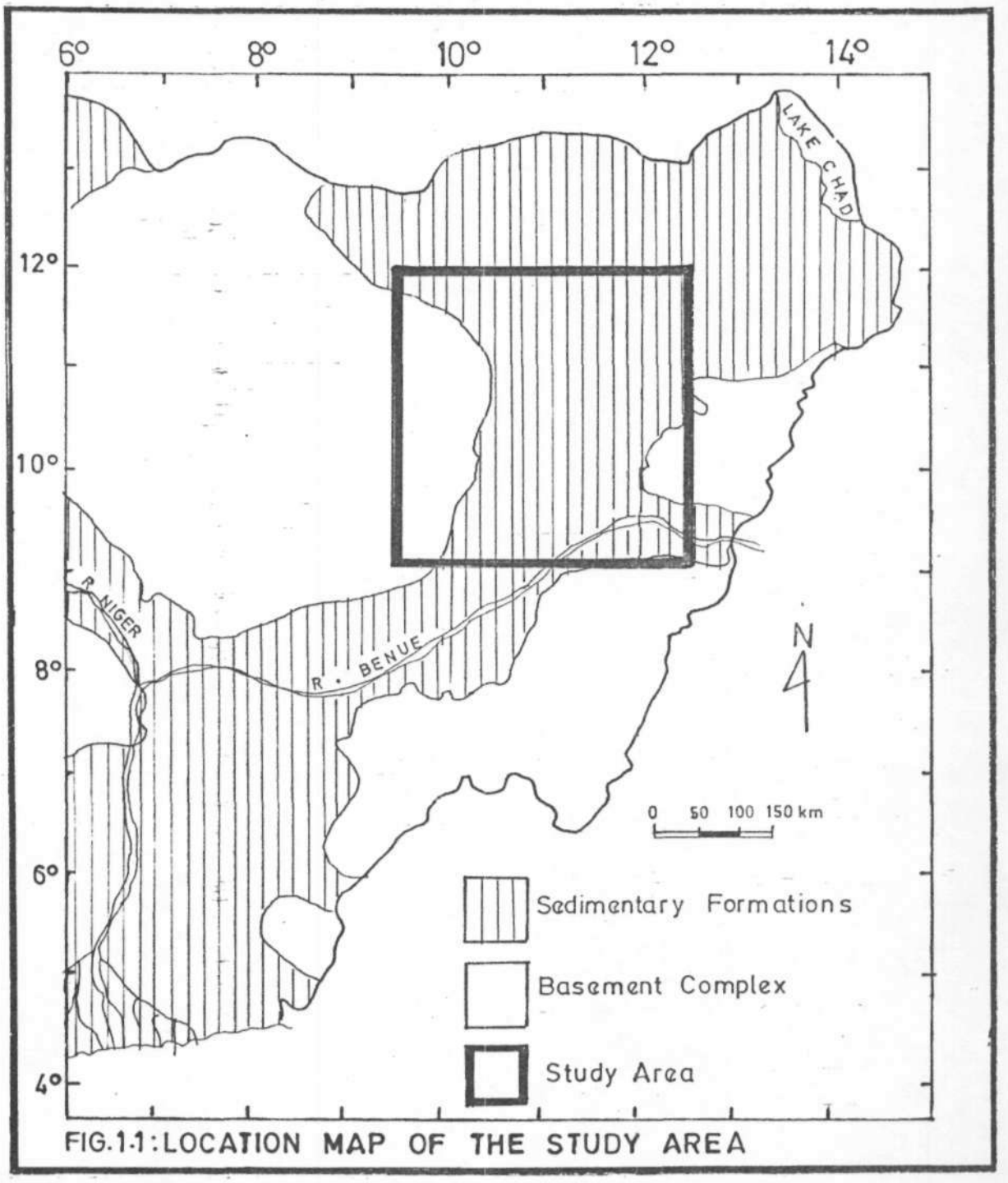


FIG.1.1: LOCATION MAP OF THE STUDY AREA

The flight parameters and other relevant information on compilation are listed on the aeromagnetic maps.

1.2 Spectral Analysis of Potential Fields

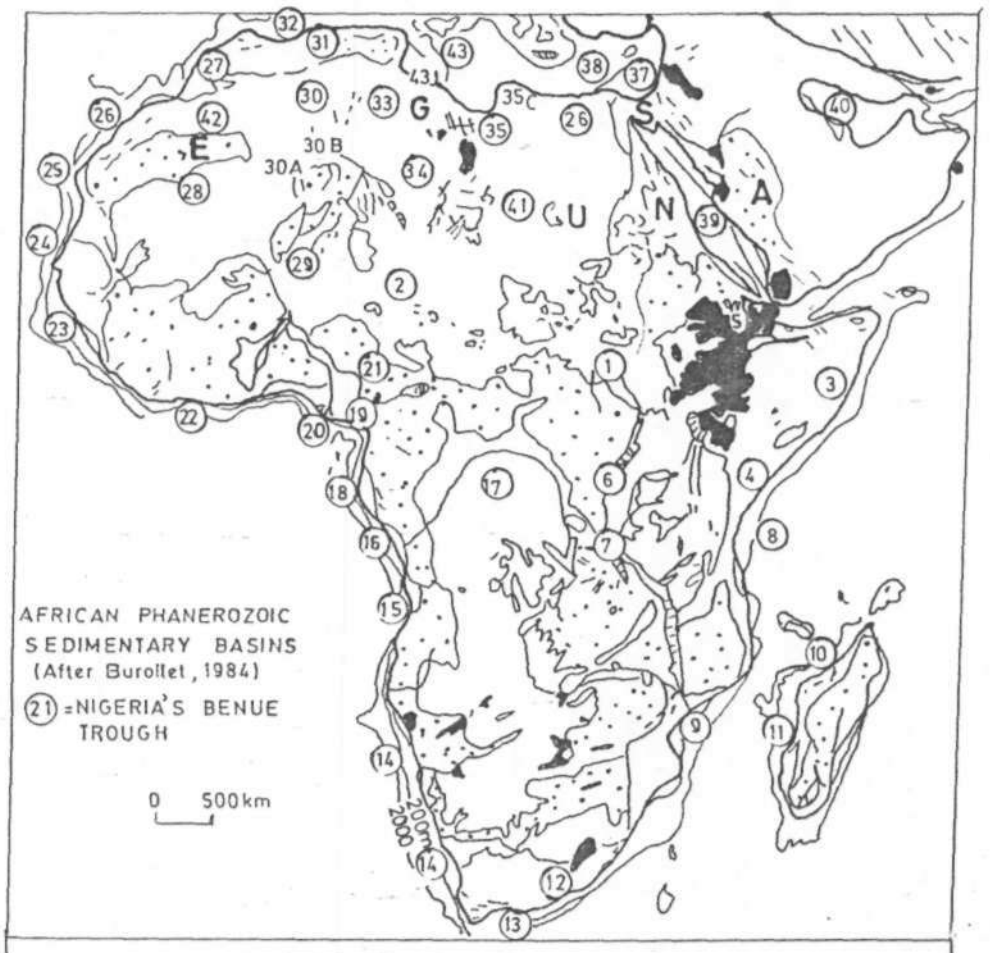
Spectral analysis in geophysics refers primarily to the process of calculating and interpreting the spectrum of a geophysical record or data. The spectrum is simply a transformation of the data from time or space domain to frequency or wave number domain respectively. This transformation is usually accomplished through the application of Fourier Transform methods. Potential field anomalies (gravity and magnetic) can therefore be represented by a one - or two-dimensional Fourier Transform consisting of various frequencies which characterize the anomalies.

The development of the spectral method and its applications in the analysis and interpretation of aeromagnetic fields can be traced back to the mid 1960s when it became a standard technique for estimating depths to buried magnetic rocks. This radical development is mainly due to the emergence of techniques for the fast computation of the Fourier Transform of large arrays of

aeromagnetic data. Some recent published results (Naidu, 1970 a; Spector and Grant, 1970; Mishra and Naidu, 1974; Curtis and Jain, 1975; Hahn et al, 1976; Pal et al., 1978; Negi et al., 1983) show that the spectral method can give reliable first order estimates of depths to the disturbing magnetic sources after a number of problems and difficulties have been overcome in the spectral calculation of the observed data. Some of these problems arise mainly from the use of a finite record of data in the analysis, and the need to have the record in digital form. The effects of these problems on the computed spectrum and their treatment are important considerations in the spectral analysis of aeromagnetic fields.

1.3 The Benue Trough

The Benue Trough is one of the known major rift systems in Africa (Figure 1.2), and forms a feature of considerable structural significance in Nigerian geology. The trough is essentially a linear sedimentary basin containing the Niger, Benue and Gongola rivers (Figure 1.3). It is an elongated trough of subsidence which trends North-easterly to attain an approximate length



Location map 1= Sudan 2=Chad 3=Somalia 4=Keny 5=Danakil 6=Rwanda Burundi 7=Tanganyika 8=Tanzania offshore 9=Mozambique 10=Madagascar Majunga 11=Madagascar Morondava 12=Karroo 13=Agulhas 14=Namibia and South Africa 15=Angola 16=Cabina, Congo 17=Zaire 18=Gabon 19=Cameroon 20=Niger 21=Nigeria's Benue Trough 22=Ivory coast and Ghana 23=Guinea 24=Senegal 25=Mauritania 26=Morocco Atlantic 27=Morocco atlas 28=Taodeni 29=Niger onshore 30=Algerian Sahara 31=Maghreb 32=Western Mediterranean 33=Ghadames 34=Murzuk 35=Syrte 36=Egypt Western Desert 37=Egypt Syrian Arch 38=Eastern Mediterranean 39=Red Sea and Suez 40=Arabo-Persian Gulf 41=Kufra 42=Tindouf 43=Pelagian-Lonan Basin. Sub-basin:— 30A=Ahnet 30B=Mouydir 35C=Cyrenaica 43J=Jeffara. Dotted area=Pre-Cambrian Shield A=Arabian E=Eglabs G=Gargaf H=Hoggar N=Nubian Massif S=Sinai T=Tibesti U=Avenat in black: volcanism

FIG.1.2 : AFRICAN SEDIMENTARY BASINS

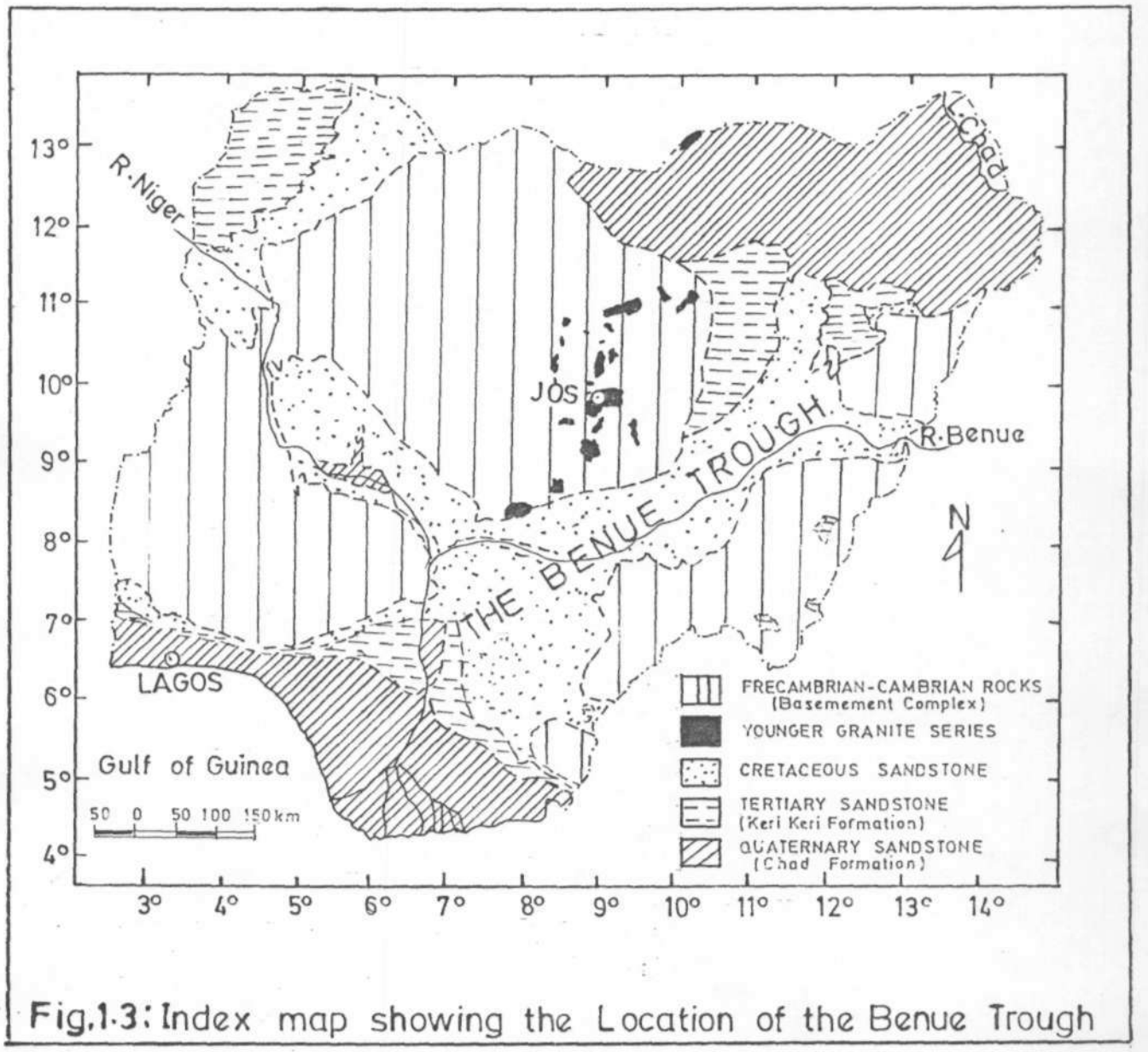


Fig.1.3: Index map showing the Location of the Benue Trough

of 800km and have a width of about 130 - 150km (Cratchley and Jones, 1965). The trough is filled with Cretaceous sediments whose ages range from Middle Albian to Maestrichtian and whose thickness generally decreases from the Lower and Middle Benue to the Upper Benue region. Boardering the sediments on either side are Pan African granites and gneisses of probable Palaeozoic age which make up the crystalline basement (Carter et al. , 1963; Oyawoye, 1972; McCurry 1976). Within the trough, there are several widely distributed ridge areas which are possibly areas of uplifted basement or basic intrusions, elongated along the main axis of the trough (Ajakaiye, 1981). Numerous basic to intermediate intrusions of various sizes also occur at different localities within the sediments. The sediments of the trough and the basement are strongly folded with a predominantly ENE-WSW fold axes aligned parallel to the main structural axis of the trough, and criss-crossed by numerous faults. The axis of the trough is also characterized by a narrow lead-zinc mineralization belt which runs from Abakaliki in the Lower Benue region to Zurak in the Upper part of the Trough.

The Benue Trough has a continous stratigraphical and structural coherence from the South-west to

the North-east through the entire length of the valley and this is shown by (Cratchley and Jones, 1965; Artsybashev and Kogbe, 1975; Offodile, 1976).:

(i) the continuity of palaeontological zonation within the marine formations.

(ii) the series of long and narrow folds with ENE-WSW axes which characterize the Cretaceous rocks from the vicinity of Abakaliki in the South-west to Gombe area in the North-east.

(iii) the narrow zone of lead-zinc mineralization with associated minor intrusions which extends from Abakaliki to Zurak, the intrusions continuing to beyond Gombe.

In general, the Benue valley exhibits a number of features common with other intra-continental rifts around the world. It is long compared with its width, it cuts through uplifted cratonic rocks, axial trending folds and faults predominate over others, there are abundant signs of volcanicity, and there are thermal and saline springs along its central axial zone (Ford, 1981). In addition to these features, the Benue Trough is known to possess some other unique properties, for example ;

(i) The width of the trough is about two or three times that of a normal rift valley (Wright, 1968) which is usually about 50 ± 15 km (Holmes, 1964).

(ii) The sediments of the trough are folded with the fold axes aligned parallel to the axis of the trough. Burke et al. (1970) asserted that the Benue Trough is the only rift valley in the world which has a fold axis parallel to its length.

For convenience, the area of the Benue Valley has been divided into three main regions of Cretaceous rocks; namely the Lower (Southwest), Middle (Lafia - Muri area), and Upper (Northeast) Benue (Figure 1. 4).

1.4 Review of Previous Geophysical Studies in the Upper Benue Trough

Until the mid-1960s the Benue Trough remained one of the geophysically unknown areas in Nigeria. But in recent years however much attention has been focussed on the geological and geophysical investigations of the trough in view of its economic potential and structural significance. The first major geophysical investigation carried out in the Benue Trough was done by Cratchley and Jones (1965). In spite of some limitations caused mainly by large station intervals (5km) and the lack of adequate roads, this pioneering geophysical study contributed

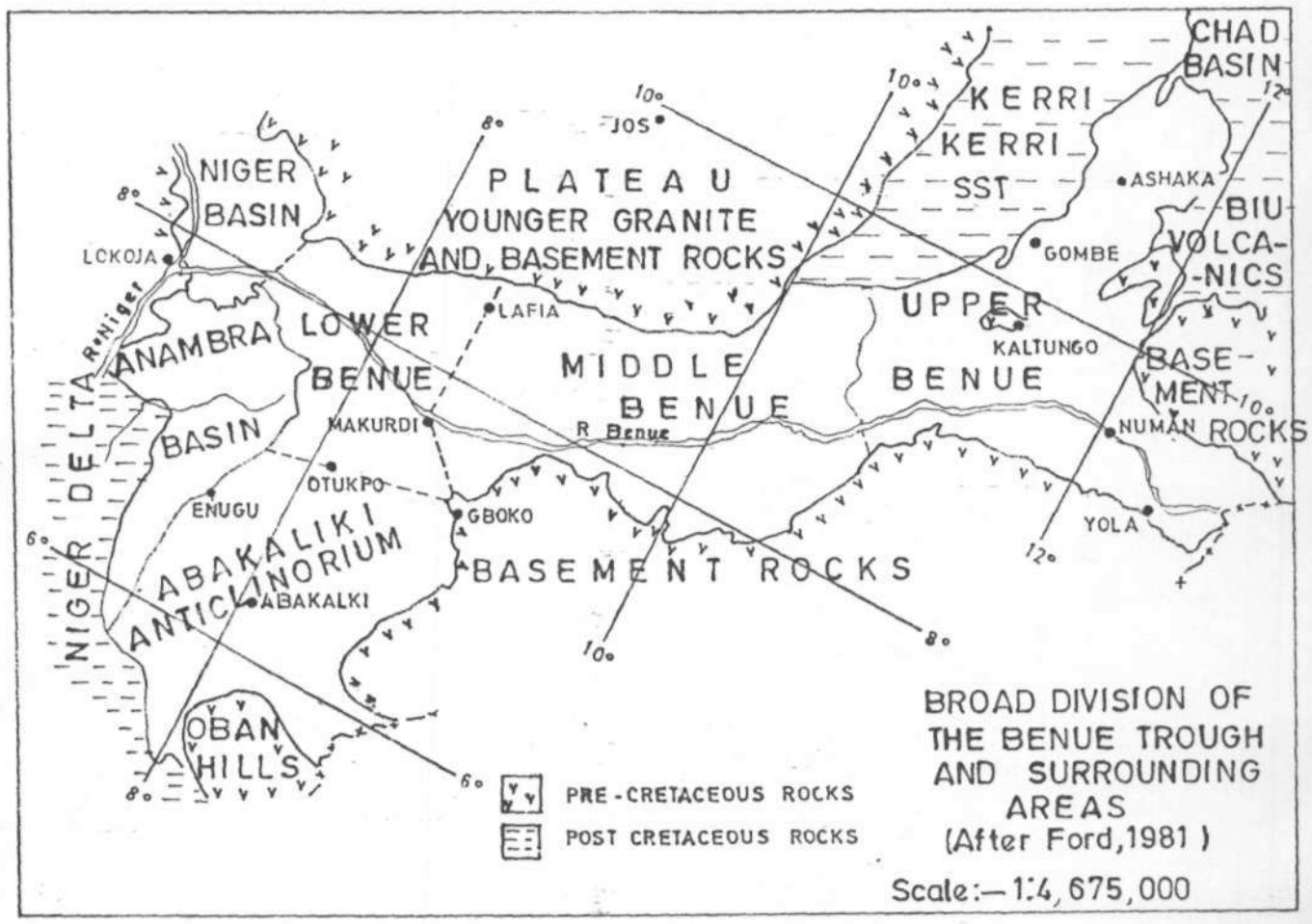


FIG. 1-4 : DIVISIONS OF THE BENUE VALLEY

enormously to the knowledge of the regional structure of the Benue Trough and have proved very useful in subsequent geological and geophysical studies in the region.

Subsequent years witnessed a remarkable increase in geophysical activities within the trough. These were largely isolated but detailed geophysical surveys employing mainly gravity and ground magnetics (Artsybashev and Kogbe, 1975; Osazuwa, 1978; Umego, 1978; Ekine, 1979; Ajayi, 1979; Myada, 1979; Adighije, 1979, 1981a, b; Osazuwa et al. 1981; Ajakaiye, 1981; Ajayi and Ajakaiye, 1981; Fairhead and Okereke, 1986). In addition to these surveys are the studies of aeromagnetic anomalies over parts of the trough (Ofoegbu, 1982; Ashiekaa, 1983; Ofoegbu, 1984a, b, c, 1985b; Ajakaiye et al., 1986).

Apart from the surveys of Cratchley and Jones (1965), Osazuwa (1978), Osazuwa et al. (1981), Ajakaiye et al. (1986) and Fairhead and Okereke (1986) which cover the Upper Benue region, the other studies were limited in scope to the Lower and Middle Benue, and to the Chad basin.

Results of studies in the trough were successful in providing useful information about the structure and tectonics of the basin. A

review of some of the results indicate that the Benue Trough is characterized by a central axial positive anomaly in the Middle and Upper Benue regions. This central axial high is flanked on both sides by some local positive anomalies and broad negative anomalies characteristic of valleys with sedimentary fills. The observed axial positive anomalies have been interpreted by some authors in terms of a zone of sizeable igneous intrusions of intermediate to basic composition occuring at very shallow depths, and uplifted blocks of near-surface basement rocks (Cratchley and Jones, 1965; Ajayi and Ajakaiye, 1981). The major negative anomalies observed in the trough have been generally associated with the presence of isolated and deep basins with thick deposits of Cretaceous sediments. In the Upper Benue Trough sediment thickness has been estimated to be 4.9 km near Numan while a thickness of 0.9km was estimated near Sangere Loko (Osazuwa, 1978). The local positive anomalies have also been interpreted as being due to numerous minor intrusions occuring within the trough. The intrusive bodies may exist predominantly within the basement or within the sedimentary rocks or both (Cratchley and Jones, 1965). Depths-to- top of these intrusions vary erratically through the entire length of the trough.

Some results of the aeromagnetic studies in the trough (Ofoegbu, 1984a) agree substantially with the interpretation of gravity anomalies over the trough (Cratchley and Jones, 1965; Osazuwa, 1978- Adighije 1979; Osazuwa et al.; 1981). These authors consider the regional positive anomalies in the trough as being due to an uplift of the mantle and a corresponding thinning of the crust.

In another study of aeromagnetic anomalies Ajakaiye et al.(1986) analysed aeromagnetic data for the Benue Trough and the neighbouring younger granite complexes, and some portions of the Chad basin. The findings from that study revealed the existence of narrow magnetic linearments in this region, indicating some possible relationship with the four main oceanic fracture zones (St. Pauls, Romanche, Chain, and Charcot) cutting the Atlantic sea floor of the West coast of Africa.

1.5 Scope and Objectives of Study

Several geophysical techniques mainly gravity, ground magnetics and aeromagnetics have been employed in the study of the various sections of the Benue Valley. Until now, the only known aeromagnetic studies of the Benue Trough are due to Ofoegbu (1982, 1984a, c, 1985b) and

Ashiekaa (1983) whose surveys were restricted mainly to the Lower and Middle Benue regions, and Ajakaiye et al. (1986) whose work covers the entire valley and the surrounding regions.

The present aeromagnetic study therefore focusses particularly on the Upper Benue Trough and appears to be the first major attempt at interpreting the aeromagnetic anomalies over the Upper Benue region by employing techniques based on spectral analysis. The objective is to investigate the lateral variation in sedimentary thickness and structure under the valley. It is hoped that this study will yield new information regarding the structure and tectonics of the Benue Trough.

CHAPTER 2

GEOLOGY OF THE UPPER BENUE TROUGH

2.1 Introduction

The geology described in this section covers an area of approximately 109,000 sq km in the North-eastern part of Nigeria, lying mostly between latitudes 09^{o} 00'N and 12^{o} 00'N, and longitudes 009^{o} 30'E and 012^{o} 30'E.

The essential geological features of the region comprise the sedimentary and volcanic rocks, ranging in age from Upper Cretaceous to Quaternary overlying an ancient crystalline basement made up mainly of Precambrian granites and gneisses.

The basement, Cretaceous sandstones and the volcanic rocks form prominent hill features at some locations in the project area. A simplified geological map of Nigeria is shown in Figure 2.1.

2.2 The Basement Complex

Most of the exposed outcrops in Nigeria belong to the basement complex which is believed to be predominantly Precambrian (Oyawoye, 1972). The crystalline basement over the Upper Benue Trough, as in most other parts of Nigeria, contains numerous major and minor intrusions. The rocks



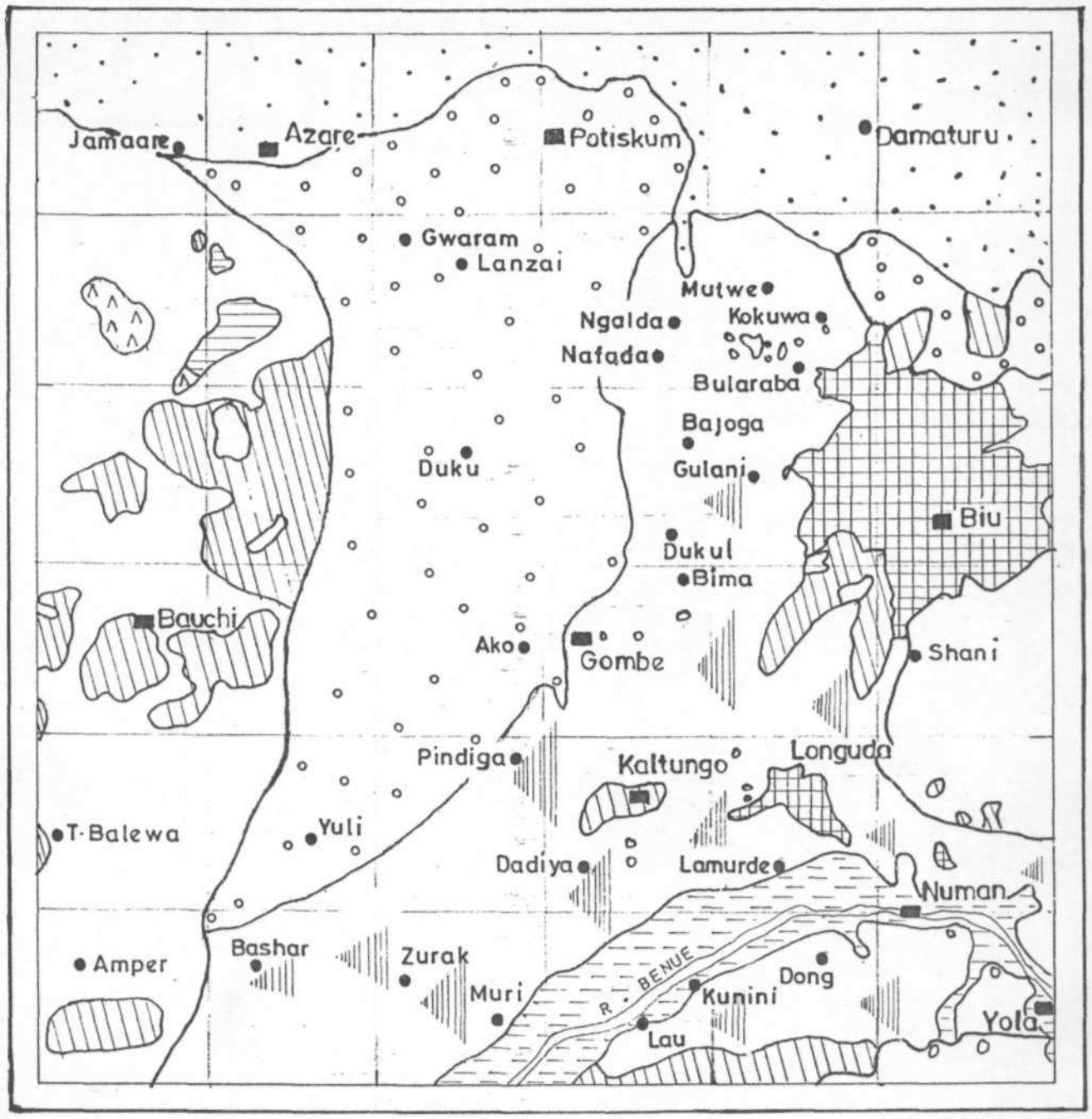
FIG. 2.1: SIMPLIFIED GEOLOGICAL MAP OF NIGERIA

that make up the basement complex are also quite numerous, and those over the project area consist mainly of quartzo-feldspathic migmatites and gneisses, quartzites, marbles and amphibolites (Carter et al., 1963). There are also numerous older and younger intrusions. Notable outcrops of the older granite rocks include the small inliers of biotite granites and gneisses that are found around Gombe and Kokuwa, and in . Bauchi area. The older intrusives are mainly granites and granodiorites while the younger intrusives are largely granitic and pegmatic types, although diorite, dolerite, and some syenites occur. Many younger intrusives of intermediate to basic character also occur with numerous associated dyke-like bodies (Oyawoye, 1972; Wright, 1976).

The crystalline basement whose topography is believed to be irregular (Carter et al., 1963) is exposed in a number of locations in the Upper Benue Valley. One of the prominent outcrops of the basement in the area include the Kaltungo basement inlier. The general geology map of the study area is presented in Figure 2.2.

2.3 Cretaceous Stratigraphy of the Upper Benue Trough.

The stratigraphy of the Cretaceous in the



LEGEND

QUATERNARY	CHAD FORMATION	ALLUVIUM SANDS AND CLAYS
TERTIARY	TERTIARY TO RECENT VOLCANICS	BASALTS
	KERRI-KERRI FORMATION	GRITS, SANDS AND CLAYS
CRETACEOUS		CLAY, SHALE, COAL, SANDSTONE AND LIMESTONE, etc.
JURASSIC	YOUNGER GRANITES	GRANITE SYENITES AND GABBRO
PRE-CAMBRIAN TO UPPER CAMBRIAN	BASEMENT COMPLEX	OLDER GRANITES UNIDIFFERENTIATED BASEMENT COMPLEX

FIG. 2.2: GENERAL GEOLOGY MAP OF THE STUDY AREA

Benue Trough has been studied and documented (McConnell, 1949; Jones,1960; Carter et al., 1963; Offodile, 1976a; Kogbe, 1981a). A general stratigraphical sequence in the Upper Benue Trough is given in Table 2.1. The stratigraphy of the Upper Benue region has been worked out as consisting of several formations of Cretaceous age. It is now known that sedimentation in the Upper Benue basin started in the Albian with the deposition of Bima sandstone whose age ranges from Middle Albian to Late Albian. The Bima sandstone is made up of a widespread series of continental grits, found at the base of the sedimentary succession directly overlying the crystalline basement floor (Carter et al., 1963). Bima sandstone is believed to vary considerably in thickness. This is due partly to the undulating topography of the crystalline floor on which the sediments accumulated, and partly due to the differing degrees of accomodation in the basins of deposition (Carter et al.,1963). It ranges in thickness from 100m to 300m and has its maximum development at the Lamurde anticline where the thickness exceeds 3000m (Offodile, 1976a).

TABLE 2.1: General Stratigraphical Succession in the Upper Benue Trough

AGE	GEOLOGICAL TIME		UPPER BENUE BASIN: LAU	ZAMBUK-GULANI	GOMBE
Paleocence					Kerri-Kerri Fm.
CRETACEOUS	MAESTRICHTIAN		Lamja sst	Gulani sst.	
	SENONIAN	Campanian	Numanha Shales		Pindiga Formation
		Santonian	Sekule Fm.		
		Coniacian			
	TURONIAN	Upper	Jessu Fm.		
		Middle			
		Lower	Dukul Fm.		
	CENOMANIAN		Yolde Fm.		Yolde Fm.
	MID-LATE ALBIAN		Bima sst.	Bima sst.	Bima sst.
Late Palaeozoic to Pre-Cambrian	BASEMENT COMPLEX				

Stratigraphy: Compiled from (Carter et al., 1963; Cratchley and Jones, 1965; Wright, 1976; Offodile, 1976; Kogbe, 1981a).

Next to be deposited in the Gombe basin and Lau basin was Yolde formation whose exact relationship to the Bima sandstone is not well known, although the formation is believed to be predominantly Cenomanian. A widespread, shallow marine transgression occured during the Lower Turonian times (Carter et al,, 1963) and it was during this period that Pindiga formation was deposited. In the Lau district the sequence of deposition was Dukul, Jessu, Sekule and Numanha formations (Carter et al., 1963; Offodile, 1976a). The Yolde formation is thus a transition between the continental Bima sandstone and the succeeding marine formations. The Dukul formation which consists mainly of shales interbedded with thin limestones, and having a total thickness of up to 100m, marked the beginning of the widespread marine transgression (Carter et al., 1963; Offodile, 1976a; Kogbe, 1981a). The Numanha and Sekule formations consist of shales and limestone levels and are Senonian in age. The Gulani sandstone consisting of a sequence of cross-bedded, massive, fine- and medium-grained sandstone is also Senonian, probably Campanian (Kogbe, 1981a). The marine conditions persisted until the Campanian-Maestrichtian and the ensuing regression gave rise to the growth of deltaic conditions associated with the deposition of

Gombe and Lamja standstones (Carter et al.,1963). The end of the Maestrichtian deposits marked the close of the Cretaceous sedimentation.

Following the development of great anticlinal structures in the Cretaceous rocks, sedimentation continued in the Palaeocene, and a younger -sequence of continental deposits, the Kerri-Kerri formation, was laid down unconformably upon the folded Cretaceous rocks in the Gombe basin. The Kerri-Kerri and Gombe formations marked the end of the sedimentary sequence in the Upper Benue Trough. This continental sedimentation was however followed by a period during which the extensive Laterite sheet overlying the Kerri-Kerri formation was formed.

2.4 Structures in the Upper Benue Trough

The major structures found in the Benue Trough are folds and faults. The trough was subject to several folding episodes, notably in the Cenomanian, Santonian, Post Maestrichtian and possibly Palaeocene (Ofoegbu, 1985a). In the Upper Benue region the structural pattern has been largely determined by the brief but severe earth movements of the Santonian. Within the sedimentary formations the structural pattern is dominated by a series of folds believed to be formed by repeated deformative forces, compressional and tensional (Carter et al., 1963). The predominatly compressional nature of

these folds is revealed by their assymetry and the reversed faults associated with them (Ofoegbu, 1985a). A major character of these folds is their consistent trend and linear dimensions. In the Upper Benue region, folding took place mainly along ENE-WSW axes, particularly in the Dadiya Kaltungo, Lamurde, Longuda and Zurak areas. The sediments of the Upper Benue are uniformly and gently folded thus suggesting the possibility of two episodes of folding within the region - a major folding episode in the Santonian and a relatively minor one in the post Maestrichtian.

The majority of faulting in the Upper Benue Trough are later events than the folding and are believed to have affected all the Cretaceous rocks. Numerous faults have been reported within the trough (Burke et al., 1970; Chukwu-Ike, 1977; Ajayi and Ajakaiye, 1981; Ajakaiye et al., 1986). Some of these faults are parallel to the axis of the folds, hence, they are thought to be strike faults (Offodile, 1976) and are known to be well developed in the Gombe basin. Another group of tension faults are also known to be present along the margins of the basement - Cretaceous contact, and in the sediments surrounding the Kaltungo inlier.

The faults show variable trends but the dominant direction lies between NNE and ENE. The major east-west faulting near Muri may account for the complicated nature of Muri and Ligiri folds (Cratchley and Jones, 1965).

2.5 Igneous Intrusions and Volcanic activity

The extensive igneous activity which took place in the Lower Cretaceous of Nigeria was concentrated within the Benue Trough and was apparently most intense during the Late Albian times (Ofoegbu, 1985a). The intrusions are widely distributed throughout the Upper Benue region, and the younger intrusives are represented by volcanic plugs, dykes, sills, or bosses in the central and southern parts of the project area. Smaller bosses and dykes are of basic and intermediate rocks and the larger basic masses occasionally produce contact metamorphism in the sediments, as well as characteristics suggestive of a close interval of time between sedimentation, folding and intrusion (Cratchley and Jones, 1965).

There is also evidence of widespread but sporadic volcanic activity extending from

Cretaceous to Recent times, and its distribution only infrequently coincides with areas of igneous activity. Prominent among the Tertiary and Recent volcanics in the region are the basaltic lavas of Biu and Longuda. In general, the occurences of igneous and volcanic activity within the trough tend to be closely associated with the lead-zinc mineralization, and there is also a marked association of the intrusions with the anticlinal structures in the trough (Cratchley and Jones, 1965; Wright, 1976).

2.6 Tectonic Evolution and Origin of the Benue Trough

Many theories and models have been proposed in an attempt to explain the structural and tectonic evolution of the Benue Trough. Accounts of these theories and models range from those based on the geomorphological evidence (King, 1950; Lees, 1952; Farrington, 1952; Cratchley and Jones, 1965) to the tectonic models of Wright (1968, 1981), Grant (1971), Burke et al.(1971, 1972), Olade (1975), Osazuwa et al. (1981) and Ofoegbu (1984a). There are other hypotheses proposed by other authors (Ayoola, 1978; Adighije, 1981; Ajayi and Ajakaiye, 1981; Benkhelil, 1982) which are complementary to the ideas already mentioned.

Although several bold attempts have been made to explain the origin of the trough the subject still remain inconclusive. Some of the theories frequently indicate lack of consistent agreement with each other, although most of the authors appear to support the idea of a rift origin. Geological and geophysical investigations by some workers in this area give ample evidence in support of the rift theory but no completely satisfactory explanation has as yet been given. However the theories have given a wider scope for further research. A completely integrated geophysical investigation covering the entire Benue Valley and the surrounding regions can provide very useful data for a better understanding of the origin and tectonic evolution of the trough.

2.7 Economic Geology of the Upper Benue Trough

The Benue Trough is generally regarded as a rift structure and is known to posses some of the familiar features found in other intra-continental rift structures around the world. It is long compared with its width, axial trending folds and faults occur, there are abundant signs of volcanicity and there are thermal and saline springs along its central, axial zone (Ford, 1981). Considering the economic potentials seen in rift environments it is reasonable

to expect the occurence of exploitable minerals in the Benue Trough. Accounts of the economic mineral resources of the Benue Trough have been reported by many authors (Carter et al.,1965; Offodile, 1976a, 1977; Ford, 1981). Offodile (1977) observed that deposits of minerals are distributed throughout the length of the trough (Figure 2.3).

The lead-zinc mineralization which occur in the sedimentary formations along the axial zone of the trough extends to Zurak and Gwana in the Upper Benue region. Further detailed prospecting and development may be necessary to determine if the quantities available are concentrated into deposits of economic interest.

Some of the best sedimentary limestones in the country are to be found in the Benue trough. Limestones occur in the Yolde, Dukul, Sekule, Pindiga and Gongila formations (Carter et al., 1963). A narrow band (5cm) of limestone outcrops over a fairly wide area about 5km south of Zurak. Many individual bandsof limestone have also been recorded in Lau, Kunini, and Dong (Carter et al., 1963), most of them between 10cm and 50cm thick.

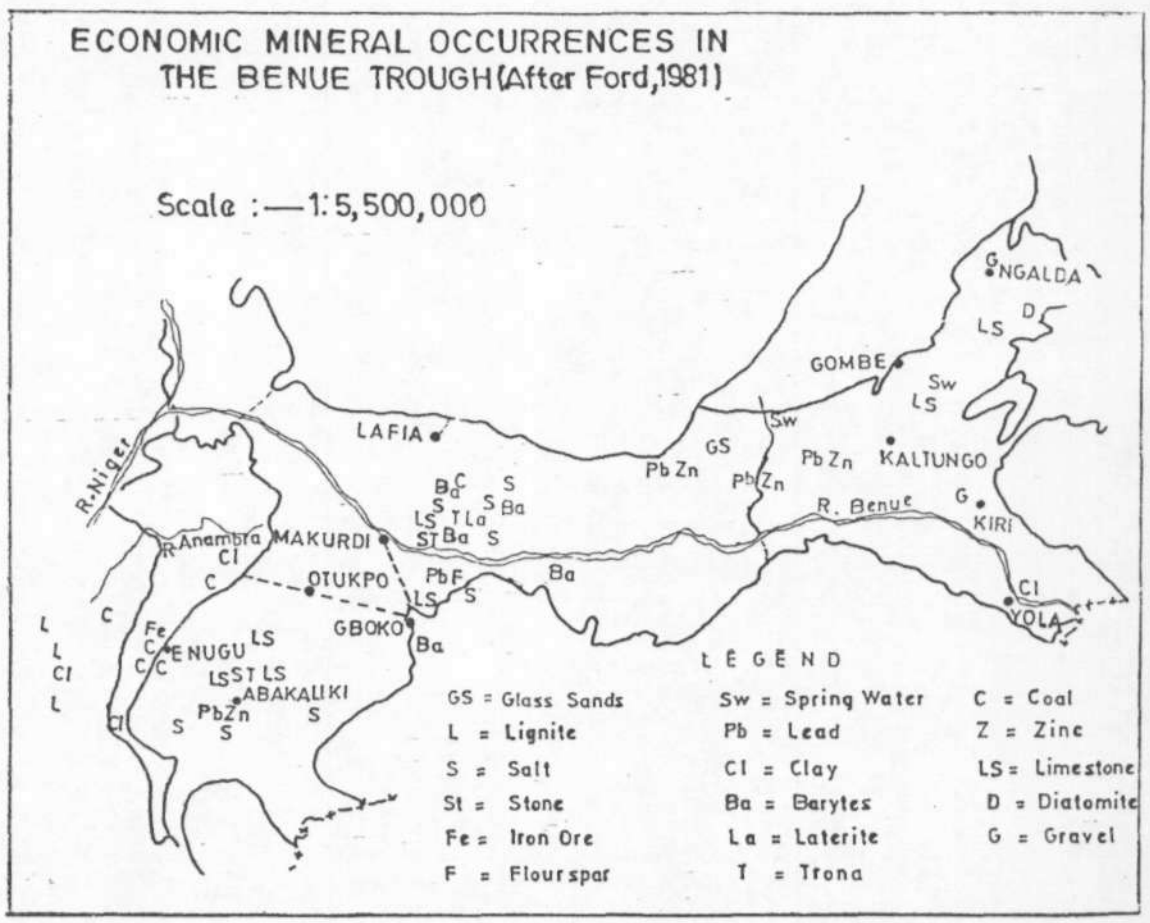


Fig. 2.3: Economic Mineral Deposits in the Benue Valley.

Thin seams of coal have also been found in the Upper Benue trough during geological mapping of parts of the trough,and in drilling for water around Gombe area (Offodile, 1976a; Ford, 1981). The coal deposits in this area are thin, impersistent and poor in quality to be of economic importance.

No deposits of chemical minerals such as solid rock salt has been reported in the Upper Benue trough but salt springs have been recorded near the western ends of Lamurde anticline and Kaltungo inlier, the concentrations being of sodium chloride. Reports of actual salinity at various sites differ widely probably due to seasonal variations resulting from admixtures of surface water (Ford, 1981).

Diatomite occurs at the extreme northern end of the Upper Benue in the form of local deposits. The deposits, scarcely up to 3m thick has been estimated to contain 55,000 tonnes of good quality diatomite (Carter et al, 1963; Offodile, 1977; Ford, 1981). Occurences in several other locations in the general area appear too small to be worth consideration for exploitation.

Abundant reserves of crushed stone aggregates, an essential commodity in building and civil engineering construction, exist in the Upper Benue trough. Within the trough the crystalline rocks are restricted to small localities such as Gombe and Kaltungo and they constitute the raw materials for

stone aggregates. Gravel has also been regarded as a raw material of possible value at Ngalda, near Nafada and at other sites in the Upper Benue.

Marine sediments, mainly clays and shales, deposited as Cretaceous sediments are exposed at several locations and in Pindiga area of the Upper Benue. These deposits have yielded useful raw materials for brick making and earthen ware pottery.

By reference to its mode of formation and probable origin, the Benue Trough holds considerable potential for minerals and industrial raw materials of possible economic value. At present the greater part of the trough particularly in the Middle and Upper Benue regions remain largely unmapped and unexplored (Ford, 1981). If a complete integrated geophysical exploration programme is applied to the search for economic mineral deposits in the Benue Valley, the rewards may be considerably greater than what we have now.

CHAPTER 3

SPECTRAL ANALYSIS OF AEROMAGNETIC FIELDS

3.1 Fourier Analysis of two-dimensional Aeromagnetic data

With the application of computerized procedures now available, Fourier analysis has become a standard technique for analysing aeromagnetic data. The usual procedure is to transform the details of the digitized total intensity aeromagnetic data over a finite area, preferably a square, into the frequency domain using the Fourier Transform methods. This approach now uses the Fast Fourier Transform (FFT) techniques. The FFT is simply a computational algorithm that can compute the discrete Fourier Transform (DFT) of a series of data samples much more rapidly and efficiently than other available algorithms.

The FFT method was infact presented many years ago, and was later rediscovered and widely publicized by Cooley and Tukey (1965). Cooley and Tukey's algorithm for one-dimensional data is easily adapted to two-dimensional data, given in a matrix form. Using this algorithm Naidu (1969), Spector and Grant (1970), Kanasewich and Agarwal (1970) and many others have analysed one-

and two-dimensional aeromagnetic data.
The increasing application of FFT methods in other fields where spectra are calculated has also given rise to a corresponding increase in the amount of literature on various aspects of the subject. Consequently new and much faster procedures for computing Fourier Transform have been published. A modified FFT, particularly useful for saving storage space and computer time in transforming two-dimensional aeromagnetic data, has been devised by Naidu (1970a).

Fast Fourier Transform of two-dimensional aeromagnetic data is usually obtained by first Fourier transforming columns (or rows) and next rows (or columns). The scheme simply follows from the Fourier Transform of a two-dimensional data matrix (Naidu, 1969; Naidu, 1970b):

$$\bar{X}(u, v) = \sum_{m=1}^{M} \sum_{n=1}^{N} X(m, n) \exp(-i(um + vn))$$

$$= \sum_{m=1}^{M} \{ \sum_{n=1}^{N} X(m,n) \exp(-ivn) \} \exp(-ium)$$

$$= \sum_{m=1}^{M} \bar{X}'(m, v) \exp(-ium)$$

.... 3.1

where $\bar{X}'(m, v)$ is a Fourier transform of the m^{th} column and M,N are the dimensions of the data matrix. The normalized power or energy spectrum of the two-dimensional aeromagnetic data is given by:

$$S'(u,v) = \frac{1}{M \times N} \left| \bar{X}(u,v) \right|^2 \qquad \ldots \quad \ldots \quad 3.2$$

In general, and for this study in particular, M = N. The number of sample points N is chosen according to the relation $N = 2^k$, for FFT analysis, where k is an integer constant.

Based on the available algorithms, the above processes have been programmed by many authors for various implementations using the binary features of a computer. For the present study an FFT subroutine written by Claerbout (1976) was used. Input to this subprogram is a complex matrix.

3.2 Data Organisation and Treatment

The data set used in this study was compiled from thirty-six half-degree aeromagnetic map sheets. The first step in the data preparation stage was to digitize each map sheet on a digitizing

grid suitable to regional work. The correct choice of the digitizing interval is an important consideration in the spectral analysis of aeromagnetic data. An incorrect choice of the digitizing step affects the retrieval of the true spectrum, and in consequence degrades the interpretational fidelity (Cianciara and Marcak, 1976; Pal et al., 1978). In order to obtain a sufficiently correct digitizing spacing, a compromise has to be sought between various considerations the most significant of which are the data length or map window in use, the sampling frequency, the nyquist frequency, the flight line spacing, the approximate depth to the magnetic sources of interest, and the wavelength of the anomalies of interest (Bath, 1974). For best results Cianciara and Marcak (1976), and Pal et al.(1978) consider the optimization of the digitization spacing very essential.

In the present study digitizing was done manually at a spacing of approximately 3km on a regular square grid of 19 x 19 data matrix per map sheet. This gave rise to a grand matrix of dimension 109 x 109 for the project area, or 11,881 data points. A digitizing interval of 3km directly imposes a Nyquist frequency of 1/6 km^{-1}.

The Nyquist frequency is the lowest frequency which is its own alias; that is the limit of both the sequence of frequencies and of the sequence of their aliases. The Nyquist frequency also known as the folding frequency is simply given by:

$$f_{nq} = \frac{1}{2}\left\{\frac{1}{\Delta x}\right\} \quad \ldots \quad \ldots \quad 3.3$$

where Δx is the sampling step.

A Nyquist frequency of 1/6 km^{-1} simply implies that magnetic anomalies less than 6km in width cannot be adequately defined with a digitizing spacing of 3km. However, Hall (1968, 1974) considers this digitizing interval suitable for the potrayal and interpretation of magnetic anomalies arising from regional crustal structures. It has also been indicated by Ajakaiye et al. (1985) that crustal anomalies are much wider than 6km and therefore lie in a frequency range for which computational errors arising from aliasing do not occur with a 3km digitizing grid.

3.2.1 Regional Field Separation

The interpretation of potential field anomalies frequently begins with some procedure which separates the residual anomalies from broader background disturbances. A popular reliable conventional approach to the anomaly separation

problem is the application of two-dimensional surface fitting calculations. With the increasing speed and capacities of present-day computers the hitherto complicated mathematical procedure of the surface fitting has largely become a routine operation.

A least square operation is usually carried out which determines a potential surface which is fitted to the observed data. Since the surface fitting technique is a least square process, the fitted surface which is the assumed regional, is a surface which will have both positive and negative differences from the observed data. In the present study the regional field was removed from the observed aeromagnetic data by fitting a first order polynomial surface to the data. The expression for the regional surface over the study area is given by:

$$F = 7792.0 - 4.66\,X - 0.9236Y \qquad \ldots \quad \ldots \quad 3.4$$

where X and Y are grid coordinates in kilometers which describe the position of the data points with respect to the origin of the two axes of the data array. A value of 25,000 gammas should be added to all map data to obtain the actual total field magnetic values.

The regional trend was subtracted from the observed aeromagnetic data to obtain the residual anomalies. The residual anomalies contain the components of the field which, presumably, are caused by the geological disturbances of interest.

3.3 Choice of Map Windows

The use of a limited record length is practically inevitable in the spectral analysis of any observed record. A direct consequence of using a finite data window in the analysis is that the true spectrum cannot be retrieved from the observed data. This means that the amplitude and phase characteristics of the resulting spectrum will suffer some distortion due to the truncation effects. Besides the size of the data window, its shape also has an important bearing on the characteristics of the computed spectrum. Hence the degree of distortion in the computed spectrum also depends on the shape of the data window.

Limitations on the choice of an appropriate window size can be imposed by such factors as the type of record in use, the resolution desired in the computed spectrum, capacity of the computer in use, and the objective of study. A large

data window will obviously lead to a better resolution in the resulting spectrum than a small data window. The use of a finite data window is equivalent to applying a rectangular data window. Figure 3.1 shows the rectangular time window and the corresponding spectral window. The effects of the data window in the frequency domain are to broaden the spectral lines and to introduce a series of spurious peaks called side lobes. The consequence of the presence of side lobes is that the spectral power from the adjoining frequencies leaks into and contaminates the frequency of interest. This is highly undesirable particularly in the neighbourhood of a spectral peak.

In order to obtain good spectral estimates Bingham et al. (1967) suggest a way of reducing the ill effect of the side lobes. The procedure is to use a window function which does not abruptly go to zero. Although this results in a wider main lobe, the objective is to have a spectral window that is concentrated in its main lobe and yet has only negligible side lobes. To achieve this effect the cosine-tapered rectangular window was used in the present study. Such an extended cosine-bell data window remains fairly flat over most of the data length, therefore preserving most of the

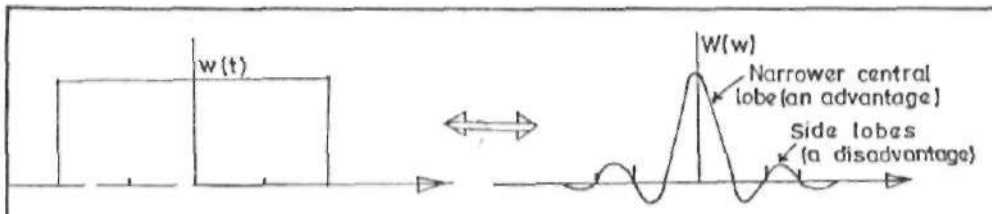


Fig. 3-1 : Rectangular data window and the corresponding spectral window

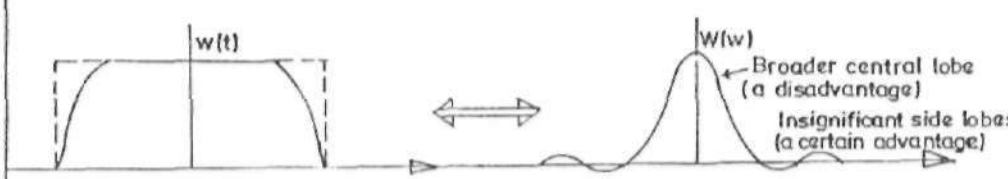


Fig. 3-2 : A cosine-bell data window and the corresponding spectral window

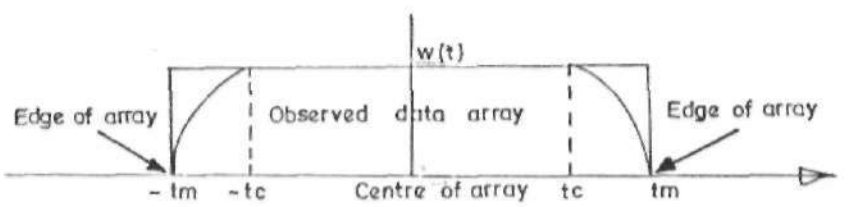


Fig-3-3 : An extended cosine-bell data window

original data set but tapers off near the two ends of the record (Figure 3.2). The tapering eliminates the high frequencies (side lobes) erroneously introduced by the sharp truncation in the rectangular data window.

An ideal taper consists of a pair of cosine bells defined as follows (Figure 3.3):

$$w(t) = \tfrac{1}{2}\left\{1 + \cos\pi\frac{(t_c - t)}{(t_c - t_m)}\right\}, \text{ for } -t_m < t < -t_c$$

$$= 1, \text{ for } -t_c \leq t \leq t_c$$

$$= \tfrac{1}{2}\left\{1 + \cos\pi\frac{(t - t_c)}{(t_m - t_c)}\right\}, \text{ for } t_c < t < t_m \qquad \ldots 3.5$$

The procedure for smoothing the shape of the data window through the application of the cosine taper was based on the basic formulas of equation 3.5. The edges of the data array were smoothly tapered by applying the cosine taper of width equal to 5 data points for the 19 x 19 data array ($\frac{1}{2}^{o} \times \frac{1}{2}^{o}$ map window); and 10 data points for the 37 x 37 (1^{o} x 1^{o} map window) and 55 x 55 ($1\frac{1}{2}^{o}$ x $1\frac{1}{2}^{o}$ map window) data arrays respectively. This reduced the grid of the unaltered data for the three data arrays in use to 9 x 9, 17 x 17 and 35 x 35.

3.4 Procedure for Spectral Depth Estimation in Magnetics.

Following the approaches of Hahn et al.(1976) and Pal et al. (1978), the procedure for the spectral estimation of depths to magnetic sources within the earth's crust starts with the calculation of the average spectrum from the spectrum matrix computed from equation 3.1 or 3.2. The first step is to subdivide the frequency intervals into subintervals representing frequencies which lie within a given interval value (Figure 3.4). The frequency interval used in the present study lies within 0.5 of an integer. The average spectrum of all the partial waves occuring within this frequency range was computed and the resulting values together form the radial spectrum of the anomalous field under study. The scheme for computing the radial spectrum for map spectra is illustrated in Figure 3.4. The upper values in each block represent the normalised energy spectrum and the values below are the frequencies.

A logarithmic plot of the radial spectrum versus frequency on a linear scale shows a series of points that may well be represented by straight lines. Most of the points due to anomalies

	0	1	2	3	4	5	6	7	8	9	10	11	12	13	14
0	13.12 0	11.13 1	9.91 2	7.09 3	7.09 4	7.31 5	5.65 6	3.30 7	4.28 8	2.59 9	-1.25 10	-1.58 11	0.53 12	-0.63 13	-0.24 14
1	11.07 1	9.19 1.41	7.68 2.24	5.00 3.16	5.07 4.12	5.16 5.10	3.48 6.08	1.23 7.07	2.29 8.06	0.46 9.06	-1.51 10.05	-3.92 11.05	-1.29 12.0	-1.80 13.04	-1.25 14.04
2	9.88 2	7.66 2.24	6.90 2.83	4.28 3.61	3.88 4.47	4.17 5.39	2.81 6.32	-0.44 7.28	1.19 8.25	-0.60 9.22	-1.38 10.20	-4.15 11.18	-1.52 12.17	-2.56 13.15	-3.42 14.14
3	6.90 3	4.70 3.16	4.31 3.61	0.31 4.24	1.30 5.00	0.72 5.83	0.23 6.71	-0.56 7.62	-3.90 8.54	-1.67 9.49	-1.33 10.44	-1.19 11.40	-1.61 12.37	-1.34 13.34	-3.19 14.32
4	6.69 4	4.53 4.12	3.68 4.47	2.93 5.00	0.77 5.66	1.23 6.40	0.64 7.21	-3.35 8.06	-3.78 8.94	-1.81 9.85	-0.75 10.77	-1.50 11.70	-2.30 12.65	-1.69 13.60	-2.99 14.56
5	7.42 5	5.33 5.10	4.73 5.39	0.63 5.83	2.51 6.40	1.42 7.07	0.17 7.81	-0.46 8.60	-0.74 9.43	-3.70 10.30	-2.97 11.18	-1.75 12.08	-1.97 13.00	-1.13 13.93	-4.02 14.87
6	5.76 6	3.34 6.08	3.12 6.32	0.88 6.71	-2.75 7.21	-0.48 7.81	0.58 8.49	-1.32 9.22	-0.62 10.00	-4.13 10.82	-3.25 11.66	-1.49 12.53	-1.86 13.42	-1.14 14.32	-3.72 15.23
7	2.22 7	0.76 7.07	1.58 7.28	-0.92 7.62	0.88 8.06	0.89 8.60	-0.36 9.22	-2.58 9.90	-1.98 10.63	-4.18 11.40	-1.29 12.21	-0.95 13.04	-3.15 13.89	-2.50 14.76	2.54 15.65
8	4.67 8	1.81 8.06	2.70 8.25	1.08 8.54	-0.36 8.94	-1.31 9.43	-0.48 10.00	-2.86 10.63	-4.85 11.31	-1.16 12.04	-5.58 12.81	-1.72 13.60	-3.10 14.42	-2.92 15.26	-2.45 16.12
9	2.97 9	1.87 9.06	-2.38 9.22	0.65 9.49	-0.25 9.85	1.13 10.30	-1.47 10.82	-1.17 11.40	-3.27 12.04	-0.85 12.37	-4.63 13.45	-1.82 14.21	-1.72 15.00	-1.06 15.81	-2.05 16.64
10	-0.72 10	-1.80 10.05	0.40 10.20	-0.09 10.44	-1.38 10.77	-0.19 11.18	-2.37 11.66	-1.80 12.21	-1.34 12.81	-2.14 13.45	-1.97 14.14	-1.11 14.87	-2.52 15.62	-1.51 16.40	-1.17 17.20
11	-4.12 11	-0.92 11.05	-0.79 11.18	-1.31 11.40	-0.87 11.70	-2.97 12.08	-1.93 12.53	-0.54 13.04	-0.75 13.60	-3.01 14.21	-3.83 14.87	-1.92 15.56	-1.84 16.28	-1.53 17.03	-1.44 17.80
12	0.77 12	-0.82 12.04	0.61 12.17	-0.25 12.37	-2.83 12.65	-2.14 13.00	-0.64 13.42	-3.16 13.89	-1.92 14.42	-4.61 15.00	-1.83 15.62	-2.45 16.28	-3.32 16.97	-1.76 17.69	-1.50 18.44
13	-0.03 13	0.20 13.04	-2.16 13.15	-0.77 13.34	-4.59 13.60	-2.31 13.93	-0.57 14.32	-2.27 14.76	-0.88 15.26	-1.55 15.81	-3.31 16.40	-0.79 17.03	-1.91 17.69	-1.89 18.34	-0.80 19.10
14	-1.08 14	-0.72 14.04	-3.89 14.14	-1.18 14.32	-2.93 14.56	-0.75 14.87	0.02 15.23	-1.30 15.65	-2.26 16.12	-6.00 16.64	-3.32 17.20	-1.45 17.80	-2.28 18.44	-1.52 19.10	-1.49 19.80

LogE	13.12	10.46	8.78	6.12	4.43	4.79	2.73	0.82	1.02	-0.35	-1.07	-2.31	-1.32	-1.75	-2.04
f	.0	1.14	2.12	3.03	4.07	5.12	6.08	7.06	8.01	9.06	10.11	11.06	12.03	13.03	14.05

FIG. 3.4 : COMPUTATION OF RADIAL SPECTRUM FROM THE SPECTRUM MATRIX

caused by bodies occuring within a particular depth range or at different levels fall on one or more straight line segments whose slope provide a measure of the mean depths to the assemblage of anomalous bodies (Spector and Grant, 1970; Hahn et al., 1976).

3.5 Slope - Depth Relation for Power Spectrum Analysis

On the assumption that the observed aeromagnetic field is due to the integrated effects of several independent ensembles of rectangular, vertical-sided parallelopipeds existing at a number of discrete depth intervals in the geologic column, Spector and Grant (1970) have shown that the variations of the radially averaged power spectrum for an ensemble of sources can be expressed as:

$$\{E(k, \theta)\} = 4\pi^2 M^2 \{\exp(-2zk)\} \{(1- \exp(-kt))^2\} \{S^2(k,\theta)\} \quad \ldots \quad \ldots \quad 3.6$$

where { } indicates the expected value, $k = (u^2 + v^2)^{\frac{1}{2}}$ = magnitude of the frequency vector , u, v are spatial frequencies in x, y directions, $\theta = \tan^{-1}$ u/v = direction of the frequency vector, M = magnetic moment per unit depth, z = the ensemble depth, t = the ensemble thickness, s = factor for the horizontal dimension of the ensemble.

Taking the average of equation 3.6 with respect to θ gives

$$\{E(k)\} = 4\pi^2 M^2 \{\exp(-2zk)\} \{(1-\exp(-kt))^2\} \{S^2(k)\} \quad \ldots \quad 3.7$$

where $\{\exp(-2zk)\}$, $\{(1-\exp(-kt))^2\}$ and $\{S^2(k)\}$ are now the depth factor, depth extent factor and the size factor respectively. The depth factor term is invariably the dominating factor in the power spectrum, such that, if the ensemble blocks are uniformly distributed in the depth range of $z = \bar{z} \pm 0.5\Delta z$ where $\bar{z}$ is the mean depth of burial of the ensemble, then the depth factor can be expressed as (Spector and Grant, 1970):

$$\{\exp(-2zk)\} = \exp(-2\bar{z}k)\ \mathrm{Sinh}(2k\Delta z)/4k\Delta z \quad \ldots \quad 3.8$$

Assuming that Δz is less than $0.5\bar{z}$ and that values of k are almost always less than $1/\bar{z}$, conditions which are generally valid in most physical situations, Spector and Grant (1970) showed that $\{\exp(-2\bar{z}k)\}$ reduces to $\exp(-2\ \bar{z}k)$. This is the dominant term controlling the spectrum shapes, and the logarithmic plot of the radially averaged power spectrum would give a straight line whose slope is equal to $-2\bar{z}$. The mean depth of burial of the ensemble is thus given by:

$$\bar{z} = -m/_2 \quad \ldots \quad \ldots \quad 3.9$$

where m is the slope of the least square line. Equation 3.9 is the basic equation for the slope - depth relation for power spectrum analysis, and can be applied directly

if the frequency unit is in radians per kilometer. If however the frequency unit is in cycles per kilometer, the corresponding relation can be expressed as

$$\bar{z} = -m/4\pi \qquad \ldots \qquad \ldots \qquad 3.10$$

3.6 Spectral Prediction of Source Depths from theoretical Models.

The spectral methods of geodata processing and analysis have been shown to provide a rapid and elegant tool for source depth prediction in gravity and magnetics (Naidu, 1969, 1970b; Treitel et al. 1971; Curtis and Jain, 1975; Pal et al. 1978; Negi et al., 1983; Connard et al., 1983; Fairhead and Okereke, 1986). For the purpose of this study a theoretical example is presented here to test the reliability of the various procedures employed in this study and hence demonstrate the efficacy of the spectral approach. The magnetic data used in this test example was derived theoretically from a computer simulation of the magnetic anomalies caused by simple two-dimensional models representing common geological forms.

Two simple models consisting of a single layer structure and a combination of regular step

structure were used (Figures 3.5 and 3.6). The single layer structure is located at a uniform depth of 500m, and the step structure has two depth levels located at 500m and 800m below the surface. The anomaly patterns of these type structures are shaped very largely by their depths and volumes, and also by the directions of their magnetization and the susceptibility contrasts.

By applying the FFT methods, a two-dimensional energy spectrum of the total magnetic field intensity anomaly over the single layer structure and the step structure was computed and analysed for source depth prediction. Figures 3.7 and 3.8 present the spectral plots for the single layer model and the step model respectively. The straight line segments on the plots were fitted by least squares. As indicated on the spectral plots the estimated depth for the single layer structure is 490m, and depths to the two disturbing interfaces of the step structure are 820m and 470m respectively. The true depths in both cases are shown in brackets.

The results of the model studies show that the depths to the top of the disturbing interfaces can indeed be estimated from the spectral analysis of the total magnetic field data in map form within a resolution limit of $\pm$ 5%.

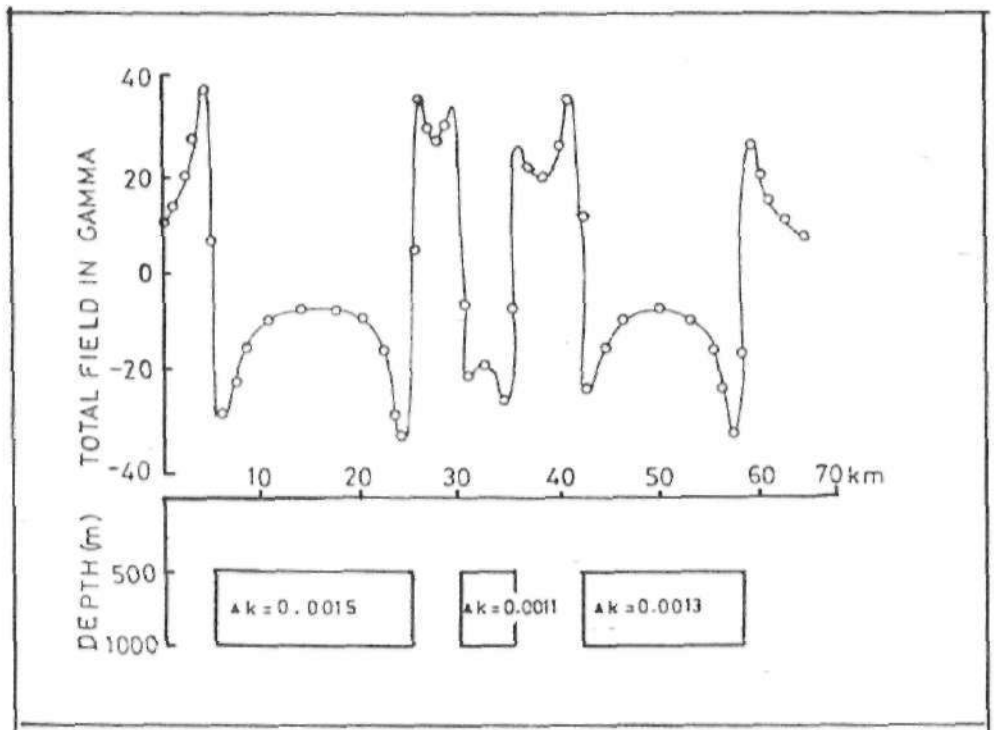


FIG.3.5 : SINGLE LAYER MODEL

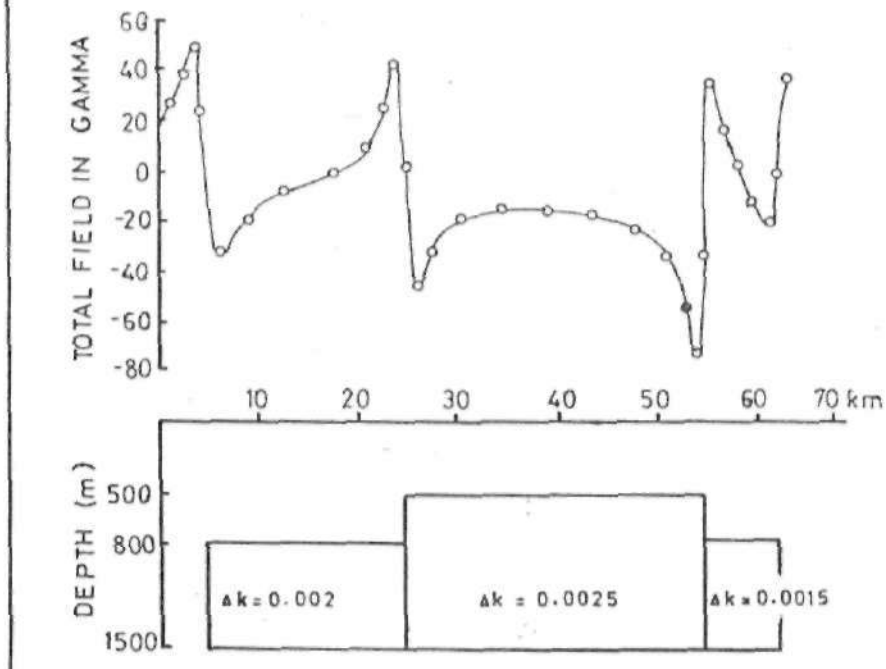


FIG.3.6 REGULAR STEP MODEL

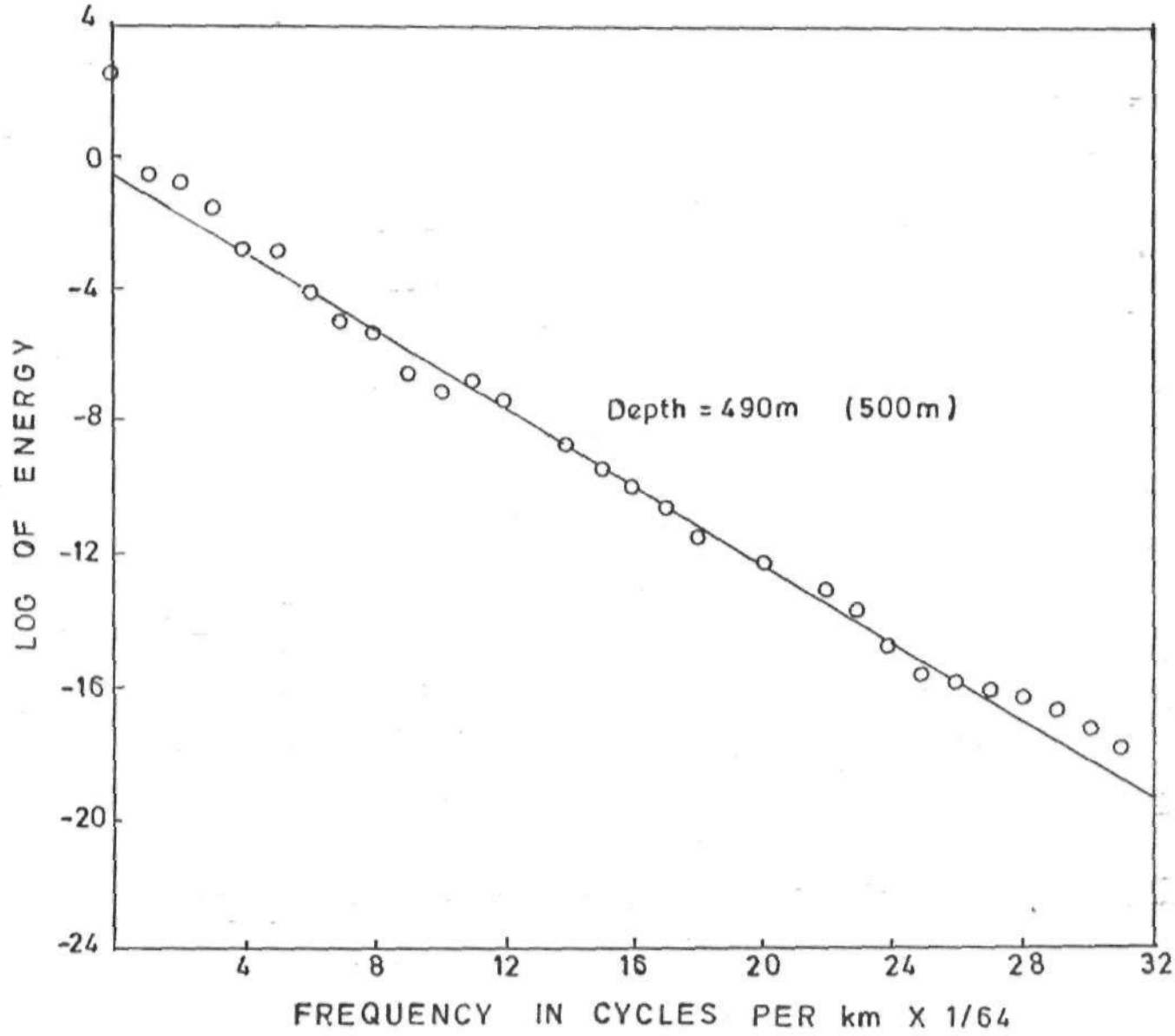


FIG. 3.7 : POWER SPECTRUM ANALYSIS FOR THE SINGLE LAYER MODEL

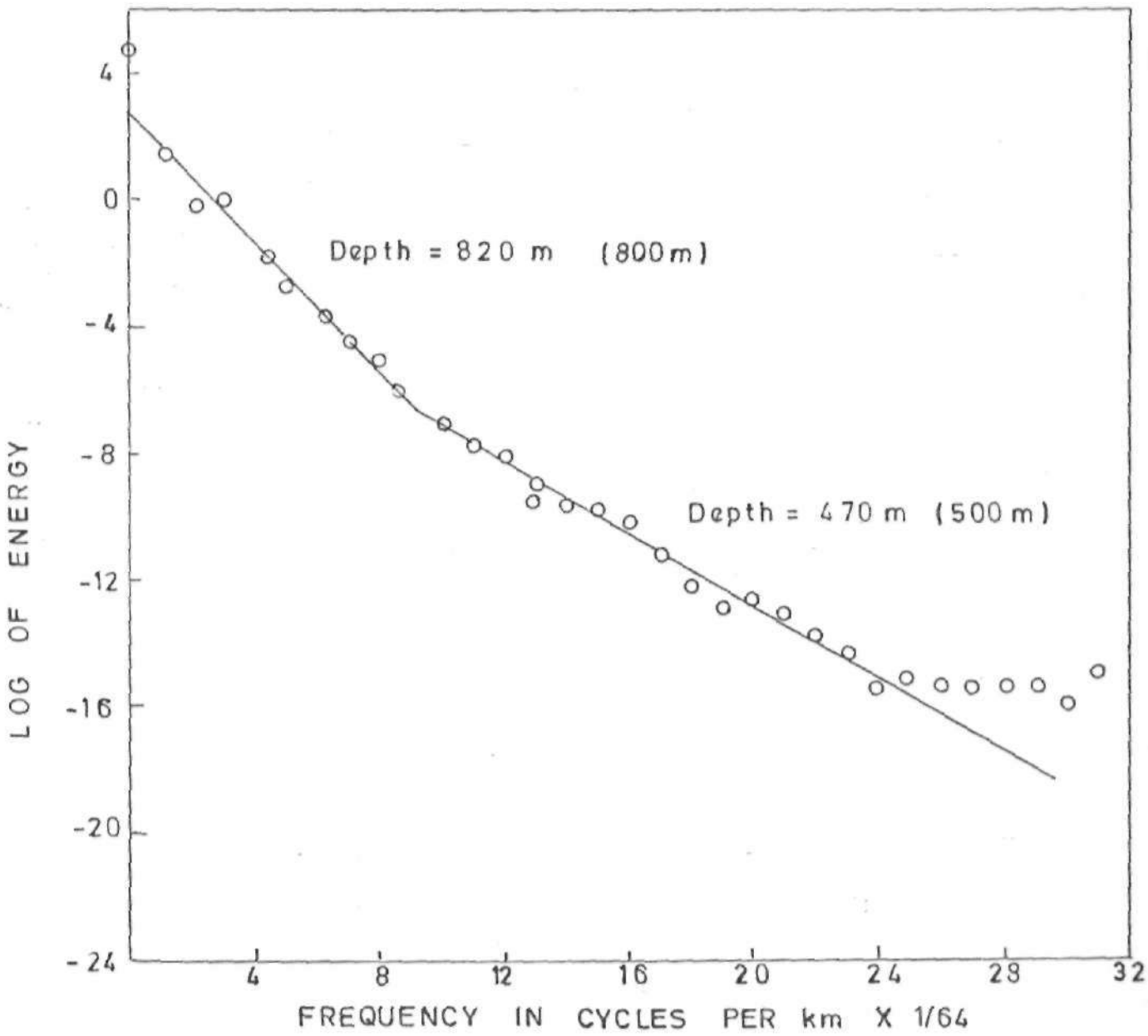


FIG.3·8:POWER SPECTRUM ANALYSIS FOR THE REGULAR STEP MODEL

CHAPTER 4

GENERAL DESCRIPTION AND QUALITATIVE INTERPRETATION OF THE FIELD ANOMALIES

4.1 Description of the anomalies and discussion of trends

The primary data used in the present study were in the form of aeromagnetic maps. Thirty-six 1: 100,000 aeromagnetic maps published in half-degree sheets were re-compiled to produce a master map of the field over the study area (Figure 4.1), with contours of total magnetic field intensities spaced at intervals of 50 gammas. The contour levels are relative to a base of 32,500 gammas.

On the basis of available geological information the study area can in general be divided into two major geological regions: the basement complex and the sedimentary formations. The sedimentary formations occupy all of the study area except the area which lie west of the boundary marked by WW ,east of EE and south of SS (Figure 4.1). These areas lie on the basement complex region. The sedimentary formations constitute the Upper Benue Trough which is part of a linear sedimentary basin that extends from the Niger delta to the Chad basin.

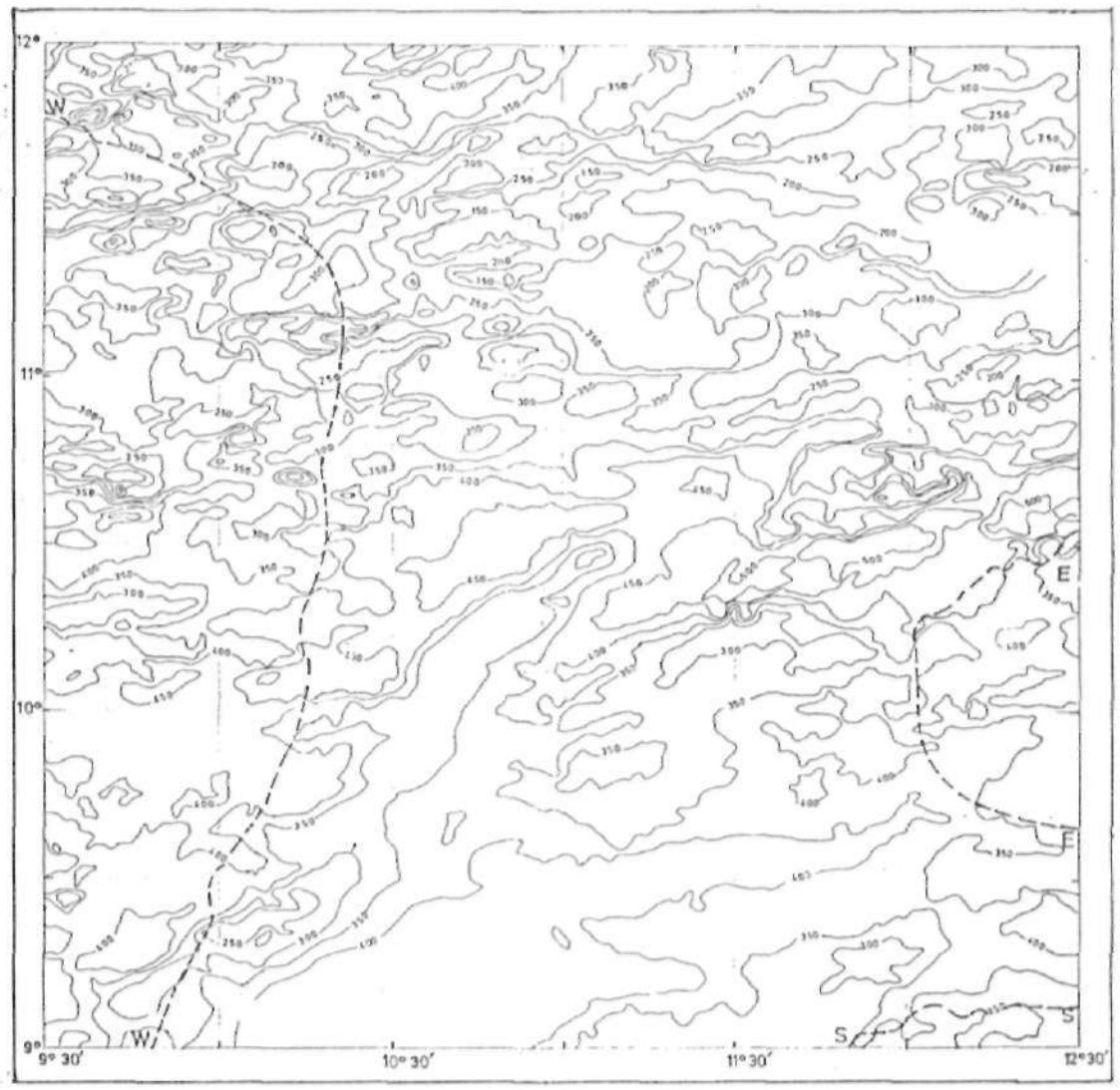


Fig. 4.1 : Total field anomaly map of the study area

The basement areas are distinguished from the sedimentary formations in the pattern of the total magnetic field anomalies in the region. Within the basement complex west of boundary WW and north of parallel 10^{o} 30', the field is characterized by a complicated distribution of high frequency anomalies. This complex pattern of anomalies with a dominant E - W trend continue for some kilometers into the sedimentary basin area NW of the study area. The same system of anomalies also occur in the east central portion of the study area, north of EE. In the western basement area south of parallel 10^{o} 30', the anomalies have a low frequency content and show similar trend as the anomalies of its northern counterpart.

In the southern portion of the trough, and in the area east of EE the most prominent trend of the low frequency anomalies is NE-SW, in contrast to the E-W anomaly trend which dominates in the Northern area and west of WW.

4.2 Correlation of the field anomalies with the spectrum plots

The study area was divided into four blocks of $1\frac{1}{2}^{o}$ x $1\frac{1}{2}^{o}$ map sizes corresponding to the broad

divisions in which the anomaly patterns seen in Figure 4.1 can be subdivided, and the spectrum corresponding to each block was plotted from the computed Fourier amplitudes (Figure 4.2). Since our interest lies in the variation of the shape of the spectrum from block to block, we have plotted only some selected sample values which occur mainly within the high frequency region of the spectrum matrix of the respective blocks. Sample values within the low frequency region in all blocks have been ignored since they show too little variations to be of any interpretational value.

The shape of the spectrum is very sensitive to the anomaly pattern particularly whenever the anomalies display some preferred orientations. Definite anomaly trends frequently have a powerful effect on the general direction and length of any of the axes of the roughly circular or elliptical spectrum. In Figure 4.2, the spectrum of block 1 is elongated in the N-S direction and this immediately suggests that the high frequency content in the region is concentrated in this direction. This also implies that the area corresponding to this block on the aeromagnetic map has its major structural trend predominantly in the E-W direction.

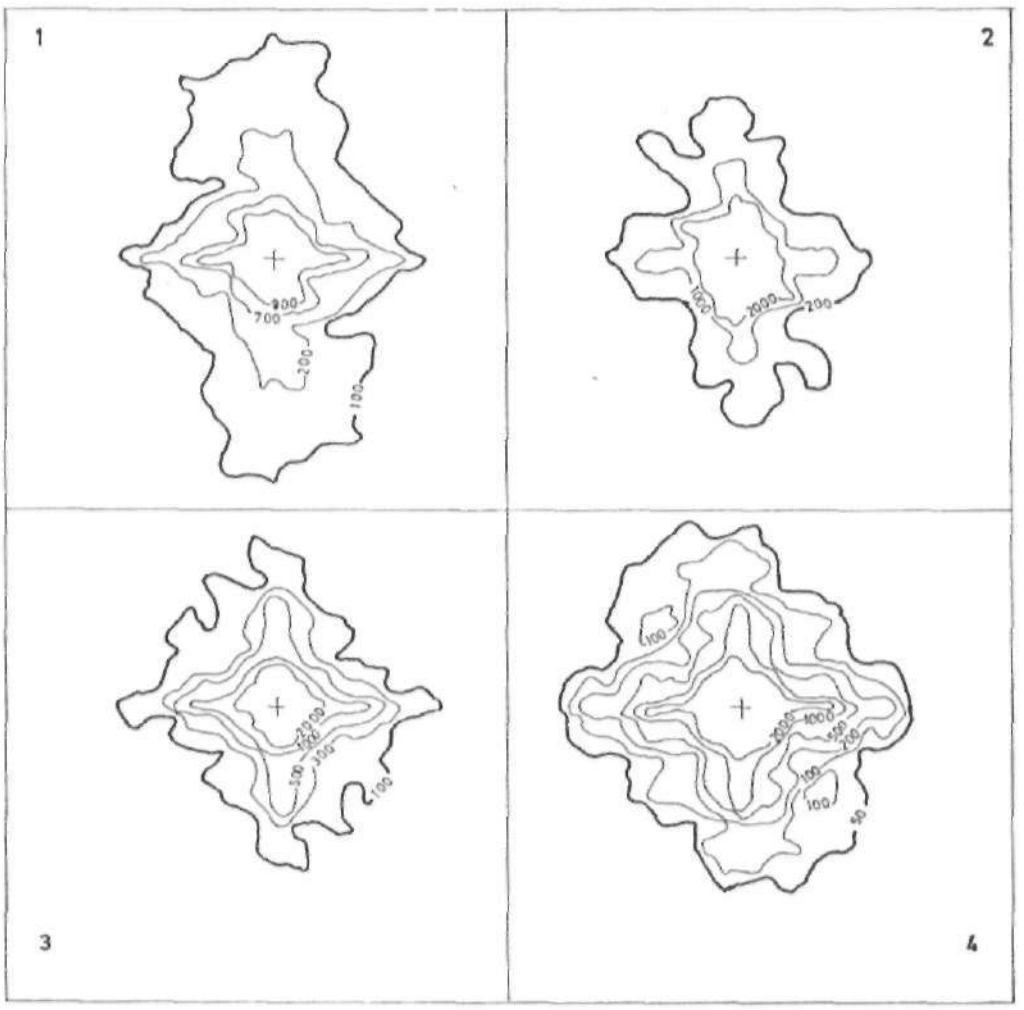


FIG. 4-2: SPECTRUM PLOTS FOR $1\frac{1}{2}^{\circ} \times 1\frac{1}{2}^{\circ}$ MAP SIZES

There is also one preferred N-S direction of strike in the shape of the spectrum of the second block. Although this has a somewhat shorter axial length in the N-S direction than for the first block it still correlates reasonably well with the E-W anomaly trends occuring within the same region on the anomaly map.

The spectrum for blocks 3 and 4 are approximately symmetrical in the four directions and do not in particular show any preferred direction although on the anomaly map, the structural trends in the adjacent regions of both blocks tend to be mainly in a general NE-SW direction with long wavelength anomalies dominating. On the west of block 3 and east of block 4 the trend is mainly E-W. Hence the mixed anomaly patterns in both blocks is consistent with the irregular spectrum shape of block 3 and the roughly circular shape of the spectrum of block 4. It is evident therefore that the major structures in this region do not exhibit any definite trend or preferred orientation.

4.3 Correlation of the Magnetic anomalies with Surface Geological Information.

For the purpose of geological and geophysical correlation in the study area, the total field anomaly map (Figure 4.1) was superimposed on the surface geological map of the area. It should be recalled that the total field anomaly map was compiled from a digitized data sampled on a 3km square grid . The implication of this sampling interval is that the narrowest feature that can be accurately defined by this map has a width of about 6km. On the other hand some of the geological boundaries on the geology map of the study area are only approximate. Therefore correlation between the two maps may be marginally affected by these limitations.

However the combined map (Figure 4.3) shows that some of the prominent features of the field anomalies correlate fairly well with the surface geological information. In general, two distinct zones are recognizable in the pattern of the observed anomalies in the study area, and these correspond to regions of exposed outcrops, and the central portion of the trough extending from the southern part through Kaltungo to a few kilometers beyoned Gombe. The main concentration of the

Fig. 4.3 : Combined geology and total field anomaly map



LEGEND

QUATERNARY		ALLUVIUM SANDS AND CLAYS
TERTIARY		BASALTS GRITS, SANDS AND CLAYS
CRETACEOUS		CLAY, SHALE, COAL, SANDSTONES, LIMESTONE
JURASSIC		GRANITE SYENITES AND GABBRO
PRE-CAMBRIAN TO UPPER CAMBRIAN		OLDER GRANITES UNDIFFERENTIATED BASEMENT COMPLEX

exposed outcrops of the older granite suite lies in the basement complex west of WW, and further north are some outcrops of younger granite bodies. Major outcrops of basement rocks also occur at Kaltungo and in the northern and south-western flanks of Biu basalts. Intense magnetic anomalies with a dominant E-W trend are concentrated in these regions of exposed outcrops from Bauchi through Azare to Potiskum, and in the area surrounding Biu. Since there are only a few outcrops in the region enclosing Azare, Lanzai and Potiskum the anomalies observed in this area are largely due to extensive igneous intrusions buried at relatively shallow depths within the sediments or possibly to the presence of shallow basement rocks.

The remainder of the sedimentary region between Bashar and Yola in the Southern part of the area, and up to the central region is characterized with anomalies of amplitudes varying between 250 and 450 gammas which are relatively regular in shape and with very gentle field gradients. These anomalies with very smooth contours trend in a general NE-SW direction and may be attributed to deep lying basement corresponding to thick cretaceous sediments.

In general, the form of the magnetic contours in the study area have given some insight regarding the structural trends in the basement. Evidently the basement in the northern half of the study area is shallower than in the southern half and is believed to slope in a general NW-SE direction. This implies that the deepest parts of the sedimentary basin may occur within the area enclosed by Muri, Gombe and Yola.

CHAPTER 5

POWER SPECTRUM ANALYSIS AND INTERPRETATION

5.1 Map Sizes and Target Depths

The use of a finite data window in either one- or two-dimensional spectral analysis is practically inevitable. Since we must always work with data of finite length or area, the target depths of interest almost invariably contribute to determine the size of map or the data length to be used in the analysis. Apart from a certain improvement in the resolution of the spectral estimates, the importance of analysing a large map lies in the fact that we can conveniently investigate deeper magnetic sources, possibly down to the Curie surface (Naidu, 1970b). For nearly all practical purposes, Naidu (1970b) considers the minimum map size to be of the order of 40 to 50 times the target depth. Using this relation as a rough guide and bearing in mind the expected maximum sedimentary thickness in the Upper Benue Valley from previous studies, three map windows were chosen and successively analysed in increasing order of map area. The objective of this approach is to carry out progressive investigation of the deeper magnetic interfaces. The map

windows are made up of:

(i) 36 blocks of $\frac{1}{2}^{o}$ x $\frac{1}{2}^{o}$ map sizes.

(ii) 9 blocks of 1^{o} x 1^{o} map sizes.

(iii) 4 blocks of $1\frac{1}{2}^{o}$ x $1\frac{1}{2}^{o}$ map sizes.

Provided there are no restrictions on either the size of the map or capacity of the computer available for use, it is possible to determine magnetic depths to the top or bottom of any lithologic interface.

5.2 Spectral Magnetic Depth Determinations

The depth results estimated from the spectral plots of each block of the three map windows investigated, and the one-dimensional North-South profile are presented in this section. The depth information obtained in all the cases are deliberately presented separately for each data window.

It should also be recalled that the aeromagnetic data was collected along flight lines spaced at 2km intervals from a survey altitude of approximately 150m above the terrain. Therefore all the depth information obtained from the spectral plots are referred to this observation level.

In order to reduce the spectral depths to the ground surface, which is our datum surface, the mean survey altitude was subtracted from the depth estimates obtained from the spectral analysis.

As discussed in sections 3.4 and 3.5, magnetic spectral depths are estimated from the slope of the least square line fitted to the power spectral plots. The inevitable presence of residual errors in the computed power spectra directly implies that numerical results derived from the slopes of the fitted lines are invariably subject to some degree of error or uncertainty. It is therefore important to assess the effect of such errors on the spectral depth estimates. Consequently an estimate of the standard errors in the depth values for the one- and two-dimensional spectral analysis, caused by errors in the slope, was carefully made. It was found that the depth estimates are accurate to within $\pm$ 5% for the one-dimensional spectral analysis, and $\pm$6% for the two-dimensional spectral analysis. It is important to remark that spectral depths are in general average depths, and individual depth estimates may have values which differ significantly from these depths.

5.2.1 Power Spectrum Analysis for $\frac{1}{2}^{o}$ x $\frac{1}{2}^{o}$ Grid.

Figure 5.1 shows the grid locations for the thirty-six blocks of $\frac{1}{2}^{o}$ x $\frac{1}{2}^{o}$ aeromagnetic maps which cover the project area, and Figure 5.2 presents the spectral depth information for each block. The first figure in each block identifies the block number, and the second and third figures refer to the deep and shallow source depths respectively.

The spectral plots for each block (e.g Figure 5.3 - 5.4) shows that the magnetic anomalies resolved by this window originate at two distinct magnetic levels as indicated by the two line segments. While the line segment which corresponds to the low frequency portion of the spectrum relates to the magnetic sources at depth, the segment occupying the high frequency end appear from noise or from shallow ensembles of sources close to the flight level. This phenomenon occurs because the shallower sources generally contibute more to the high wavenumber

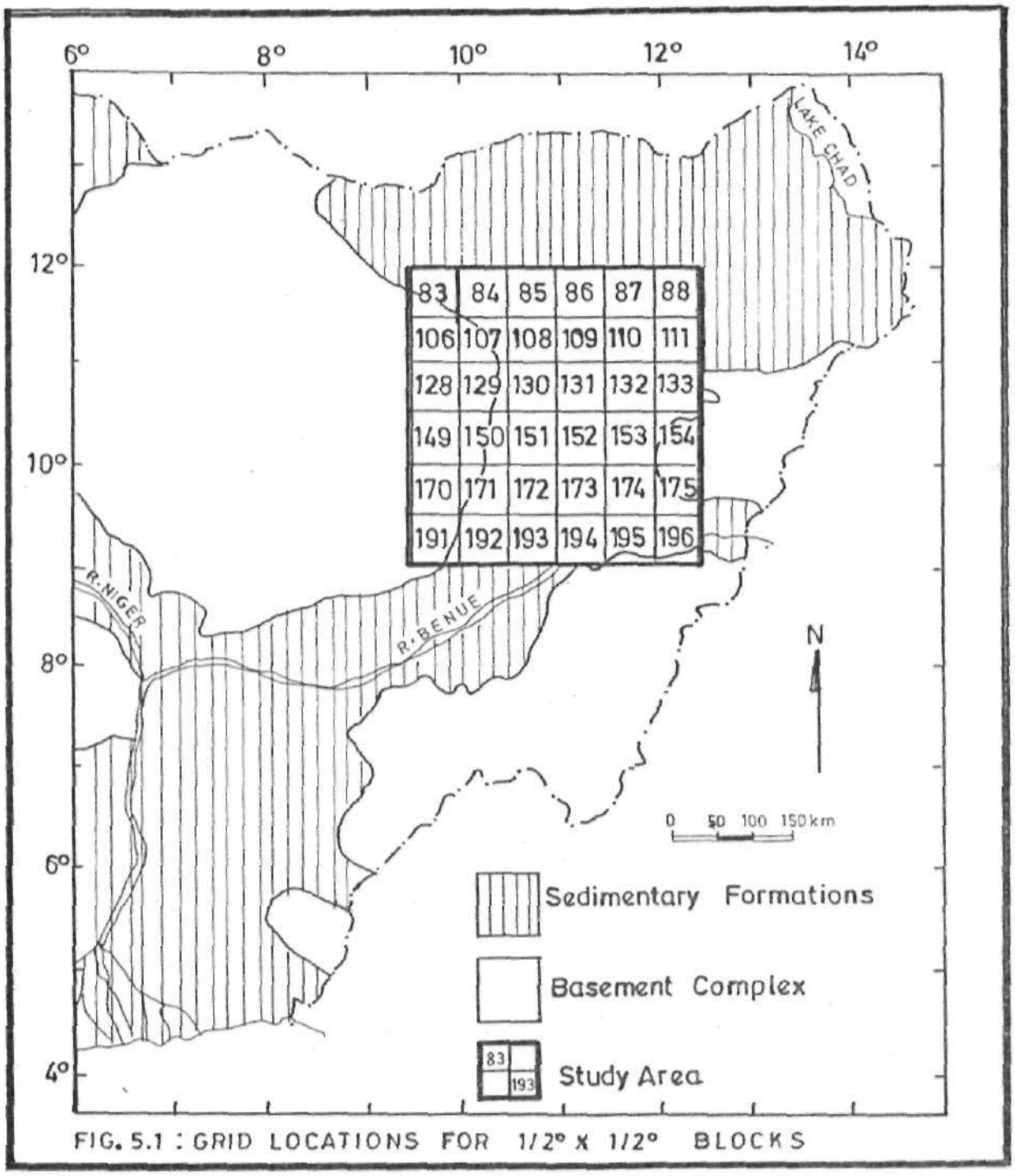


FIG. 5.1 : GRID LOCATIONS FOR 1/2° X 1/2° BLOCKS

83 1·43 0·36	84 2·00 0·17	85 2·04 0·14	86 2·28 0·14	87 2·52 0·26	88 2·21 0·19
106 1·38	107 1·94	108 2·16 0·21	109 2·33 0·46	110 2·16 0·12	111 2·23 0·07
128 1·43	129 2·04 0·09	130 2·43 0·29	131 2·48 0·63	132 2·14 0·26	133 2·23
149 2·04	150 2·26 0·12	151 2·38 0·17	152 2·55 0·29	153 2·26 0·04	154 2·35 0·12
170 2·45	171 2·45 0·07	172 2·60 0·09	173 2·43 0·43	174 2·38	175 2·50 0·07
191 2·06 0·24	192 2·52 0·21	193 2·62 0·12	194 2·62 0·17	195 2·45 0·17	196 2·48 0·48

FIG.5.2 ; SPECTRAL DEPTHS FOR 1/2° x 1/2° BLOCKS

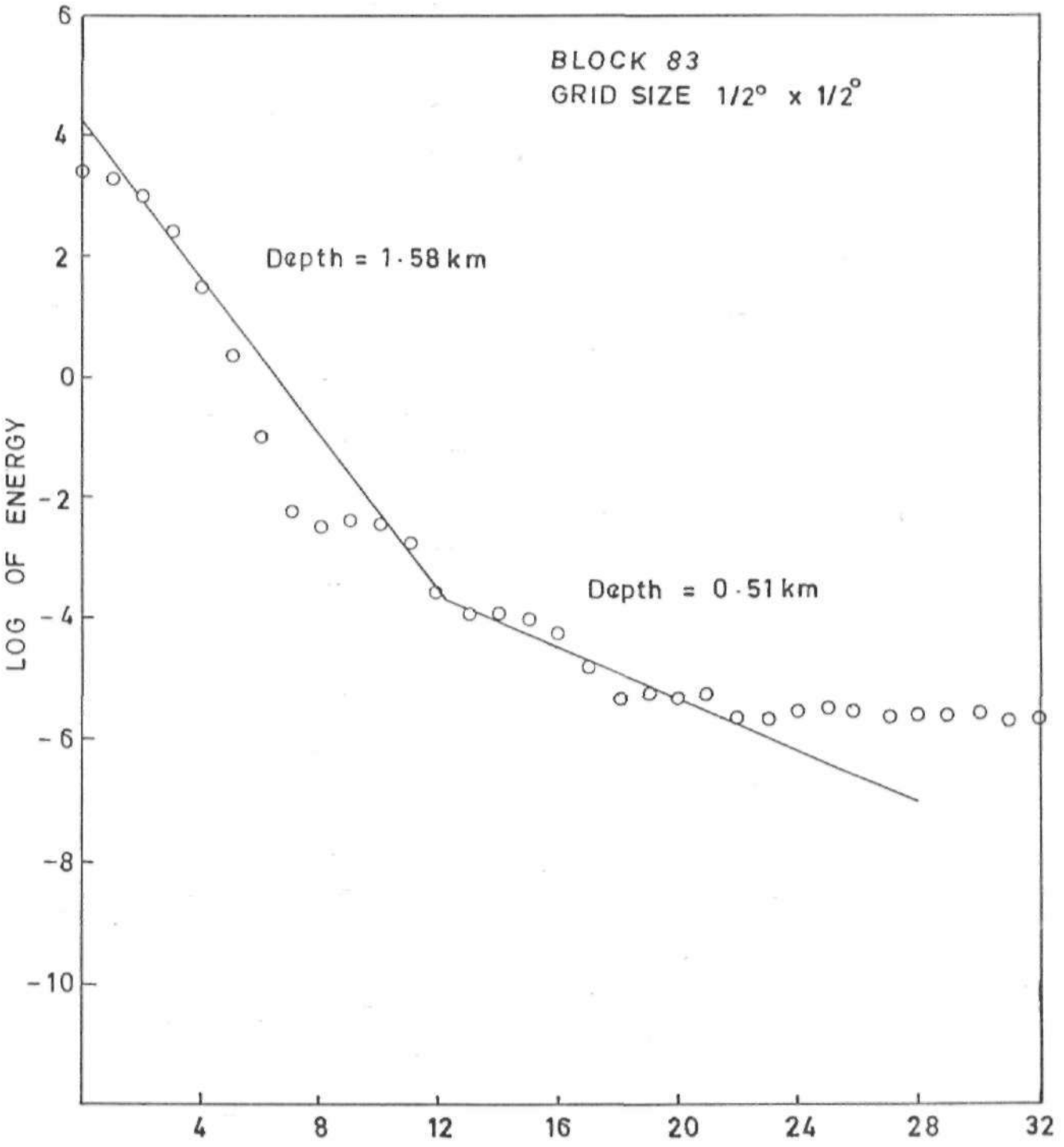


FIG. 5.3 : POWER SPECTRUM ANALYSIS FOR BLOCK 83

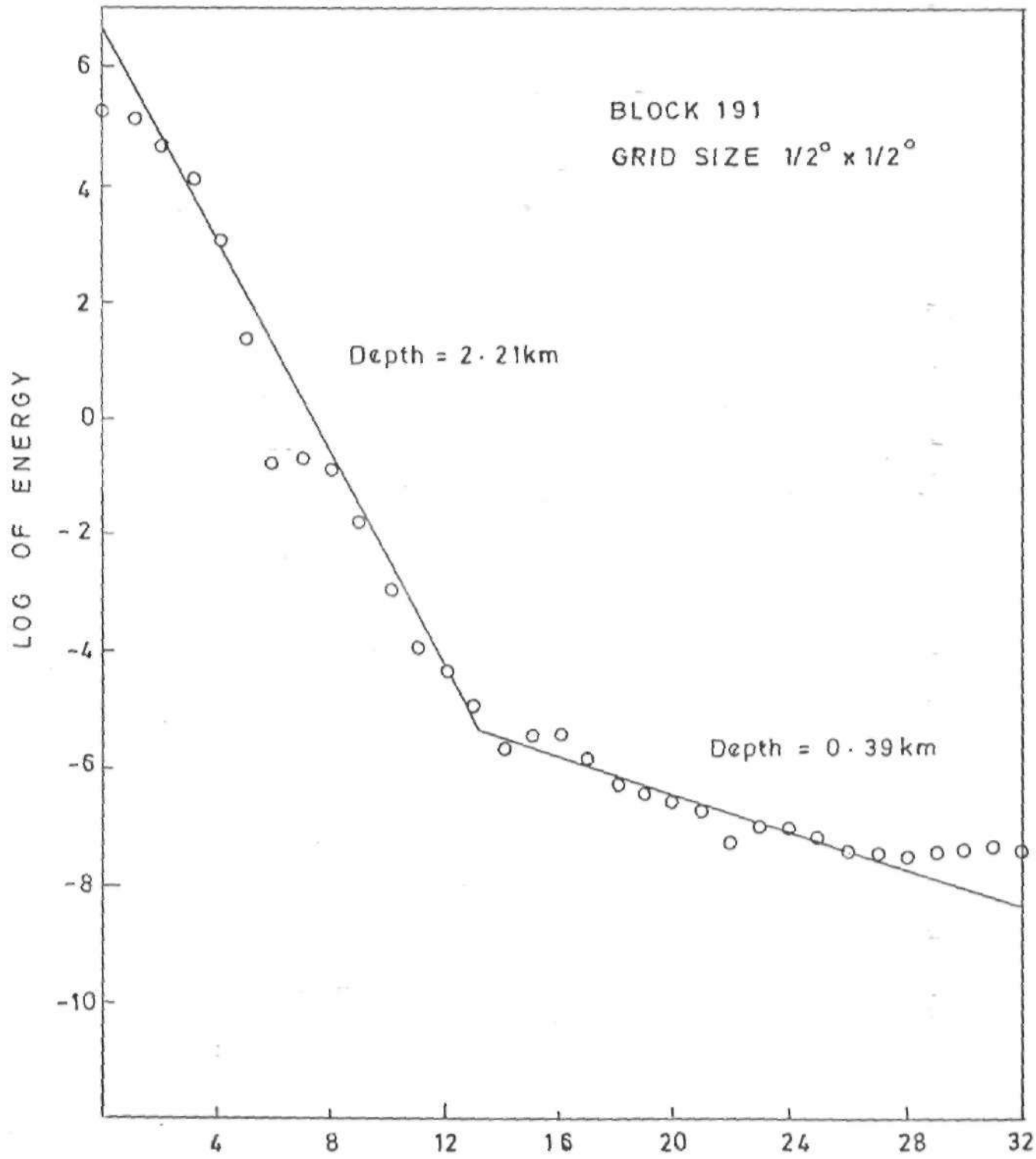


FIG. 5.4 : POWER SPECTRUM ANALYSIS FOR BLOCK 191

components than the deeper sources do. One difficulty with this is that the higher wavenumber components tend towards increasingly smaller magnitudes and hence become harder to estimate accurately. Spectral magnetic depths determined from the low frequency region are therefore more reliable than spectral depths made from the high frequency portion of the spectrum. It would be observed that the low frequency portion of all the spectra computed for this window show unexpected roughness (see also Appendix A). This complication in the spectra may be attributed to the fact that the majority of sources in the area appear to be depth limited primarily because of the size of the map window investigated. This fact has been verified aposteriori and subsequently confirmed by using larger map sizes. The spectra computed from $1^{o} \times 1^{o}$ and $1\frac{1}{2}^{o} \times 1\frac{1}{2}^{o}$ grids show significant improvement and are certainly much better behaved than the spectra for $\frac{1}{2}^{o} \times \frac{1}{2}^{o}$ grid. It is therefore possible that the uneveness in the spectra for this grid size may marginally affect the depth information obtained from the spectral plots.

It should be observed from Figures 5.1 and 5.2 that blocks 106, 128, 149 and 170 lie entirely on the basement complex. The power spectral plots for these blocks (Figure 5.5 - 5.8) show that the high frequency end of the spectra for each block

is dominated by near-surface contribution due to the shallow basement. The spectral depths corresponding to the first segment in the low frequency region for each of these blocks may therefore relate to magnetic sources lying within the basement. It may also be observed that blocks 83, 107, 129, 150, 154, 171, 175, 191, 195 and 196 (Figure 5.2) contain significant parts of more than one geologic province such that portions of these blocks lie in the basement region and in the sedimentary formations as outlined by the location of the infered basement - Cretaceous boundary in these areas. The geologic and physiographic complexity of these areas may perhaps affect the spectral depth determinations for these blocks. However it is doubted if this problem is serious in the present case because of the generally good continuity between the depth values for these blocks and the neighbouring blocks. A comparison of the deep source depths for blocks 83 and 84, 107 and 108, 129 and 130, 150 and 151, 171 and 172, and 191 and 192 (Figure 5.2) reveals a general increase in the source depths from those blocks sharing two geological provinces to their immediate eastern neighbours lying entirely on the sediments. The spectral depths estimated from the first segments for these blocks most probably refer to the basements in these localities.

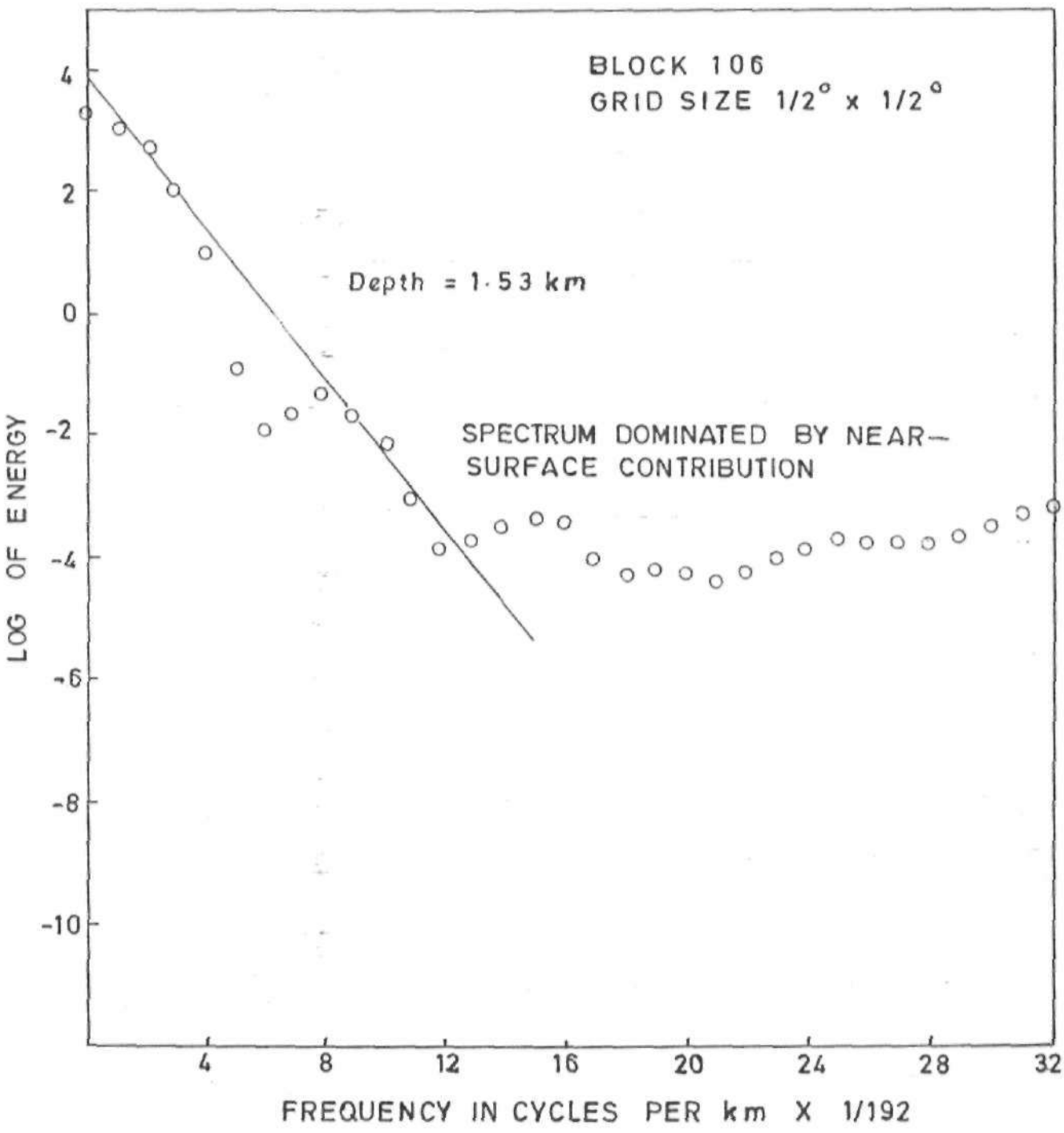


FIG. 5. 5: POWER SPECTRUM ANALYSIS FOR BLOCK 106

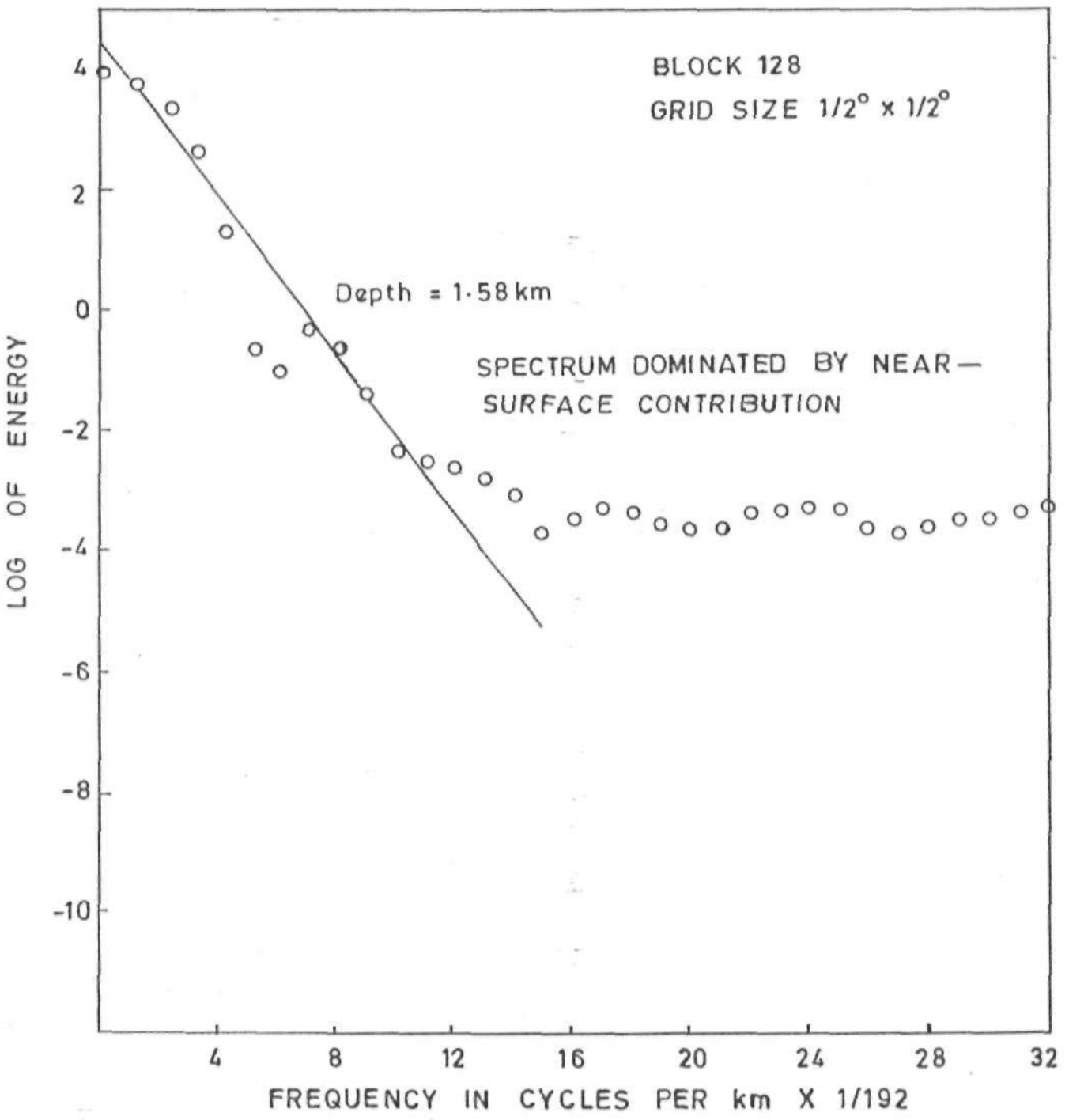


FIG.5.6:POWER SPECTRUM ANALYSIS FOR BLOCK 128

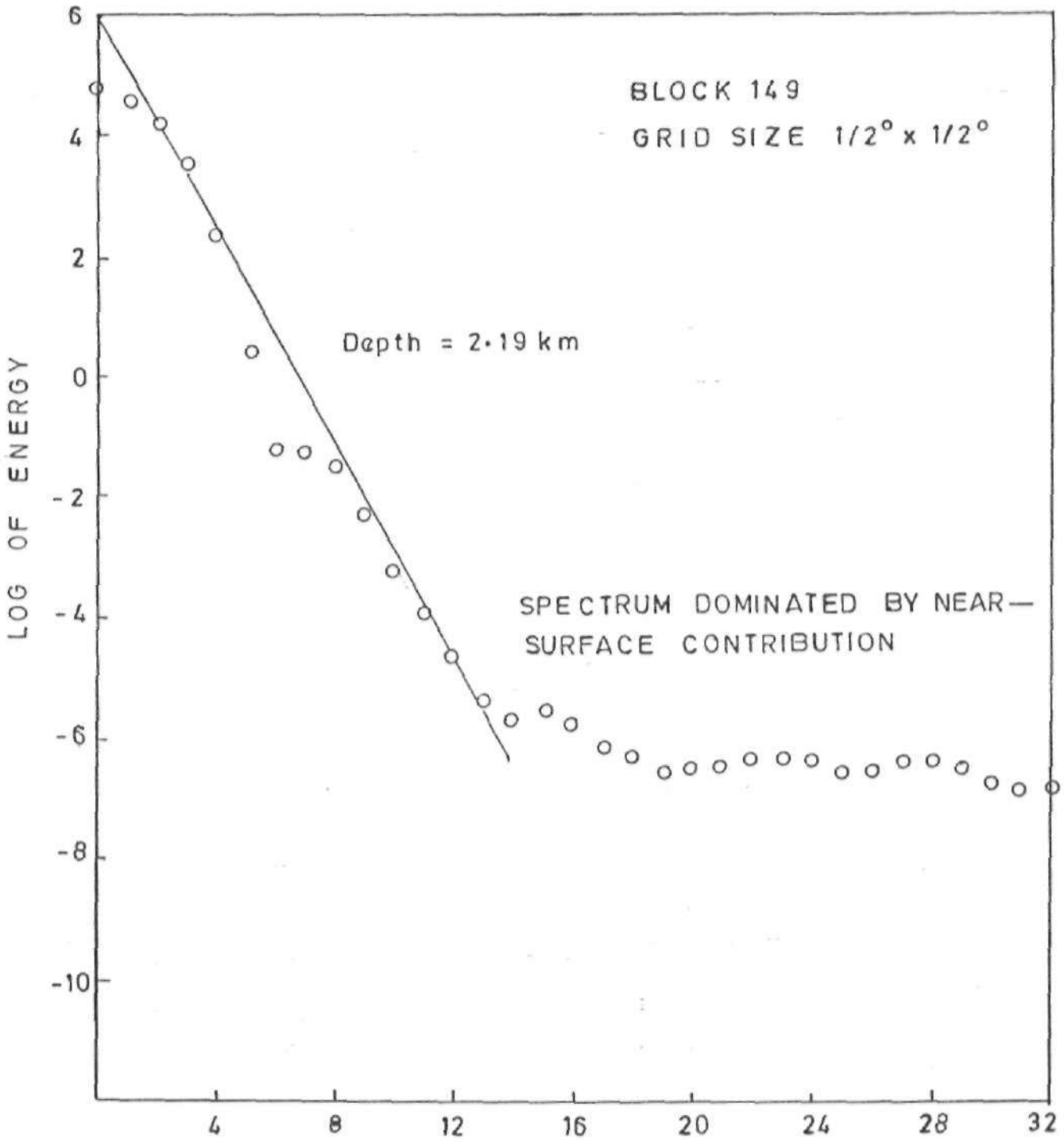


FIG. 5.7: POWER SPECTRUM ANALYSIS FOR BLOCK 149

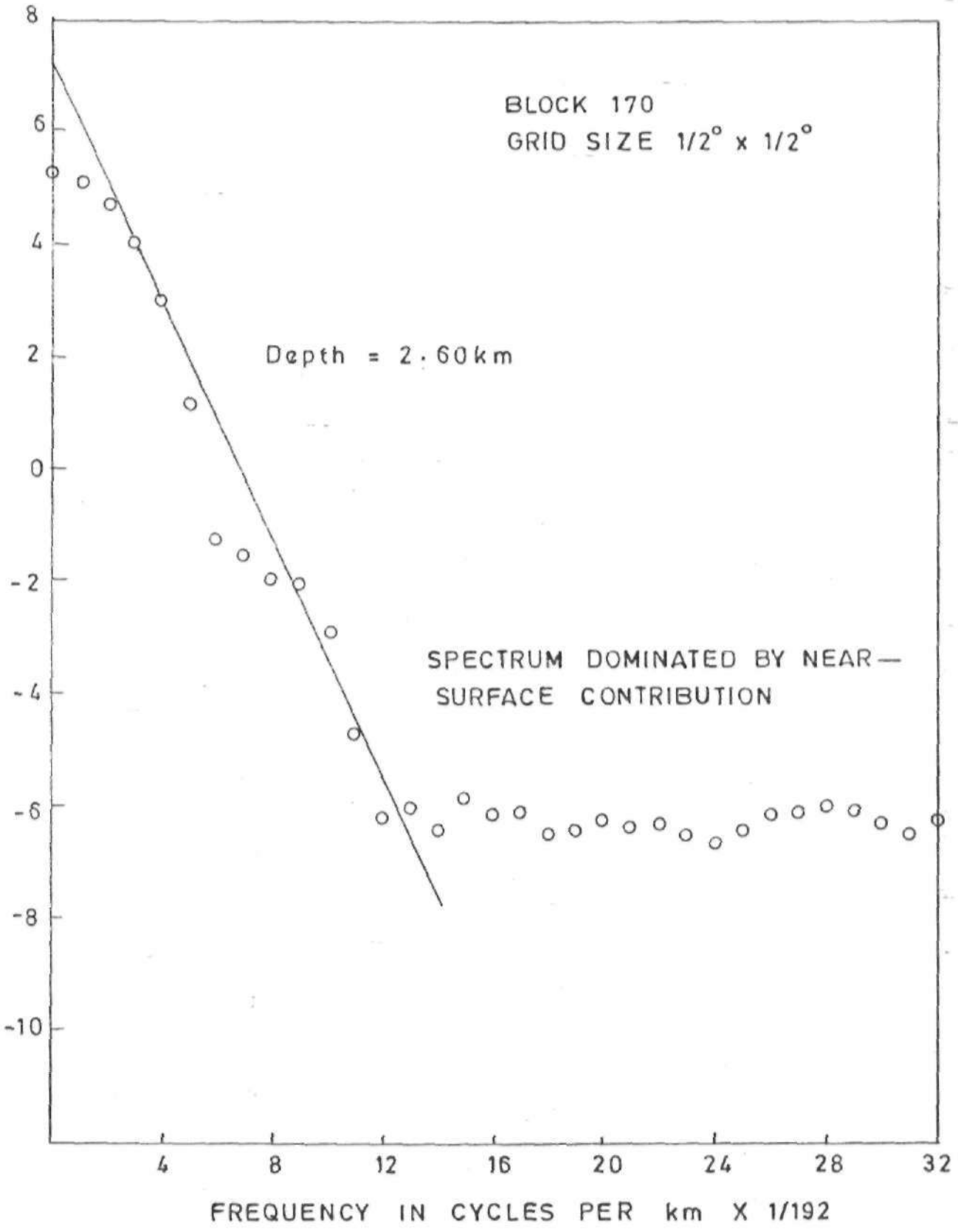


FIG. 5.8: POWER SPECTRUM ANALYSIS FOR BLOCK 170

The high frequency portion of the spectral plots for blocks 107, 133 and 174 (Figure 5.9 - 5.11) show that the magnetic sources in these areas may be attributed to shallow magnetic rocks on or near the surface. Surface geological information show that extensive outcrops of highly magnetic younger granite suites cover considerable portions of block 107, and this may have given rise to the shape of the spectrum for this block. The recent basaltic flows in Biu and Longuda also may have contributed significantly to the high frequency portion of the spectra for blocks 133 and 174, and this affected the spectra of these blocks in the same manner.

Depth results from the remaining blocks show that the mean depths to the basement in the study area show a gentle general southward increase with mean values ranging from 2.25km in the northern area to 2.50km in the south. Mean depths to shallow sources in the region vary between 0.12 and 0.63km and may in general be attributed to shallow intrusions or near-surface basement rocks. The shallower depths below 0.12km are assoicated with noise or with the surface conditions due to irregular topographic relief. The spectral plots for the remaining blocks are presented in Appendix A.

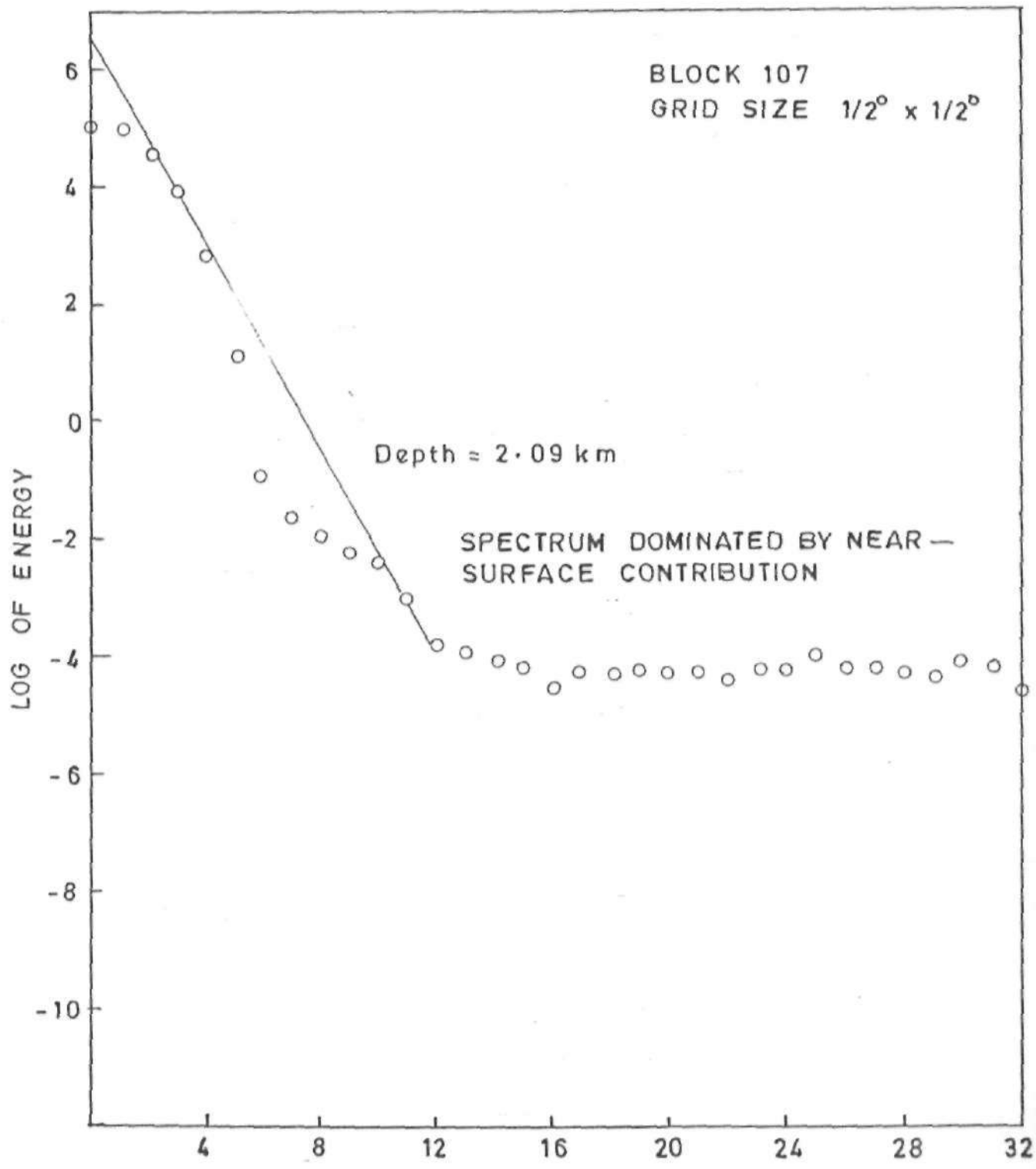


FIG. 5.9 : POWER SPECTRUM ANALYSIS FOR BLOCK 107

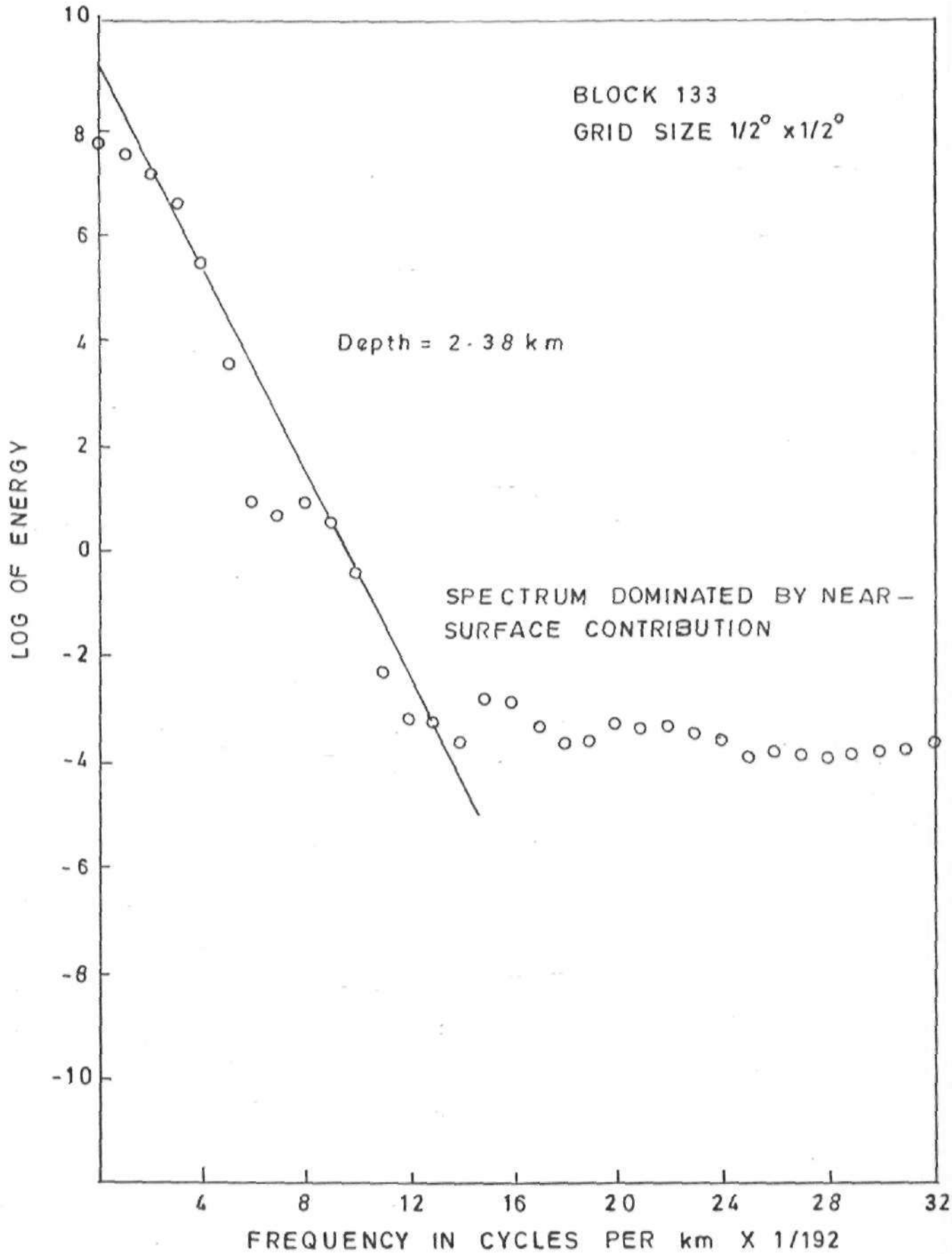


FIG. 5·10 : POWER SPECTRUM ANALYSIS FOR BLOCK 133

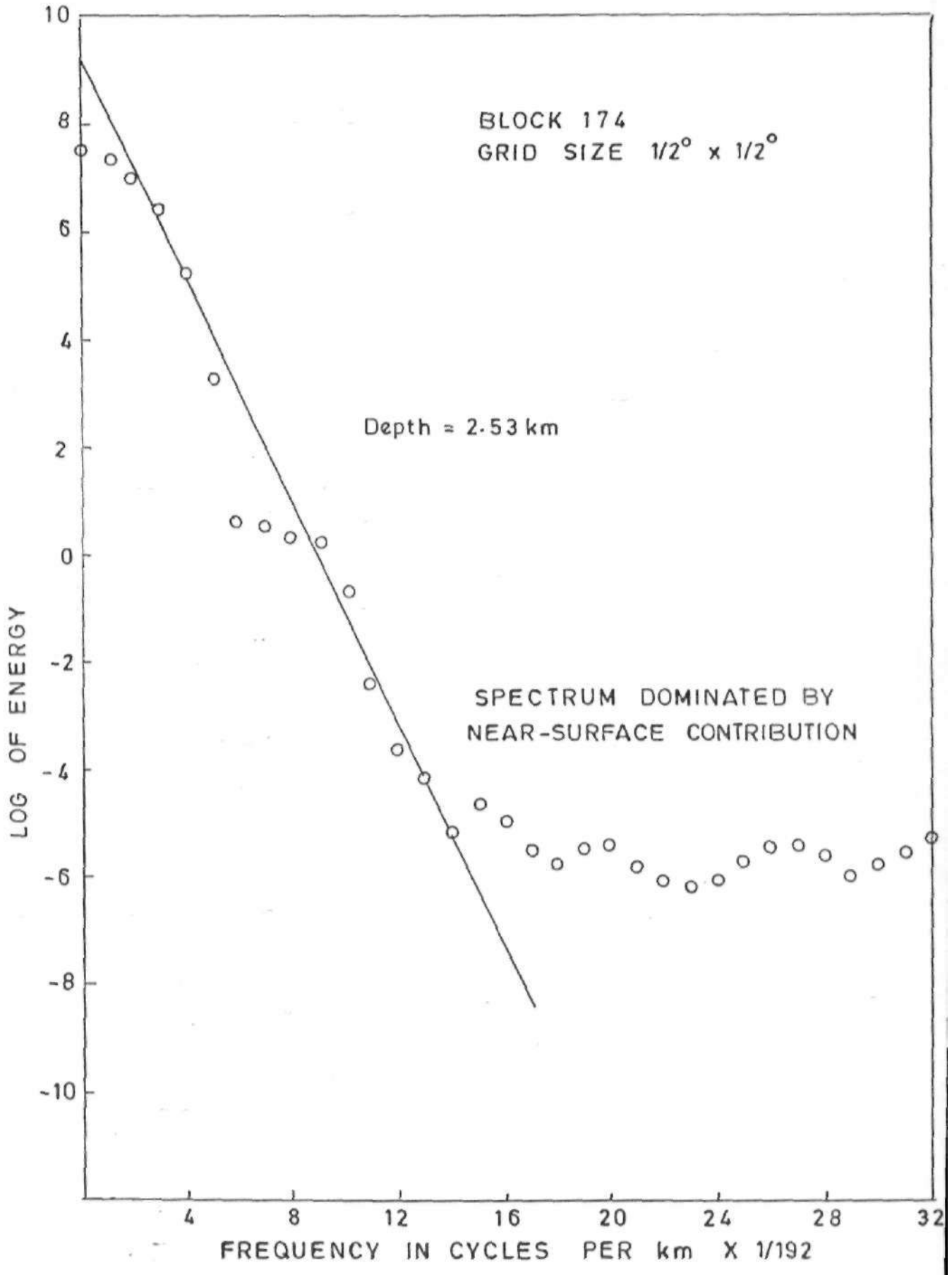


FIG.5.11: POWER SPECTRUM ANALYSIS FOR BLOCK 174

5.2.2 Power Spectrum Analysis for 1^{o} x 1^{o} Grid.

Figure 5.12 shows the grid locations and the spectral depth estimates for the 9 blocks of 1^{o} x 1^{o} map size, and Figures 5.13 - 5.16 present the log-power spectra for selected blocks. The spectral plots show that the deep source depths for all the blocks appear generally slightly higher than the corresponding source depths obtained from the $\frac{1}{2}^{o}$ x $\frac{1}{2}^{o}$ grids. For example, the deep source depth for block 3 of the 1^{o} x 1^{o} grid (Figure 5.12) is 2.76km and the mean depth value for the four corresponding blocks of the $\frac{1}{2}^{o}$ x $\frac{1}{2}^{o}$ grids (Figure 5.2) is 2.30 km. This is not suprising since grids of 1^{o} x 1^{o} map size should be able to resolve even deeper depths more accurately. For this reason, it is believed that the spectral depths for both grids refer to more or less the same magnetic level which corresponds to the surface of the magnetic basement. Support for this assertion can be found in the general southward increase in the estimated depths for the 1^{o} x 1^{o} grid, which is consistent with the trend observed in the $\frac{1}{2}^{o}$ x $\frac{1}{2}^{o}$ blocks. Shallow source depths for the 1^{o} x 1^{o} grid also show similar variations as the corresponding depth values for the $\frac{1}{2}^{o}$ x $\frac{1}{2}^{o}$ grid, and are therefore

1 2·50 0·30	2 2·65 0·09	3 2·76 0·15
4 2·50 0·23	5 2·73 0·19	6 2·71 0·23
7 2·77 0·25	8 2·73 0·09	9 2·83 0·31

FIG. 5.12 : GRID LOCATIONS AND SPECTRAL DEPTHS FOR 1° x 1° BLOCKS

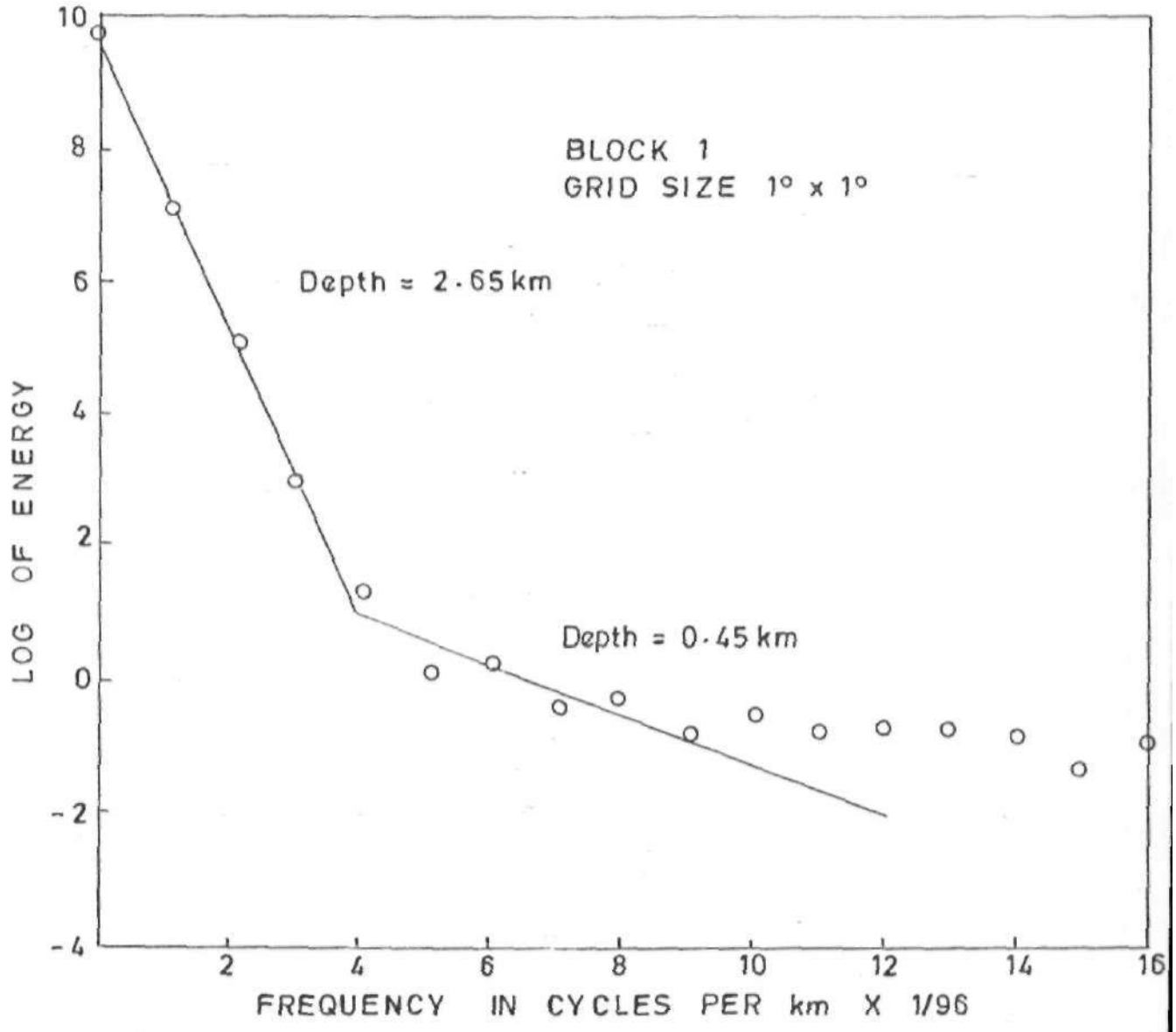


FIG. 5.13 : POWER SPECTRUM ANALYSIS FOR BLOCK 1

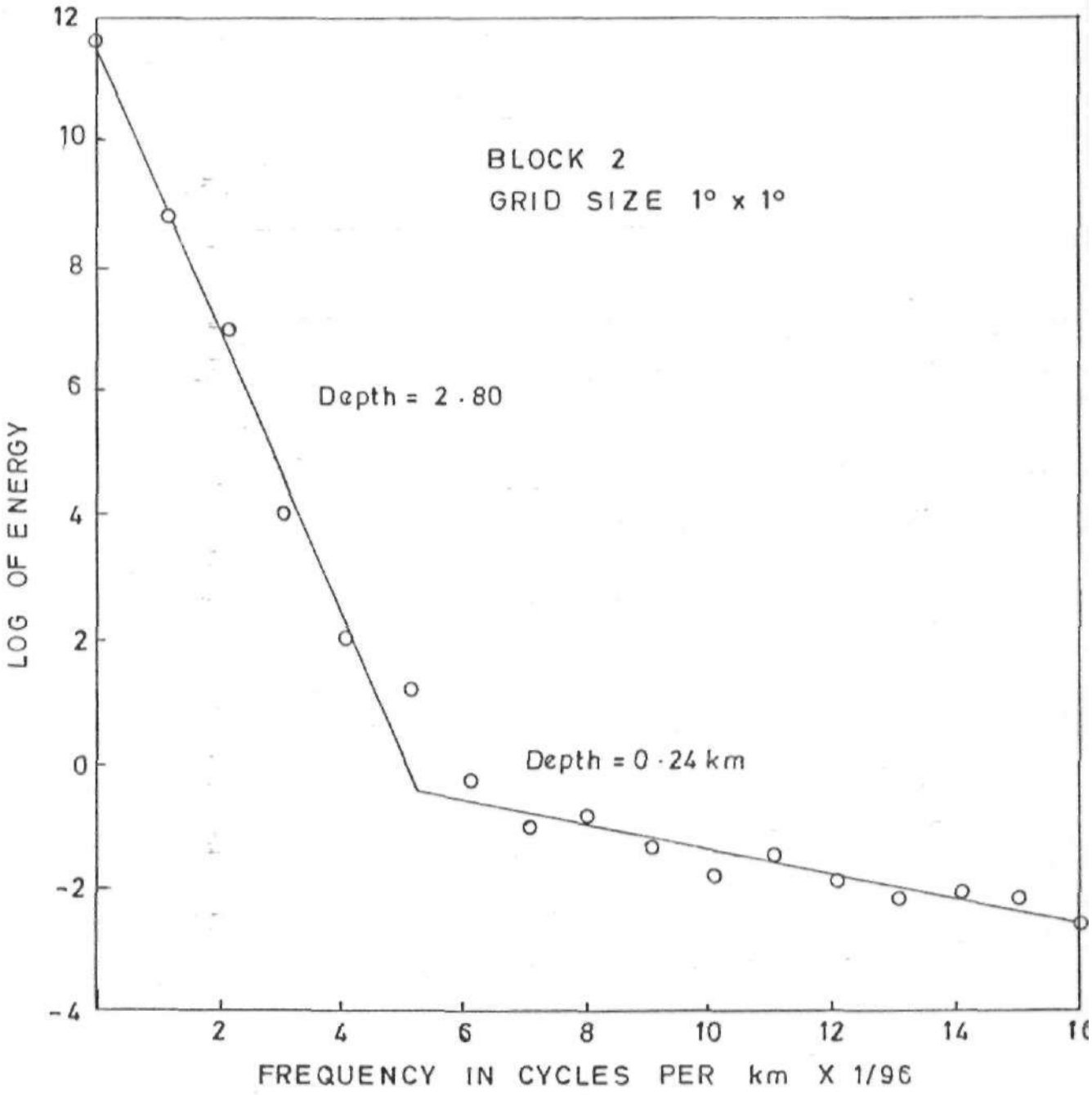


FIG. 5.14 : POWER SPECTRUM ANALYSIS FOR BLOCK 2

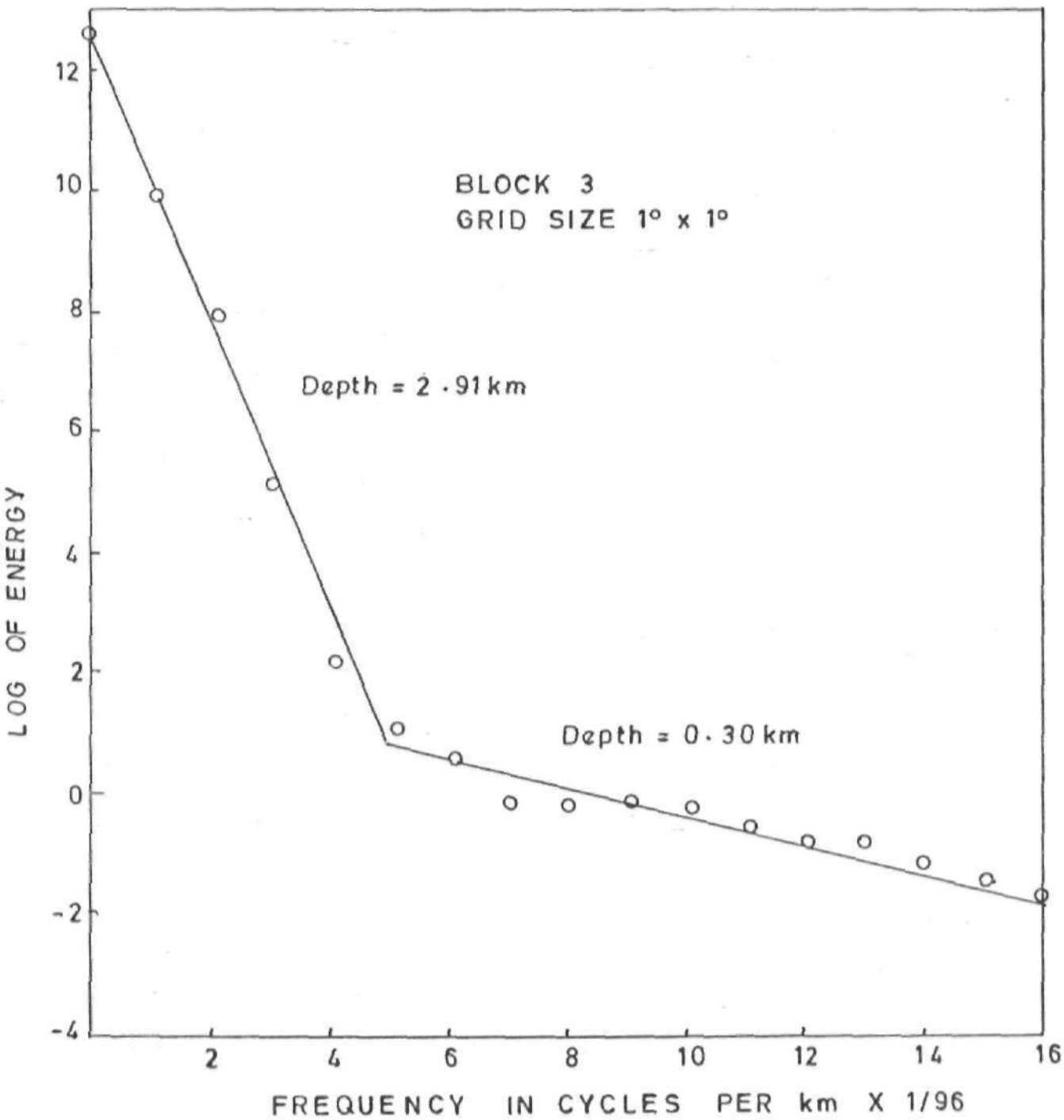


FIG.5.15: POWER SPECTRUM ANALYSIS FOR BLOCK 3

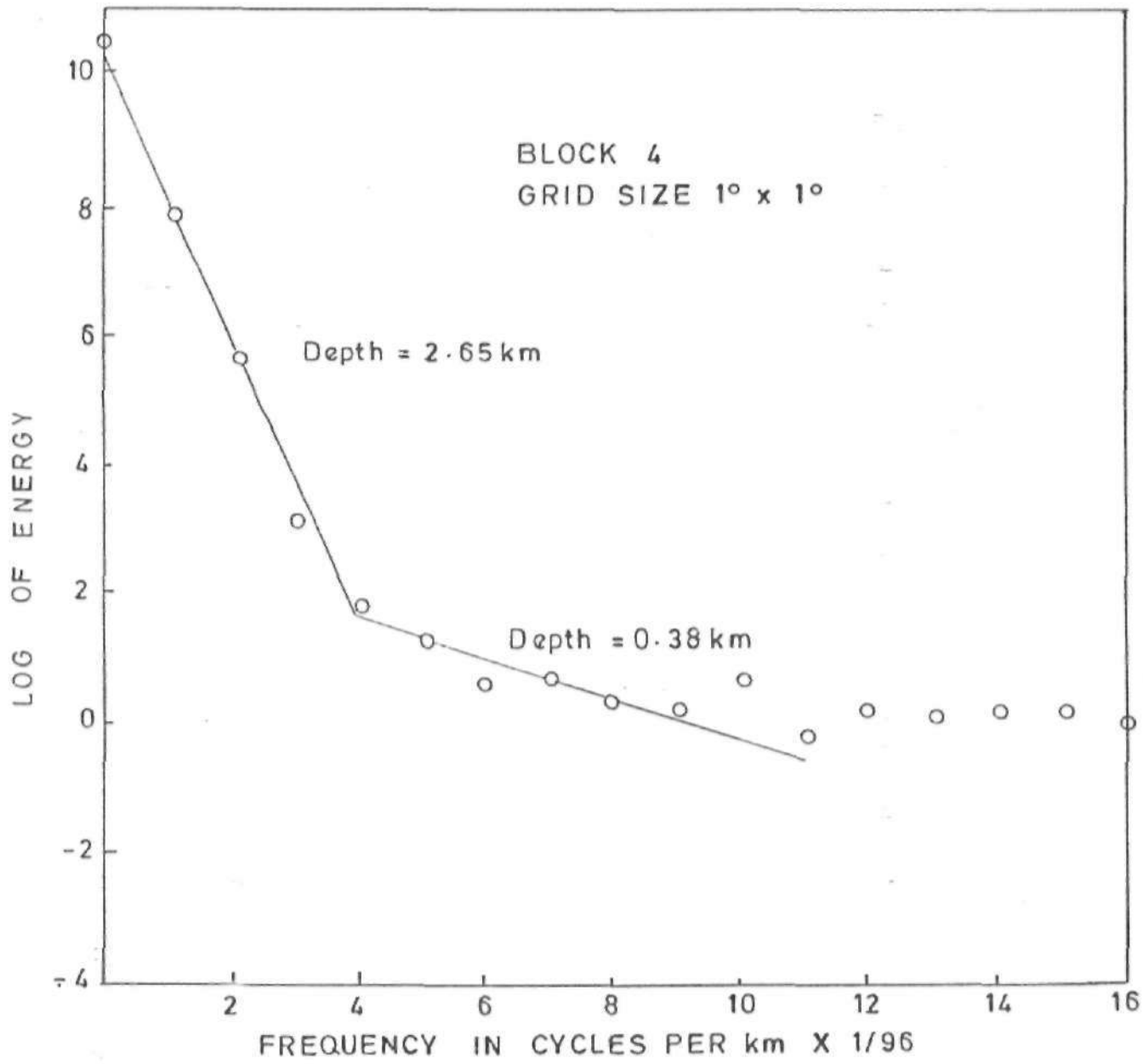


FIG.5.16: POWER SPECTRUM ANALYSIS FOR BLOCK 4

attributable to shallow magnetic sources on or near the surface.

One possible cause for the discrepancy in the spectral depth estimates for the two grid sizes might be found in the use of 32 x 32 data points in the spectral analysis of the $1^{o} \times 1^{o}$ grid instead of the actual data size of 37 x 37, plus perhaps some complementary values to satisfy the FFT requirement of $N = 2^{k}$. Another possible explanation for this discrepancy is that each of the four blocks in the $\frac{1}{2}^{o} \times \frac{1}{2}^{o}$ grid and the corresponding block in the $1^{o} \times 1^{o}$ grid will appear distinctive in magnetic character when analysed separately, such that the same technique for depth estimation may not necessarily yield the same results in both cases.

The power spectral plots for the remaining blocks are presented in Appendix B.

5.2.3 Power Spectrum Analysis for $1\frac{1}{2}^{o} \times 1\frac{1}{2}^{o}$ Grid.

Figure 5.17 presents the spectrally determined depths for the four blocks and Figures 5.18 - 5.21 show the spectral analysis for the four windows of $1\frac{1}{2}^{o} \times 1\frac{1}{2}^{o}$ map size. The

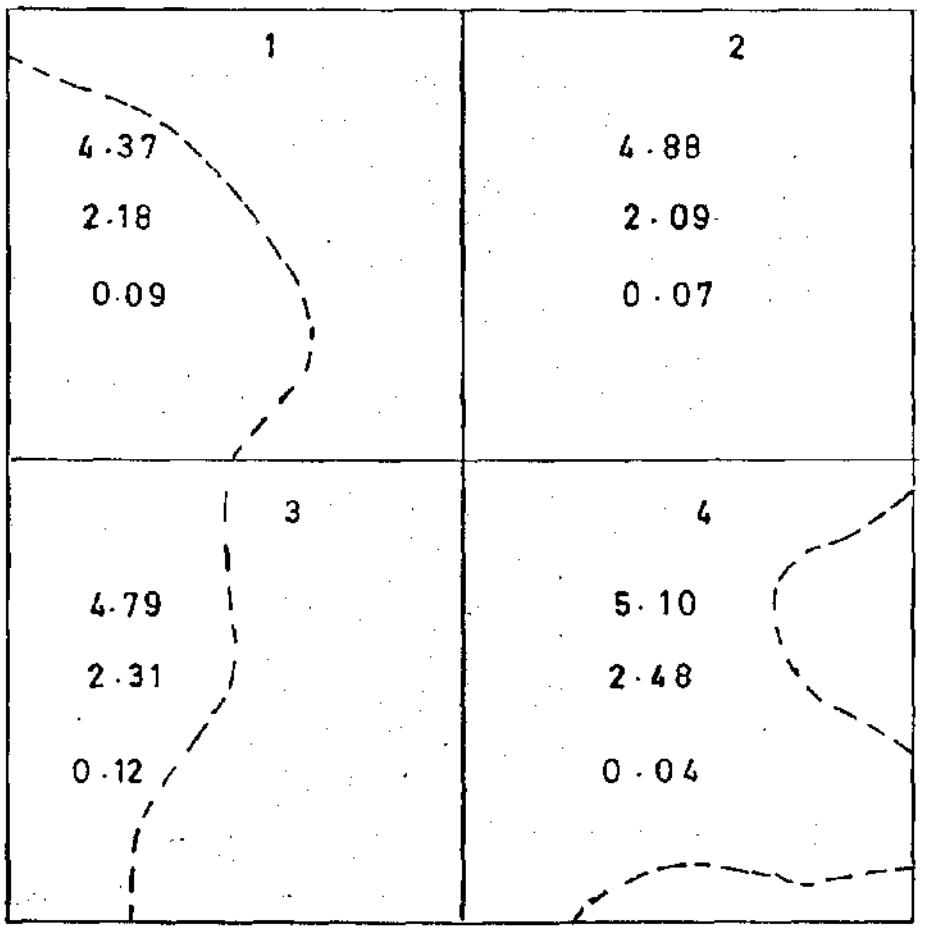


FIG.5.17: GRID LOCATIONS AND SPECTRAL DEPTHS FOR $1\frac{1}{2}^{\circ} \times 1\frac{1}{2}^{\circ}$ BLOCKS

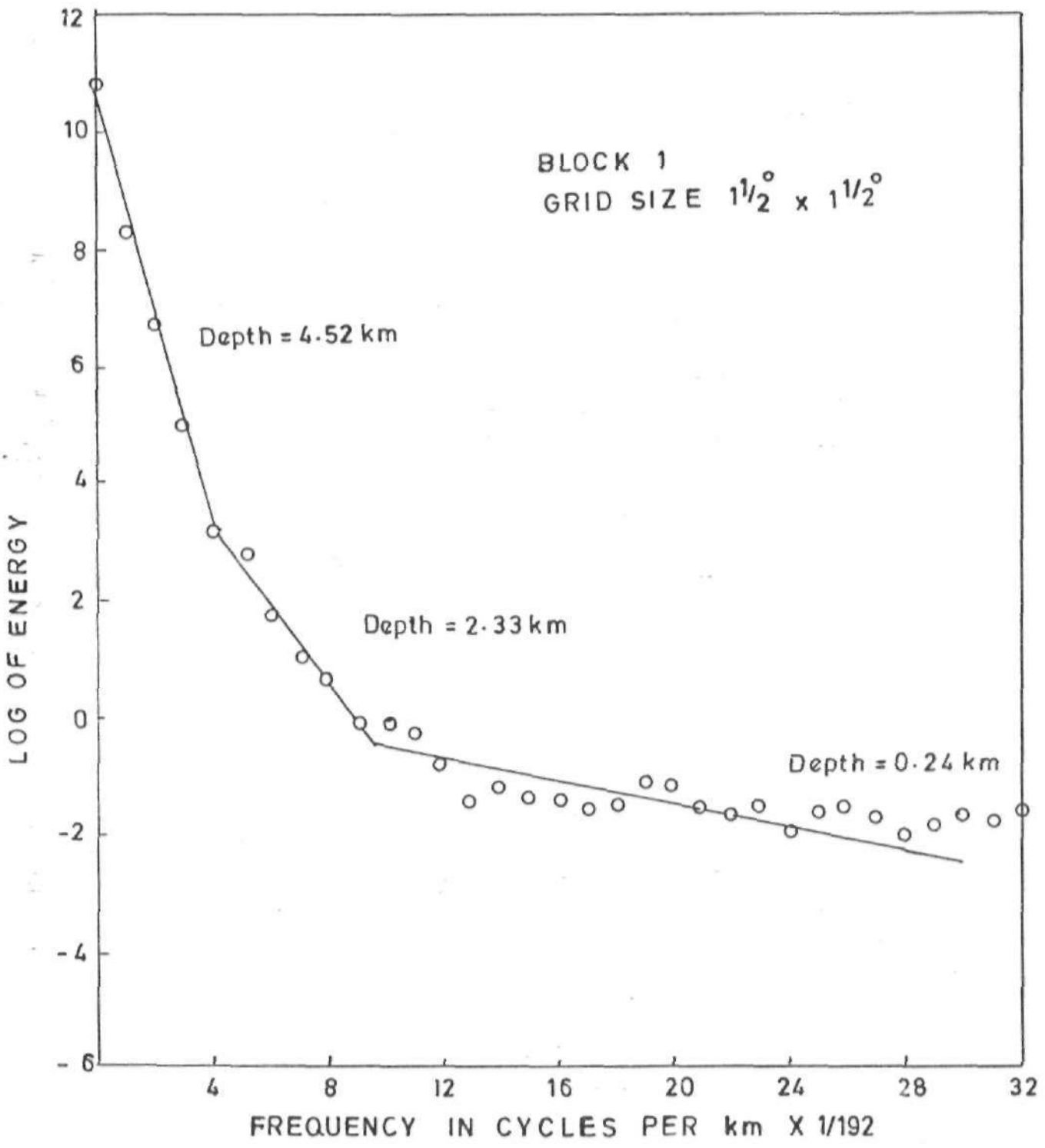


FIG.5.18 : POWER SPECTRUM ANALYSIS FOR BLOCK 1

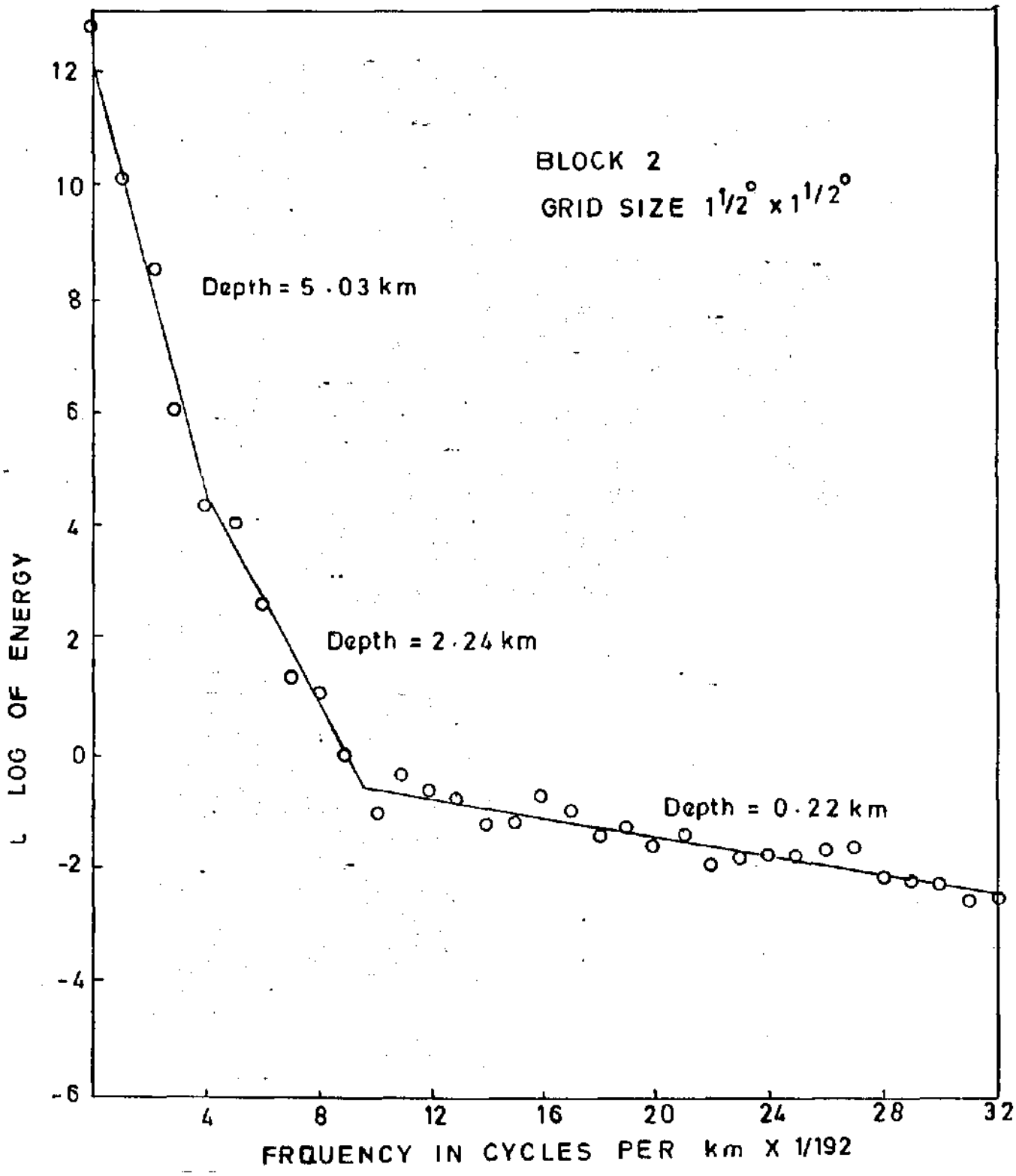
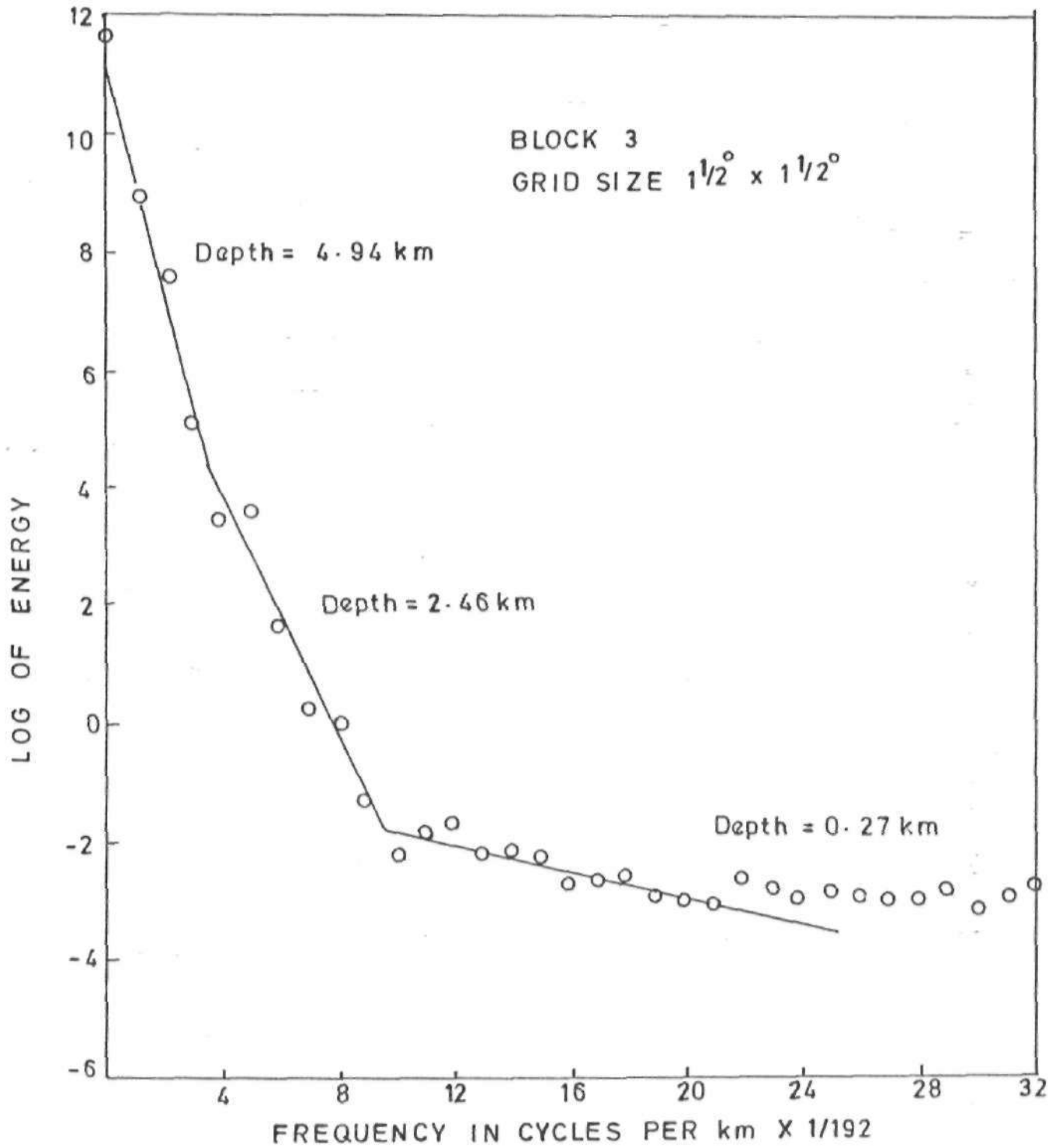


FIG-5-19: POWER SPECTRUM ANALYSIS FOR BLOCK 2



FIG·5·20: POWER SPECTRUM ANALYSIS FOR BLOCK 3

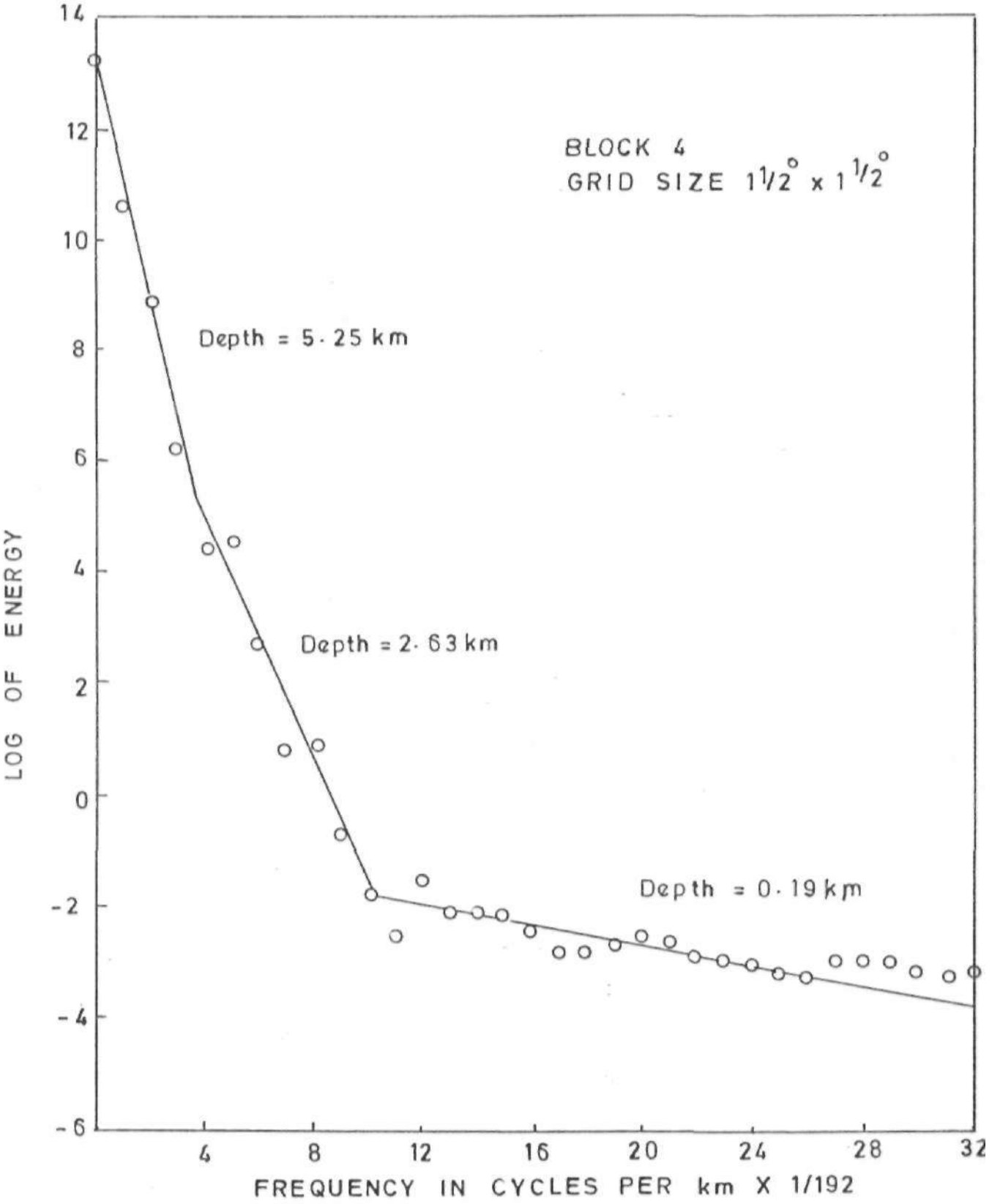


FIG. 5.21: POWER SPECTRUM ANALYSIS FOR BLOCK 4

spectral plot for each window clearly indicates the presence of three ensembles of sources in the area. While the line segment which dominates the low frequency portion of each spectrum relates to deeper magnetic sources, the segment occupying the mid-frequencies is from intermediate sources and the segment which occupy the high frequency end results from noise and shallow ensembles of sources. The magnetic anomalies in the region therefore originate at three distinct magnetic levels beneath the survey altitude.

Among the three grid sizes investigated, the $1\frac{1}{2}^{o}$ x $1\frac{1}{2}^{o}$ grid contains the highest percentage of information and this explains the significantly deeper source depths which averages 4.80km resolved by this window. The spectra for all the grids show similar deep source depths varying from 4.37km to 5.10km below the ground surface, and these may probably result from similar sources. While this is not an unreasonable depth for the surface of the geologic basement in some sections of the Benue Valley (Lower and Middle Benue in particular) it is believed that for the Upper Benue this magnetic level corresponds to some layer of highly magnetic intra basement granitic intrusives, probably of Cretaceous or Cenozoic age or to some basalt flows or both.

Similarly the intermediate depths appear continous between the four grids and may possibly result from the same sources as the spectral depths obtained from the low frequency portion of the $\frac{1}{2}^{o}$ x $\frac{1}{2}^{o}$ and 1^{o} x 1^{o} grids. These lines of average depth evidently represent the general average depth of the magnetic layers corresponding to the basement surface.

The shallow depths predicted from the linear segment occupying the high frequency region of the spectra for the four grids are so small that any magnetic sources attributable to this level would have to lie very close to the ground surface. These depths range from 0.09km in the NW grid to 0.12km in the SW and from 0.04km in the SE to 0.07km in the NE, and are in general associated with noise and other surface sources close to the survey altitude.

5.2.4 Power Spectrum Analysis for a North-South Profile

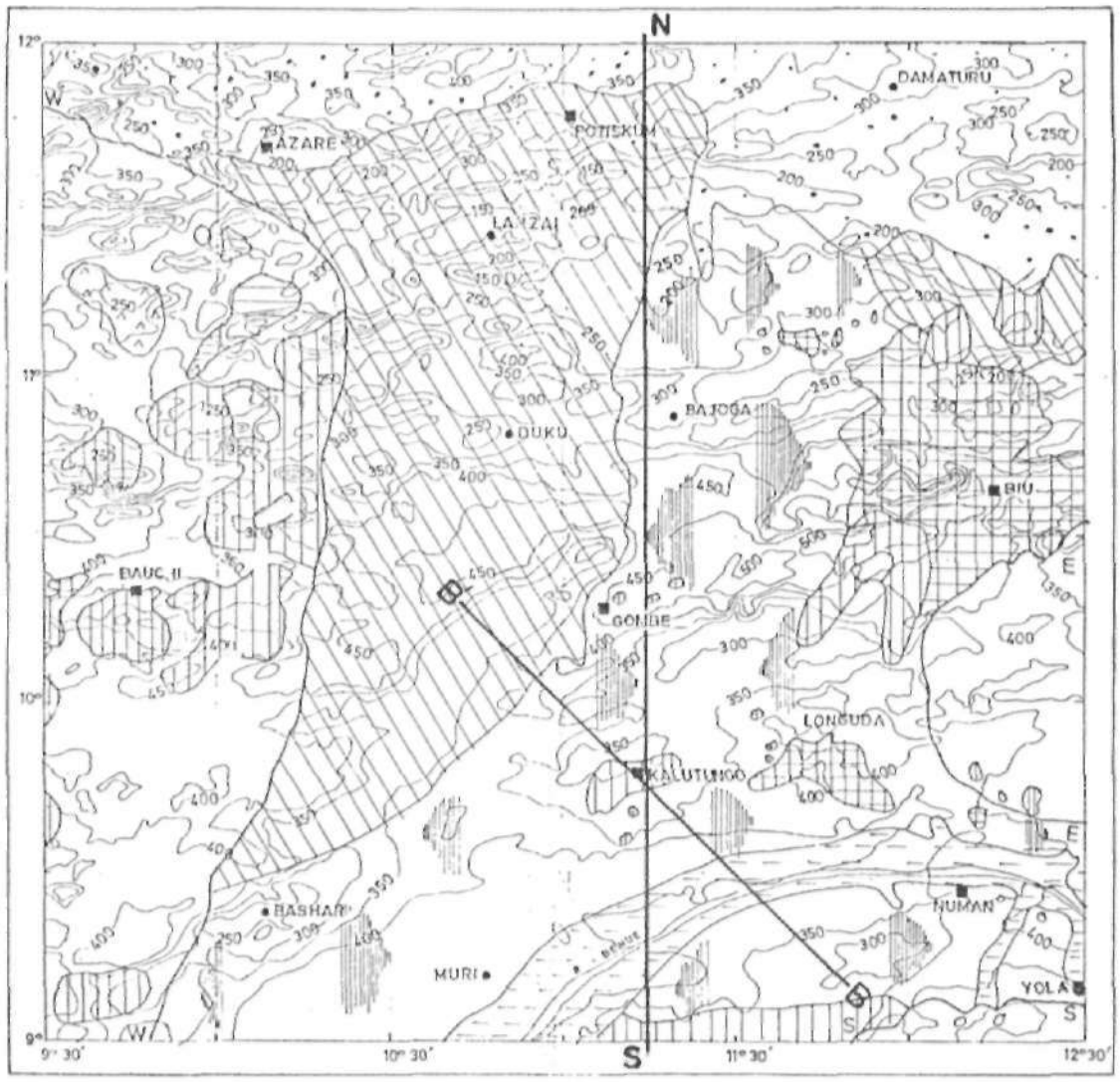
In order to assess the reliability of the spectral depths determined from the gridded magnetic data, a North-South traverse line which runs across the project area along longitude 11^{o} 15' (Figure

5.22) was selected for a one-dimensional spectral depth determination scheme based on profile data alone. The traverse line was sampled at 1km interval to ensure that all details necessary for the interpretation are included.

The interpretation has been carried out by one-dimensional power spectrum analysis for the entire window length of approximately 324km. Figure 5.23 shows the result of the analysis. The spectral plot shows that seven ensembles of sources can be clearly discerned. These are approximated by seven straight line segments which correspond to the average depths-to-tops of the different magnetic layers resolved by this window.

Interpretation of the whole profile yields depth information down to a horizon which corresponds probably to the crust-mantle interface at a mean depth of 31.52km below the ground surface. Table 5.1 shows a comparism with other depths obtained for the crustal thickness from other independent surveys.

Fig. 5.22 : Combined geology and total field map with locations of interpreted profiles



LEGEND

QUATERNARY		ALLUVIUM
		SANDS AND CLAYS
TERTIARY		BASALTS
		GRITS, SANDS AND CLAYS
CRETACEOUS		CLAY, SHALE, COAL, SANDSTONES, LIMESTONE
JURASSIC		GRANITE
		SYENITES AND GABBRO
PRE-CAMBRIAN TO UPPER CAMBRIAN		OLDER GRANITES
		UNDIFFERENTIATED BASEMENT COMPLEX

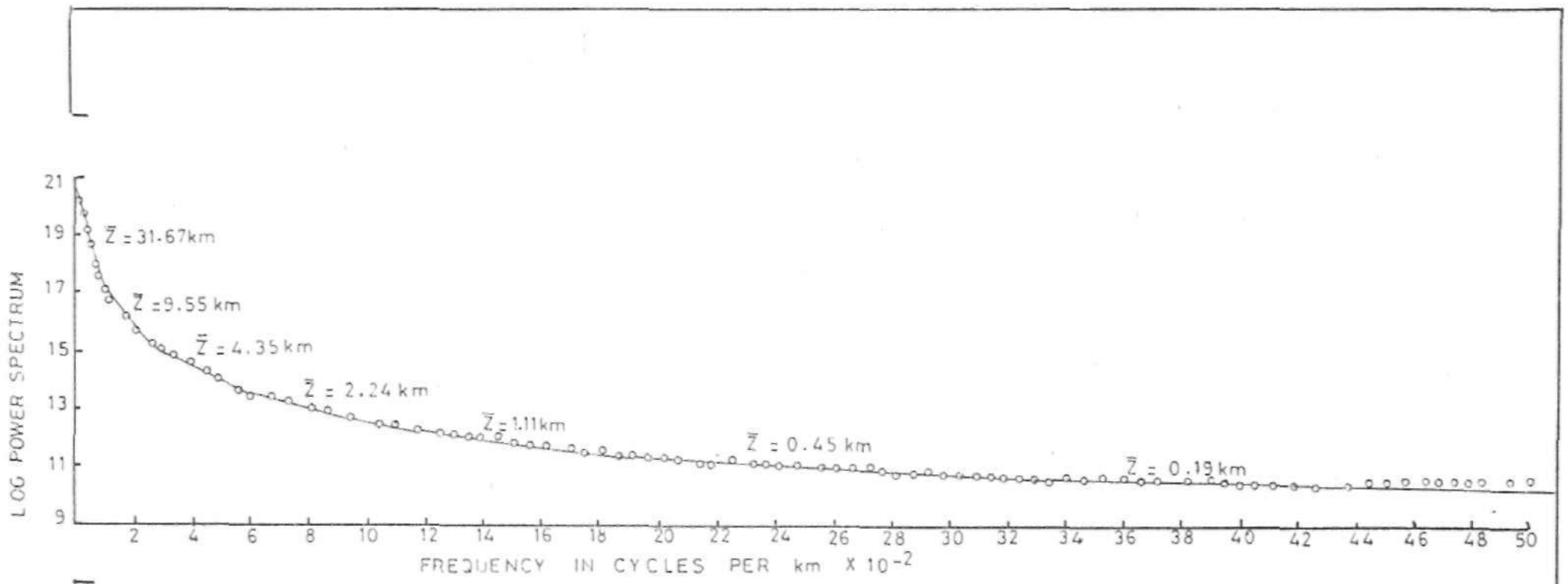


FIG.5.23: SPECTRAL ANALYSIS OF A NORTH–SOUTH PROFILE ALONG LONGITUDE 11° 15'

Table 5.1: Crustal thickness in the Benue Valley

Author(s)	Crustal thickness km
Kogbe and Artsybashev (1977)	22.0 - 37.0
Osazuwa (1978)	25.0 - 28.0
Adighije (1979)	27.0 - 28.5
Present study	31.52 $\pm$ 1.54

The 9.40km depth probably relates to some highly magnetic deep intra crustal structures. The one-dimensional spectral approach is able to resolve such deep source depths primarily because of the large gate length used in the analysis. The source depth of 4.20km below the datum surface is comparable in magnitude to the deep source depths obtained from the $1\frac{1}{2}^{o}$ x $1\frac{1}{2}^{o}$ window and may as well originate from similar sources within the basement. Similarly the 2.10km depth is consistent with the range of depths estimated from the intermediate segments in the $1\frac{1}{2}^{o}$ x $1\frac{1}{2}^{o}$ grid (Figure 5.17) and the deep source depths for the 1^{o} x 1^{o} and $\frac{1}{2}^{o}$ x $\frac{1}{2}^{o}$ grids (Figures 5.2 and 5.12). This depth range has

been interpreted as mean depths to the magnetic basement underlying the sedimentary basin.

The two-dimensional spectral analysis do not show any detectable layer corresponding to 0.96km depth level resolved by the one-dimensional spectral analysis. This is probably due to the radial averaging over large map areas investigated in the two-dimensional spectral approach. It is therefore suggested that this depth relates to some local feature along the profile and may be ascribed to some major units of buried magnetic basement rocks. Shallow source depths occur at 0.30km and 0.04km below the ground surface. While the 0.30km depth relates to some shallow intrusive material, the 0.04km depth appears from noise or from sources near the surface.

In general the depth information obtained from the one-dimensional spectral approach are consistent with the results of the two-dimensional spectral magnetic depth determination. However, while the two-dimensional spectral method gives depth information for map spectra corresponding to a given map area the one-dimensional approach yields depths along a profile and therefore local features along the

profile may influence depth estimates obtained from the one-dimensional analysis.

5.3 Two-Dimensional Model Interpretation.

One aeromagnetic profile was taken across the study area and interpreted in terms of two-dimensional structures since majority of the observed anomalies are mostly two-dimensional. **Fig**ure 5.22 shows profile BB' which lies predominantly in the sedimentary formations. The total field magnetic anomaly along the profile was sampled at 0.5km intervals and subsequently interpreted strictly in terms of a combined effect of a uniformly magnetized metamorphic basement and basic intrusive bodies of variable sizes and magnetization. These bodies may occur largely either within the basement or within the Cretaceous sediments.

The model interpretation was carried out by determining the magnetic effects of the proposed hypothetical bodies; comparing their calculated magnetic effects with the observed magnetic effects and offering some realistic interpretation. Modelling was facilitated by using a computer routine based on the algorithm of Talwani and Heirtzler (1964).

The starting depths for the surface of the geologic basement and the locations of the intrusive bodies were reliably computed by the Werner deconvolution method, through the application of a highly efficient computer program (Ojo, Personal Communication). To this was added the geological constraint imposed by the Kaltungo basement outcrop. The best fitting model obtained for the profile is shown in Figure 5.24, with surface geological information along the profile. The suceptibility ranges for the various rock types and the contrasts obtained for the modelled bodies are of the same order of magnitude as values obtained during field observations by Osazuwa (1978).

The model shows varying thicknesses of sedimentary deposits along the profile. A minimum thickness of about 2.0km and a maximum of about 8.0km was modelled. Initial suggestions for the presence of a massive granitic body "A" with a negative susceptibility contrast of -0.000625 at a mean depth of 3.0km, and a highly susceptible intrusive structure 'C' with a susceptibility value of 0.002500 occuring at a depth of 6.0km within the basement was provided from the results of the Werner deconvolution studies. It has also been observed that anomalies

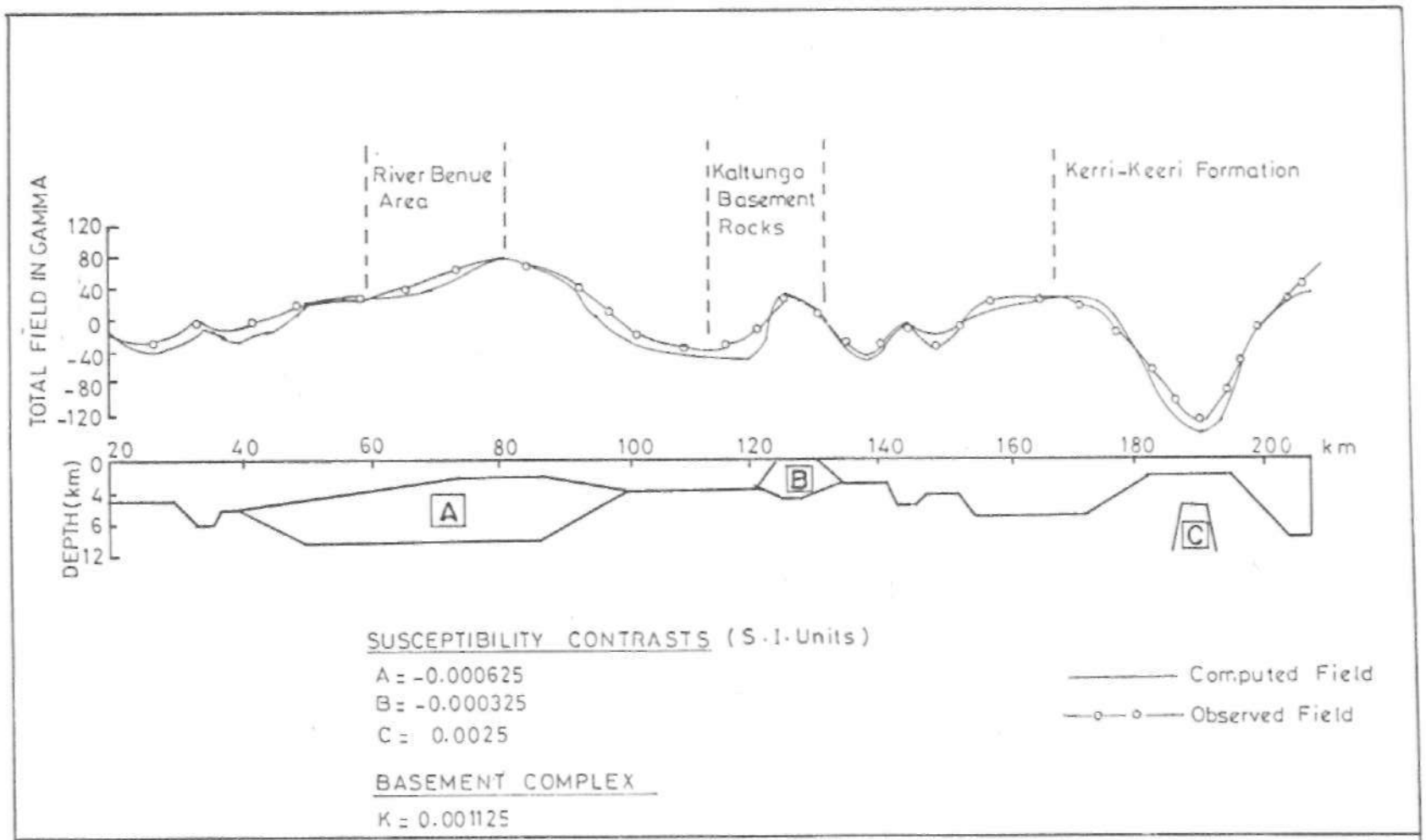


FIG. 5.24: TWO DIMENSIONAL MODEL INTERPRETATION FOR PROFILE BB'

due to these model intrusives are consistent with the gravity anomalies of parts of the Upper Benue (Osazuwa, Personal Communication).

The depth information from the spectral analysis along with the results of the model interpretation suggest that the thickest sedimentary deposits occur in the southern section of the project area, and that the sediments thin down in a general northward direction.

5.4 Structural Implications of the Interpreted Results.

The spectral magnetic depth estimation method has been used to determine the average depths to the magnetic basement and the numerous intrusions in the Upper Benue Valley. The results show clearly a quantitative picture of the thickness of the sedimentary section across the study area. The results also indicate that several igneous intrusions of basic to intermediate rocks in the study area occur at mean depths ranging from 0.26km to 4.8km in different localities either within the sediments or within the basement. Some of these intrusions as indicated by the two-dimensional model interpretation occur at depths of up to 6.0km. Spectrally determine depths

ranging between 2.0km and 2.60km refer to the magnetic layers corresponding to the basement surface, or to the basalt flows on the surface of the basement or to some major intrusions into the basement and the sediments.

The extensive igneous activity which took place in the Lower Cretaceous and the widespread but sporadic volcanism which occured in the basin throughout the Cretaceous and during Recent times suggest that the magnetic basement in some sections of the trough is no longer likely to appear as a distinct horizon with significant contrasts of magnetization. The intrusions (igneous sills, dykes, and plutons) may be so numerous in some localities that any weakly magnetic layers are no longer discernible. It is possible therefore that the much younger, intensely magnetized intrusives lying either within or outside the basement may effectively mask the true basement surface in some areas. Hence the intermediate mean depths recorded from the spectral plots for all the data windows might refer either to the basement surface or to the top of some intrusions or both. However, viewed on a broad scale, our results show that deeper intrusive structures emplaced within the basement lie at a depth which

ranges from 4.37km to 5.10 km. The existence of these deeply rooted intrusions within the trough suggests the probability of the existence of deeply penetrating fractures in the area.

Other structural features outlined by the spectral depths are a southerly dip of the basement or magnetic surface from depths ranging from 2.25km in the northern part of the region to 2.60km at the southern edge; and some indication of the magnitude of the structural relief on the basement surface. It should be appreciated that these depth values are necessarily mean depths. Consequently actual depths higher or lower than the estimated mean values may either relate to some locally deep sections containing thick sedimentary sequences or to uplifted basement rocks. This view is supported by the results of the two-dimensional model interpretation which shows a minimum sediment thickness of 2.0 km along the profile and a number of isolated depressions containing thick sedimentary sequences of the order of 8.0km.

CHAPTER 6

REVIEW AND CONCLUSIONS

6.1 Review and Discussions

A field example has been presented using both the one- and two-dimensional spectral analysis of magnetic interpretation to determine depths to magnetic basement and the numerous intrusions in the Upper Benue basin. A two-dimensional model interpretation for a chosen profile was also presented as a supplementary technique.

The utility of the spectral magnetic depth determination method lies in the fact that it provides a computationally simple and rapid scheme to obtain average depths to the magnetic basement in sedimentary basin areas. The calculations may be made directly from the total field intensity magnetic data in profile or map form.

There is in general good agreement with respect to the results obtained from the various interpretation methods employed in this study. Apart from the deep source depths of 31.52km and 9.40km resolved by the one-dimensional spectral analysis, the shallow source depths are consistent with results obtained from the three map windows used in the two-dimensional spectral method. The deep source depths picked by the one-dimensional spectral analysis

is due to the large profile length and perhaps the smaller sampling interval used in the analysis. The two-dimensional spectral analysis on the other hand yielded carefully determined depths but could not resolve depths deeper than 5.0km mainly due to the map size used in the analysis.

Some of the features revealed by the two-dimensional model interpretation (Figure 5.24) also appear on the Bouguer gravity anomaly map of a portion of the study area. An obvious example is the large granitic mass 'A' (Figure 5.24) which lies on the basement along the profile. The position of the top and bottom of the body was first indicated by the Werner deconvolution modelling, and the susceptibilty contrast was that required to obtain a good fit with the observed anomaly. This fact also applies to the large intrustion 'C' which occurs at a depth of 6.0km under the Kerri-Kerri formation (Figure 5.24).

Some degree of correlation has been achieved between the geology and the aeromagnetic profile as evidenced by the Kaltungo basement rocks which outcrop to the surface. The model (Figure 5.24) shows that the trough along the profile is underlain by a mass of basement rocks whose

depth of burial increases progressively from either flanks of the Kaltungo basement outcrop. Some locally deep sections are also indicated in the model.

'In general, sediment depths obtained from the present study vary between 0.14km and 2.83km in the project area. A comparism with the results of previous estimates from gravity and magnetic data indicate that results obtained in the present work conform well with other geophysical estimates. On the basis of residual Bouguer gravity anomalies and magnetic anomalies over the Upper Benue area, Osazuwa (1978) and Osazuwa et al.(1981) obtained sediment thickness ranging from 0.9km to 2.2km for gravity data, and sediment depths varying between 0.9km and 4.9km for magnetic data. The thickest sedimentary deposit corresponding to 4.9km was recorded near Numan which is located in the deepest sedimentary region outlined in this study. Since the mean sedimentary thickness recorded for this region in the present study is 2.83km, the thick sediment sequence of 4.9km suggests the possibility of the existence of some locally deep sections in this area.

Until now there has not been any programme for a comprehensive mapping of the basement in the Benue Trough. Known basement depths in the basin are mainly estimated by rule of thumb or from isolated surveys based mostly on two-dimensional standard profile interpretations of gravity and magnetic data(Osazuwa, 1978; Ofoegbu, 1984a). Depth information obtained from some of these surveys most often refer to depths-to-source of individual anomalies. While the spectral approach cannot be expected to have the resolution theoretically achievable by analyses carried out on individual anomalies, it can lead to the determination of mean depths to major and minor units of buried magnetic rocks and to the magnetic basement underlying a sedimentary basin (Treitel et al., 1971). In basement mapping therefore the depth to source ofany individual anomaly will be of less significance than an average depth to a group of bodies (Curtis and Jain, 1975).

6.2 Summary and Conclusion

The results of one- and two-dimensional spectral analysis show clearly the variation in sedimentary thickness and the magnitudes of the

structural relief on the surface of the basement. The power spectral plots for all the windows analysed give four depth ranges namely: 9.40 - 31.52km, 4.37 - 5.10km, 2.0 to 2.83km, and 0.04km to 0.96km. The 4.37-5.10km depths have been interpreted as being due to anomalies generated by source bodies lying within the basement. While the 9.40km and the 31.52km source depths refer to some intra crustal source structures and the crustal thickness in the region respectively, the mean depth values varying between 2.0km and 2.83km refer to the basement surface. This depth range indicate clearly the magnitude of the undulations of the basement topography throughout the study area. The topography of the basement surface has a corresponding relationship to the structure of the sedimentary strata. The basement surface shows a general trend from shallow in the NW and NE to deep in the south central area.

Shallow source depths in the range of 0.04km to 0.12km generally appear from noise and surface sources, and source depths up to 0.96km relate to the numerous source bodies within the sediments, and near-surface basement rocks. Some of these bodies have been interpreted as regions of intrusions and metamorphism which may differ structurally or appear homogenous depending on their age and depth of burial.

Our results have demonstrated the applicability of the spectral method of magnetic interpretation in estimating depths to the basement and hence the variations in sedimentary thickness in the study area. The method is also suitable for estimating the crustal thickness beneath large rifted continental areas such as the Benue Trough.

However much still remains to be done in the Benue Valley and other sedimentary basin areas in Nigeria. It would no doubt be desirable to carry out a more detailed study of the entire Benue Trough and perhaps the neighbouring Chad basin with techniques based on one - and-two dimensional spectral analysis of aeromagnetic data. This arrangement should be supplemented by a large scale depth determination scheme by Werner deconvolution method, along profiles spaced at 1km intervals. In all cases the aeromagnetic data should be sampled at 2.0km spacing in order to ensure proper definition of sources. Further surveys employing more sophisticated but highly reliable methods may also be planned.

The objective of this new approach is to produce basement contour maps for the entire basin. A magnetic basement map can determine those basin areas where the sediments are thick enough to make reasonable petroleum prospects and to guide later exploration in the region.

REFERENCES

Adighije, C. (1979). Gravity field of Benue Trough, Nigeria. Nature Phys. Sci., pp 199-201,

Adighije, C. (1981a). Gravity Study of Lower Benue Trough, Nigeria. Geol. Mag., 118, pp. 50 - 67.

Adighije, C. (1981b). A gravity Interpretation of the Benue Trough, Nigeria. Tectonophys., 79, pp. 109 - 128,

Ajakaiye, D.E. (1981). Geophysical Investigations in the Benue Trough - a review. Earth Evolution Sci., 2, pp 110-125.

Ajakaiye, D.E.; Hall, D.H. and Millar, T.W. (1985). Interpretation of aeromagnetic data across the central crystalline shield area of Nigeria. Geophys. J.R. astr. Soc, , 83 pp 503-517.

Ajakaiye, D.E.; Hall, D.H.; Millar, T.W.; Verheijen, P.J.T.; Awad, M.B.; and Ojo S.B. (1986). Aeromagnetic anomaly and tectonic trends in and around the Benue Trough, Nigeria. Nature Phys. Sci., 319 (6054), pp. 582 -584.

Ajayi, C.O. (1979). A detailed gravity survey of the Middle Benue, Nigeria. Unpublished Ph.D thesis. Ahmadu Bello University, Zaria, Nigeria.

Ajayi, C.O. and Ajakaiye, D.E. (1981). The Origin and peculiarities of the Nigerian Benue Trough: another look from recent gravity data obtained from the Middle Benue. Tectonophys., 80, pp 285 - 303.

Artsybashev, V.A. and Kogbe, C.A. (1975). Crustal Structure of the Benue Valley area Nigeria. Geol. Rdsch. 64, pp 324 - 329.

Ashiekaa, J.A. (1983). Structural Analysis of the Benue Trough, Nigeria from Geophysical data. Unpublished MSc. thesis. Ahmadu Bello University, Zaria, Nigeria.

Ayoola, E.O. (1978). Sedimentology of the Middle Benue Trough, Nigeria. Unpublished Ph.D thesis. University of London.

Bath, M. (1974). Spectral Analysis in Geophysics. Elsevier Pub. Co. Amsterdam.

Benkhelil, J. (1982). Benue Trough and Benue Chain. Geol. Mag., 119, pp 155-168.

Bingham, C., Godfrey, M.D., and Tukey, J.W. (1967). Modern techniques of power Spectrum estimation. IEEE Transactions on Audio and Electroacoustics, Vol. AU-15, pp. 56 - 66.

Burke, K.; Dessauvagie, T.F. J. and Whiteman, A.J. (1971). Opening of Gulf of Guinea and the geological history of the Benue depression and Niger Delta. Nature Phys. Sci. 233, pp. 51-55.

Burke, K.; Dessauvagie, T.F.J. and Whiteman, A.J. (1972). Geological history of the Benue Valley and adjacent areas. In: Dessauvagie, T.F.J and Whiteman, A.J. (Ed.) African Geology - Ibadan University Press.

Burollet, P.F. (1984). Intracratonic and Pericrationic Basins in Africa. Sedi. Geol., 40, (1-3): pp. 33-49.

Carter, J.D.; Barber, W. and Tait, E. A. (1963). The geology of parts of Adamawa, Bauchi and Borno Provinces in Northern Nigeria. Bull. geol. Surv. S Nigeria, No. 30.

Chukwu-Ike, I.M. (1977). Regional Photogeological Interpretation of the tectonic features of the Central Nigerian Basement Complex - a statistical based study. Unpublished Phd. thesis University of London.

Cianciara B. and Marcak H. (1976). Interpretation of gravity anomalies by means of local power spectra. Geoph. Prosp., 24, pp. 273 - 286.

Claerbout, J.F. (1976). Fundamentals of geophysical data processing: with applications to Petroleum Prospecting. McGraw-Hill Book Co., New York.

Connard, G.; Couch, R. and Gemperle, M. (1983). Analysis of aeromagnetic measurements from the Cascade Range in Central Oregon. Geophys., 48 (3): pp. 376 - 390,

Cooley, J.W. and Tukey J.W. (1965). An algorithm for the machine computation of complex Fourier series Math. Comput., 19, pp 297-301.

Cratchley, C.B. and Jones, G.P. (1965). An interpretation of the geology and gravity anomalies of the Benue Valley, Nigeria. Geophys. Pap. Overseas geol. Surv. London No. 1.

Curtis, C.E. and Jain, S. (1975). Determination of Volcanic thickness and underlying structure from aeromagnetic maps of the Silet area of Algeria. Geophys., 40 (1): pp. 79-90.

Ekine, A.S. (1979). Gravity Survey around the Wase-Akiri Salt Spring area in the Middle Benue Valley. Unpublished M.Sc. thesis. Ahmadu Bello University, Zaria, Nigeria.

Fairhead, J.D. and Okereke, C.S. (1986). Depths to major density contrast beneath the West African rift system in Nigeria and Cameroon based on the spectral analysis of gravity data. Paper presented at the AGERA Conference, Jos, 1-5 December.

Farrington, J.F. (1952). A preliminary description of the Nigerian lead zinc field. Econ. Geol., 47, pp 583-608.

Ford, S.O. (1981). The economic mineral resources of the Benue Trough. Earth Evolution Sci., 2, pp. 154-163.

Grant, N.G. (1971). South Atlantic Benue Trough and Gulf of Guinea Cretaceous Tripple junction. Bull. geol. Soc., AM., 82, pp. 2295 - 2298.

Hahn, A.; Kind, E.G. and Mishra, D.C. (1976). Depth estimation of magnetic sources by means of Fourier amplitude Spectra. Geoph. prosp., 24, pp. 278-308.

Hall, D.H. (1968). Regional magnetic anomalies, magnetic units and crustal structure in the Kenora district of Ontario. Can. J. Earth Sci. 5, pp. 1127-1296.

Hall, D.H. (1974). Long wavelength aeromagnetic anomalies and deep crustal magnetization in Manitoba and North western Ontario, Canada J. Geophys. 40, pp. 403-430.

Holmes, A. (1964). Principles of Physical Geology. Nelson Book Co.

Jones, G.P. (1960). Depositional history of the Bima Sandstone of north-eastern Nigeria. Paper presented at C.C.T.A Conference on Geology, Kaduna, Northern Nigeria, February, 1960.

Kanasewich, E.R. and Agarwal, R.G.(1970). Analysis of combined gravity and magnetic fields in wave number domain. J. Geoph. Res., 75, pp. 5702-5712.

King, L. C. (1950). Outline and deposition of Gondwana-Land. Geol. Mag., 87, pp. 353-359.

Kogbe, C.A. (1981a). Attempt to correlate the stratigraphic sequence in the Middle Benue Basin with those of the Anambra and Upper Benue Basins. Earth Evolution Sci., 1, 139 - 143.

Lees, G.M. (1952). Foreland folding. Quart. J. Geol. Soc., 108, pp. 1 - 34.

McConnel, R.B. (1949). Notes on Lead-Zinc deposits of Nigeria and Cretaceous Stratigraphy of Benue and Cross River valleys. Geol. Surv. Nigeria. Report No. 752.

McCurry, P. (1976). The geology of the Precambrian to Lower palaeozoic rocks of Northern Nigeria- a review. In: Kogbe, C.A. (Ed.) Geology of Nigeria - Elizabeth Pub. Co., Lagos, pp. 15-39.

Mishra,D.C. and Naidu, P.S. (1974). Two-dimensional power spectral analysis of aeromagnetic fields Geoph. Prosp., 22, pp. 345-353.

Myada, E.E. (1979). Mafa-Dikwa geophysical anomalies and their interpretation. Unpublished Ph.D thesis. Ahmadu Bello University, Zaria, Nigeria.

Naidu, P.S. (1969). Estimation of spectrum and cross spectrum of aeromagnetic fields using fast digital Fourier transform (FDFT) techniques. Geoph. prosp. XVII, pp. 344-361.

Naidu, P.S. (1970a). Statistical Structure of aeromagnetic field. Geophys., 35(2): pp. 279-292.

Naidu, P.S. (1970b). Fourier transform of large scale aeromagnetic field using a modified version of fast Fourier transform. Pageoph., 81(4): pp. 17-25.

Negi, J.G.; Agrawal, P.K. and Rao, K.N.N. (1983). Three-dimensional model of the Koyna area of Maharashtra State (India) based on the spectral analysis of aeromagnetic data. Geophys., 48 (7): pp 964 - 974.

Offodile, M.E. (1976). The Geology of the Middle Benue, Nigeria. Palaeo. Institute, University of Uppsala, Special Vol. 4.

Offodile, M.E. (1976a). A review of the Geology of the Cretaceous of the Benue Valley. In: Kogbe C.A. (Ed.) Geology of Nigeria - Elizabeth Pub. Co. Lagos pp. 319 - 330.

Offodile, M.E. (1977). The economic significance of some of the Cretaceous events in the Benue Valley. J. Min. and Geol., 14(2): pp 67 (abstract).

Ofoegbu, C.O. (1982). Methods of interpreting magnetic anomalies with application to the Minch dyke and mangetic anomalies over the Lower and Middle Benue Trough of Nigeria. Unpublished Phd. thesis. University of Durham.

Ofoegbu, C.O. (1984a). Interpretation of aeromagnetic anomalies over the Lower and Middle Benue Trough of Nigeria. Geophys. J. R. astr. Soc., 79, pp. 813-823.

Ofoegbu, C.O. (1984b). A model for the Tectonic evolution of the Benue Trough of Nigeria. Geologische Rundschau, 73(3): pp. 1007-1018.

Ofoegbu, C.O. (1984c). An aeromagnetic study of the Lower Benue Trough, Nigeria. Revista Brasileira de Geociencias,14(1): pp. 54 - 59.

Ofoegbu, C.O. (1985a). A review of the geology of the Benue Trough, Nigeria. J. Afric. Earth Sci., 3(3): pp. 283 - 291.

Ofoegbu, C.O. (1985b). Interpretation of an aeromagnetic profile across the Benue Trough. J. Afric. Earth Sci., 3(3): pp 293-296.

Olade, M.A. (1975). Early Cretaceous basalt volcanism and initial continental rifting in Benue Trough, Nigeria. Nature Phys. Sci., 273, pp. 458 - 559.

Osazuwa, I.B. (1978). Gravity and Magnetic Survey of the Upper Benue Trough. Unpublished MSc. thesis. Ahmadu Bello University, Zaria Nigeria.

Osazuwa, I.B.; Ajakaiye, D.E. and Verheijen, P.J.T (1981). Analysis of the Structure of part of the Upper Benue Rift Valley on the Basis of New geophysical data. Earth Evolution Sci., 2, pp. 126-135.

Oyawoye, M.O. (1972). The Basement Complex of Nigeria. In: Dessauvagie, T.F.J. and Whiteman, A.J. (Ed.) African Geology - Ibadan University Press, pp 67-103.

Pal. P.C.; Khurana, K.K. and Unnikrishnan, P. (1978). Two examples of spectral Approach to source depth estimation in gravity and magnetics. Pageoph., 117, pp. 772 - 783.

Spector, A. and Grant, F.S. (1970). Statistical models for interpreting aeromagnetic data. Geophys.35, pp. 293-302.

Talwani, M. and Heirtzler, J. (1964). Computation of Magnetic anomalies caused by two-dimensional structures of arbitrary shape. In: Parks, G.A. (Ed.) Computers in Mineral Industries.

Treitel, S., Clement, W.G. and Kaul, R.K. (1971). The spectral determination of depths to buried magnetic basement rocks. Geophys. J.R. astr. Soc. 24, pp. 415-428.

Umego, M.N. (1978). Gravity investigations around the Ribi salt spring. Unpublished MSc. thesis. Ahmadu Bello University, Zaria Nigeria.

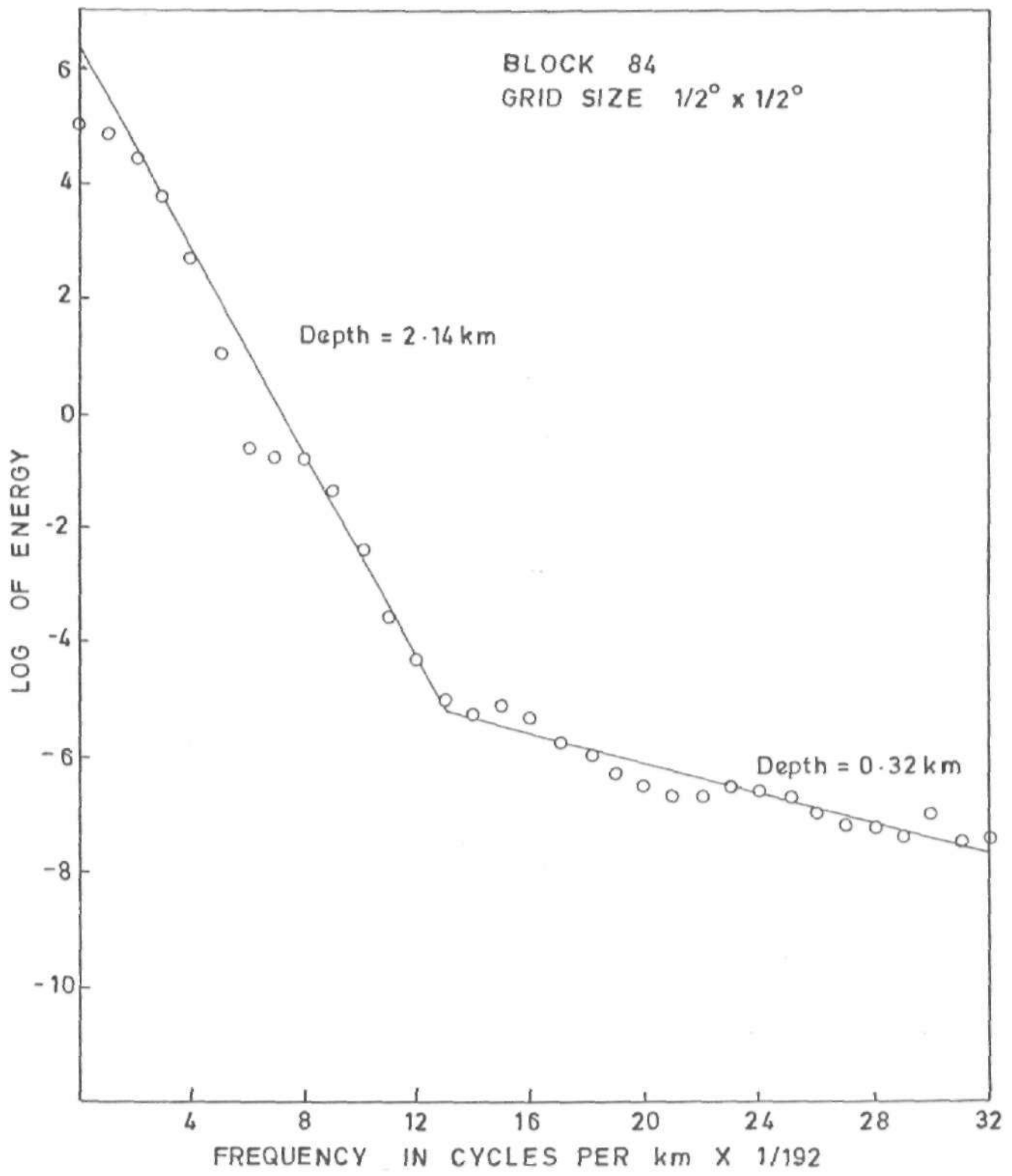
Wright, J.B. (1968). South Atlantic continental drift and Benue Trough. Tectonophys., 6, pp. 301 - 309.

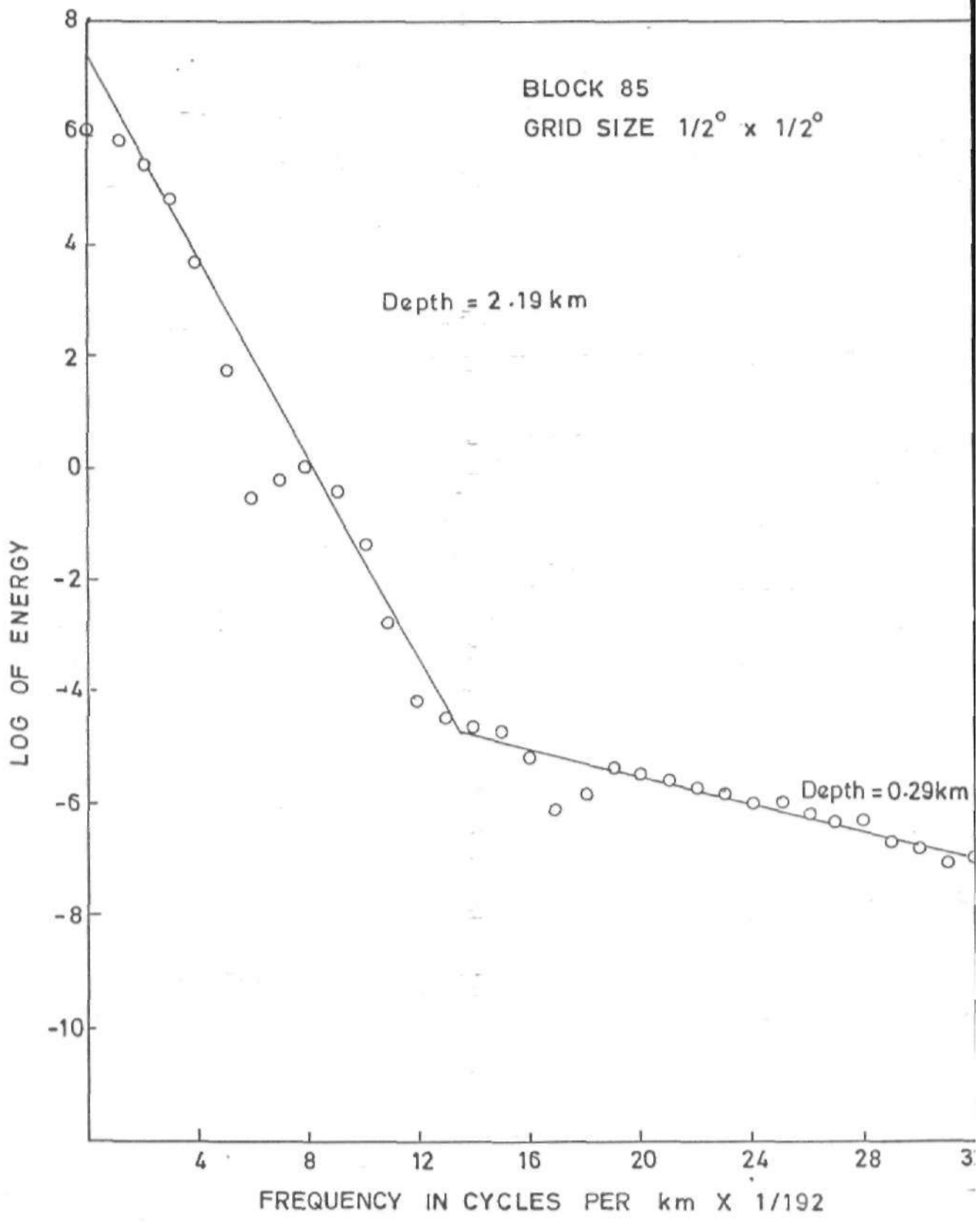
Wright, J.B. (1976). Origins of the Benue Trough: a critical review. In: Kogbe, C.A. (Ed.) Geology of Nigeria - Elizabeth Pub. Co., Lagos.

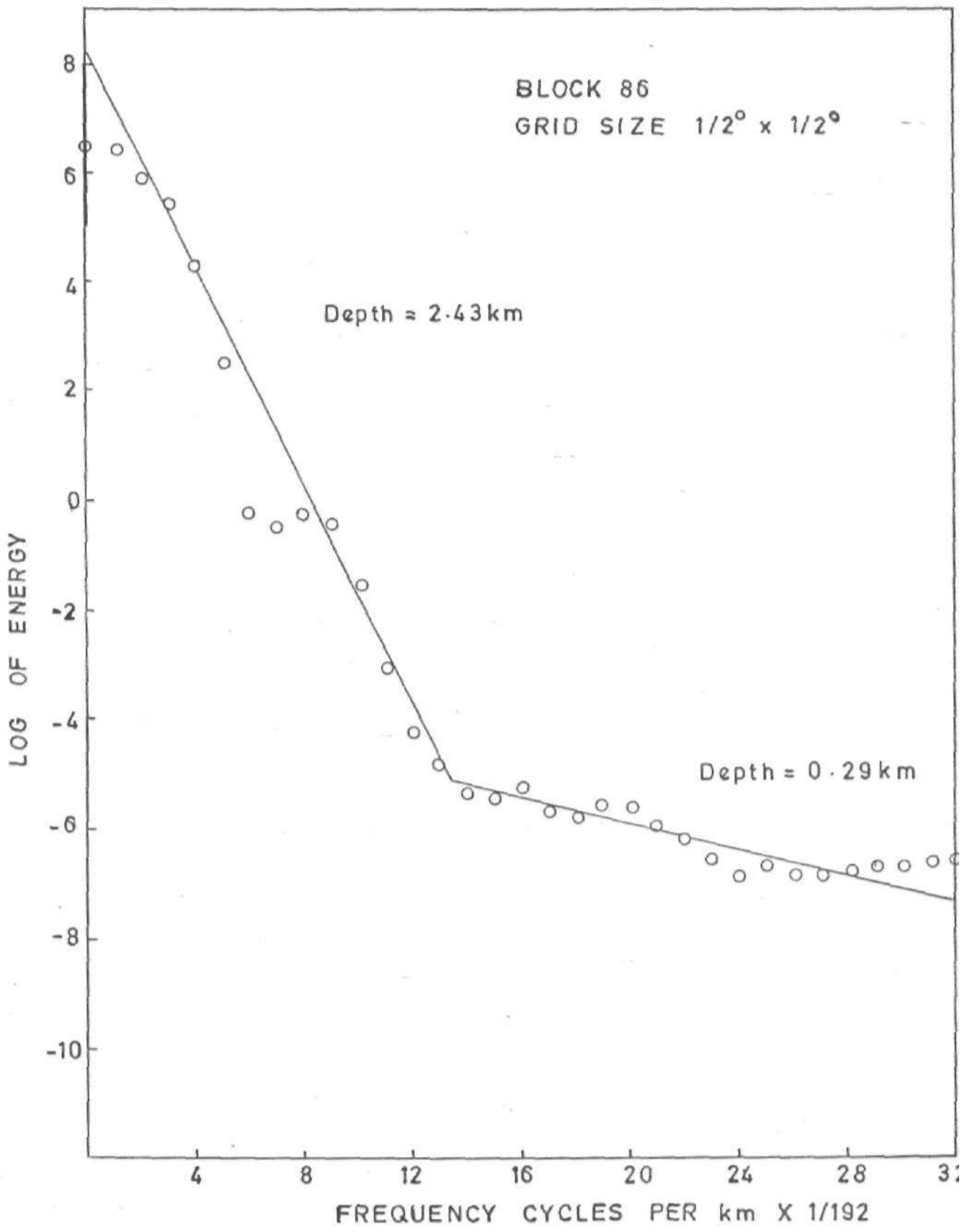
Wright, J.B. (1981). Review of the origin and evolution of the Benue Trough in Nigeria. Earth Evolution Sci., 1, pp. 98 - 104.

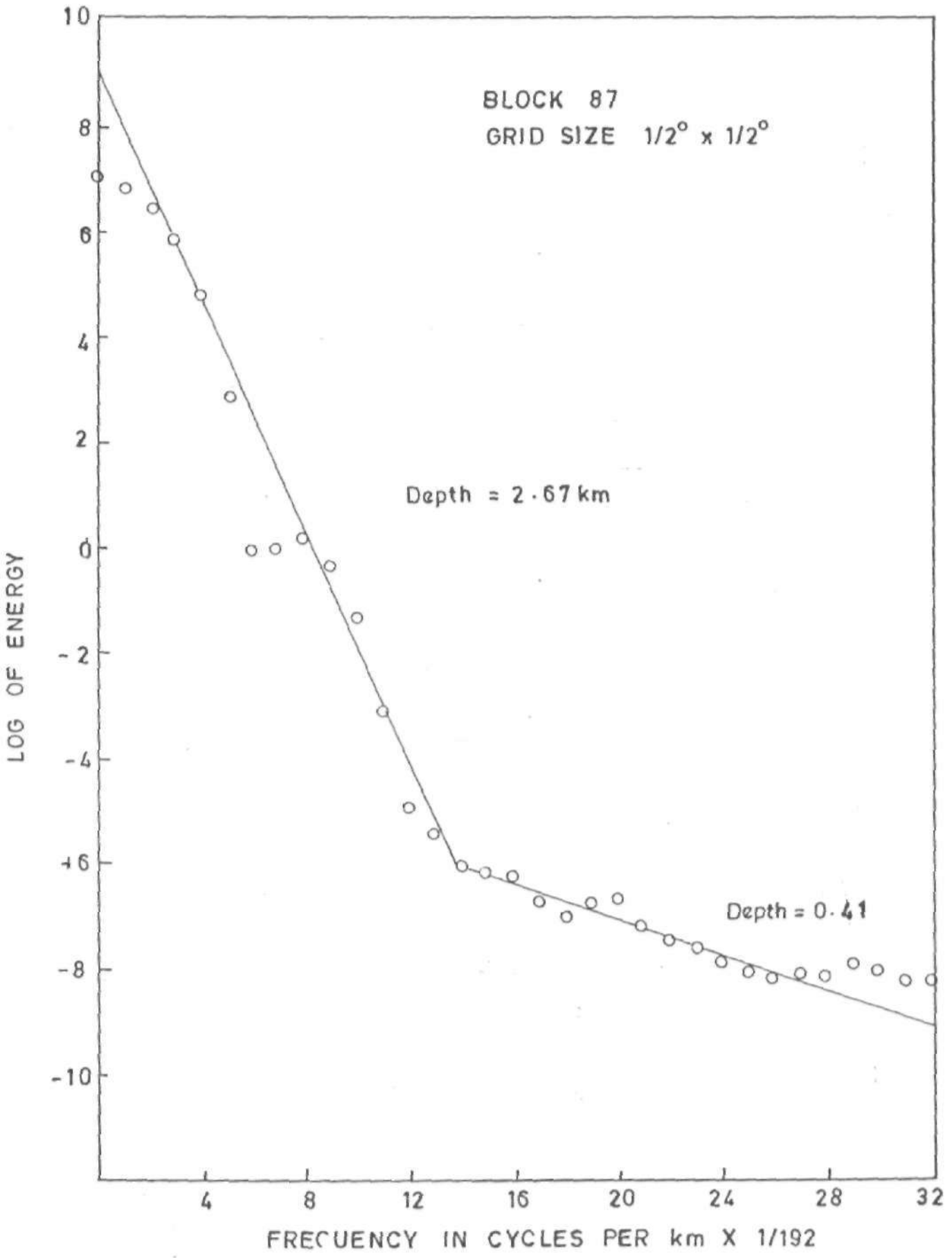
APPENDIX A

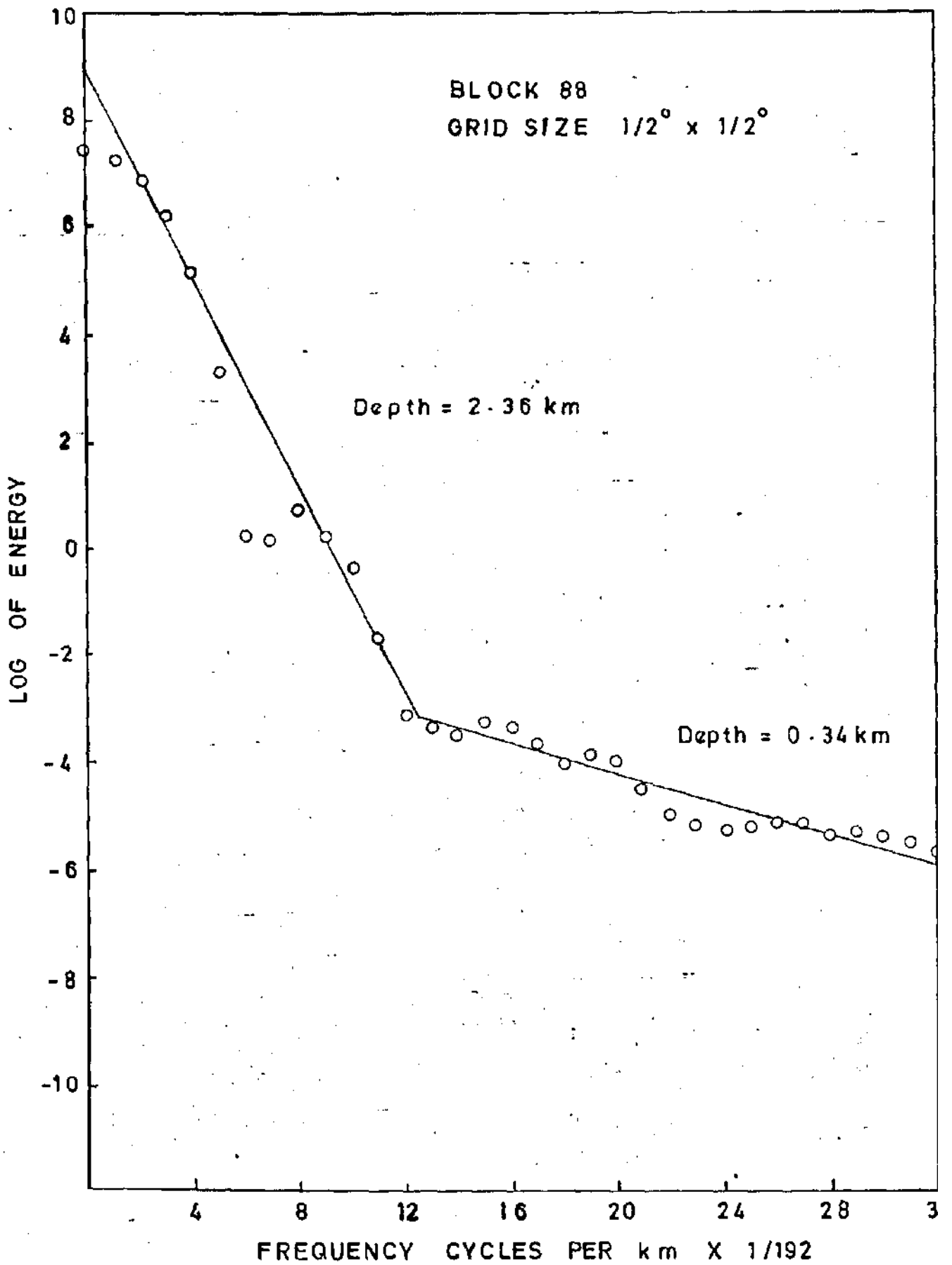
Spectral Plots for the $\frac{1}{2}^{o}$ x $\frac{1}{2}^{o}$ Blocks

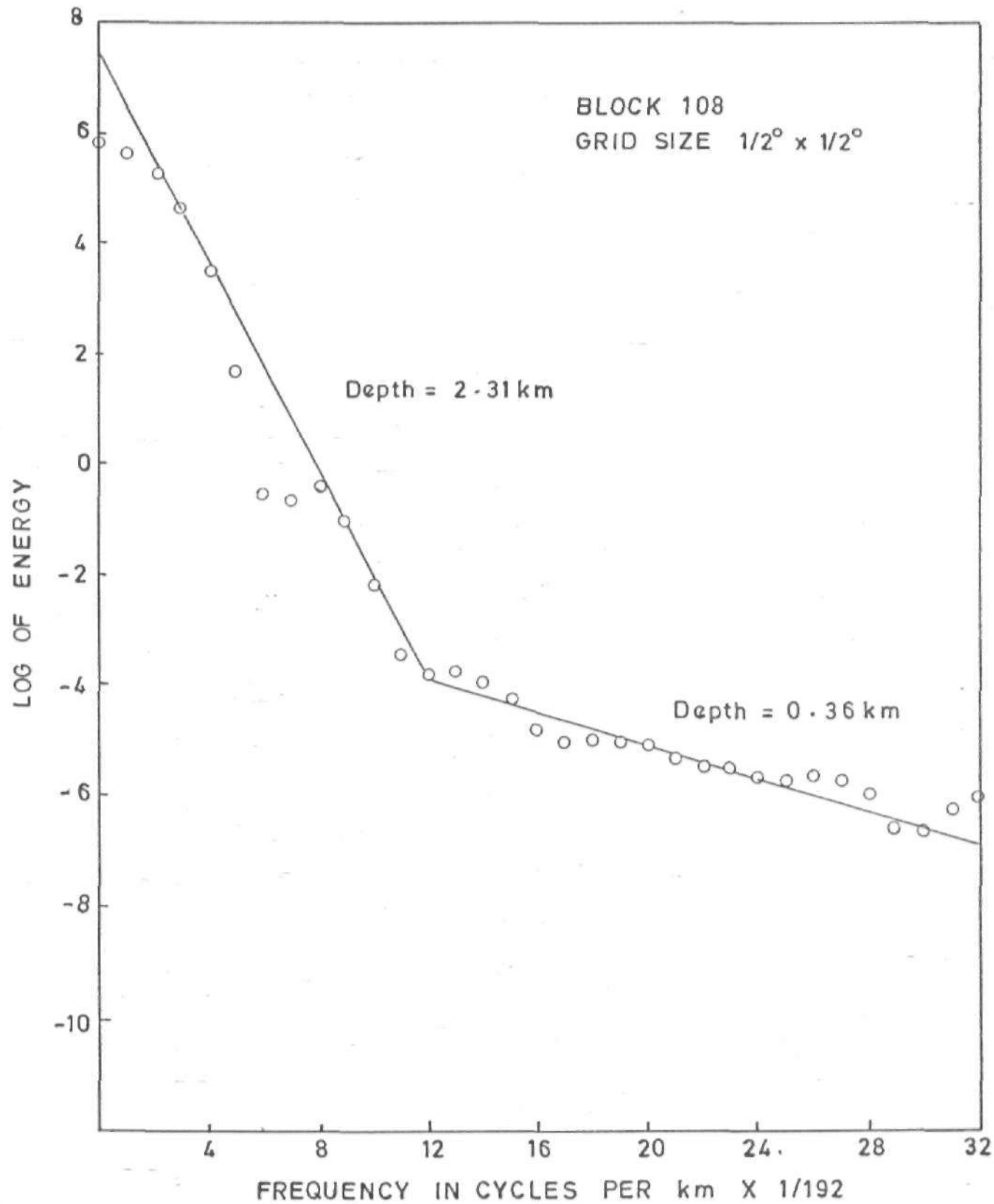

BLOCK 84
GRID SIZE 1/2° x 1/2°
Depth = 2·14 km
Depth = 0·32 km
LOG OF ENERGY
6
4
2
0
-2
-4
-6
-8
-10
4
8
12
16
20
24
28
32
FREQUENCY IN CYCLES PER km X 1/192

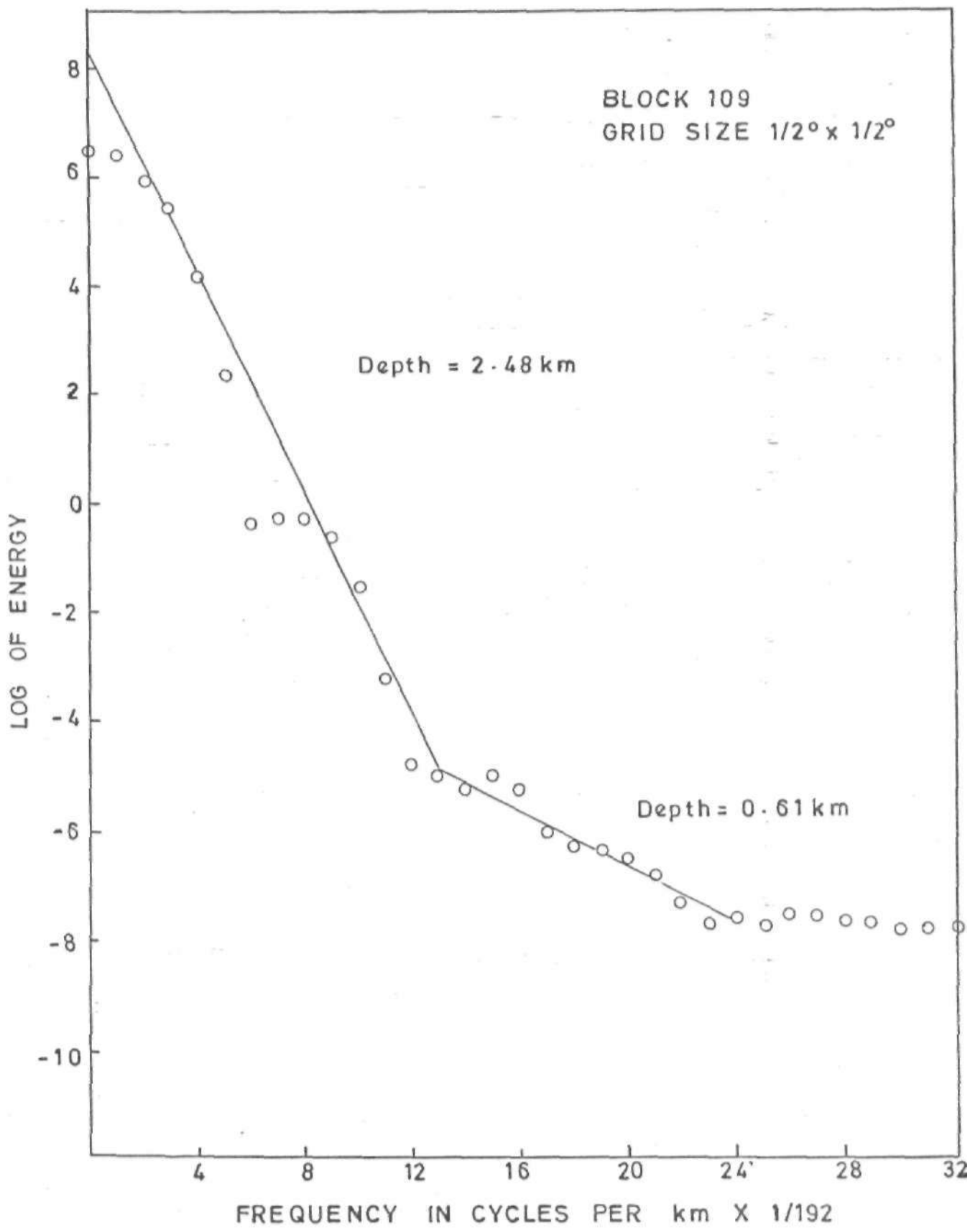

BLOCK 85
GRID SIZE 1/2° x 1/2°
Depth = 2.19 km
Depth = 0.29km
LOG OF ENERGY
8
6
4
2
0
-2
-4
-6
-8
-10
4
8
12
16
20
24
28
FREQUENCY IN CYCLES PER km X 1/192

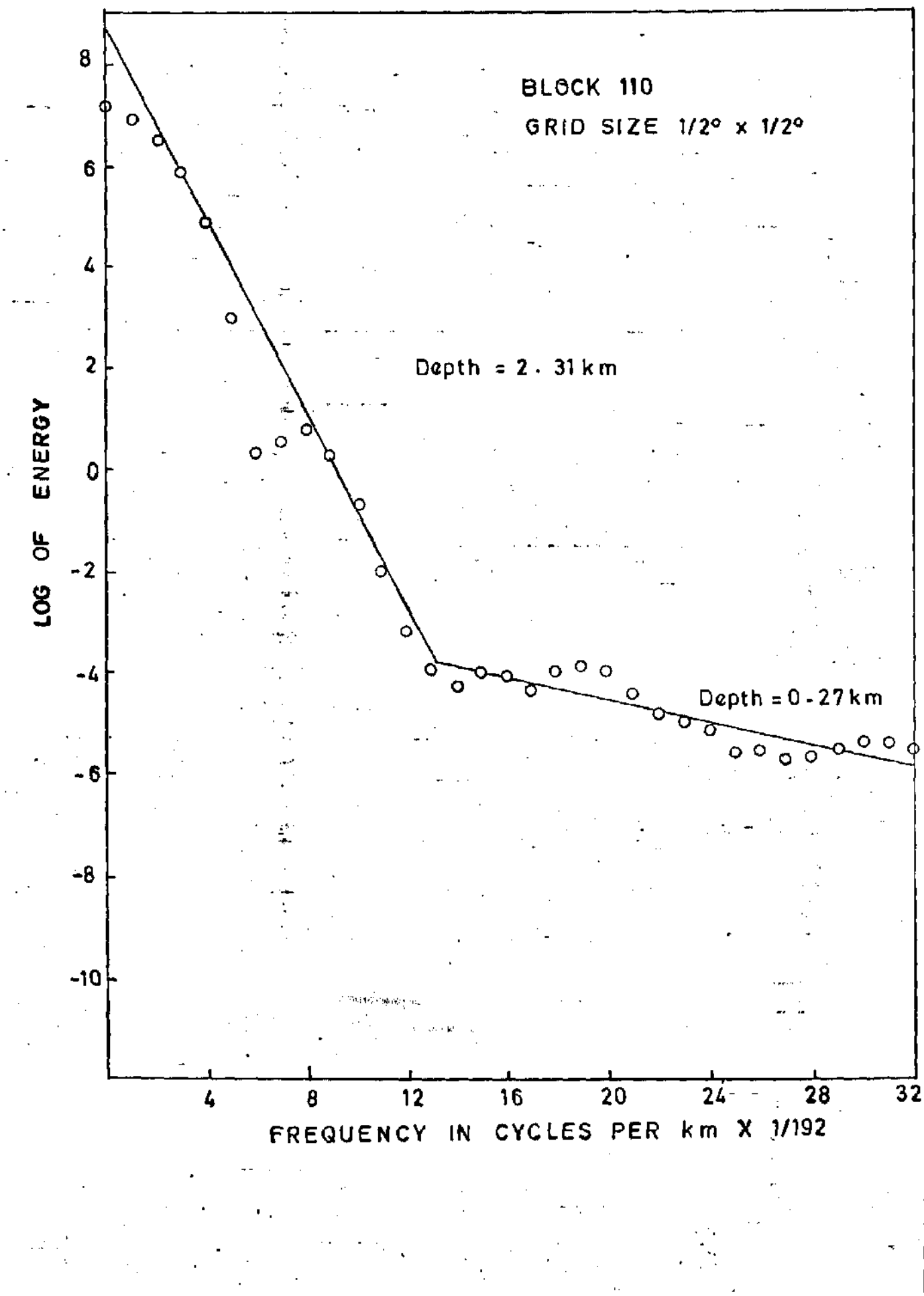

BLOCK 86
GRID SIZE 1/2° x 1/2°
Depth = 2·43km
Depth = 0·29km
LOG OF ENERGY
8
6
4
2
0
-2
-4
-6
-8
-10
4
8
12
16
20
24
28
FREQUENCY CYCLES PER km X 1/192

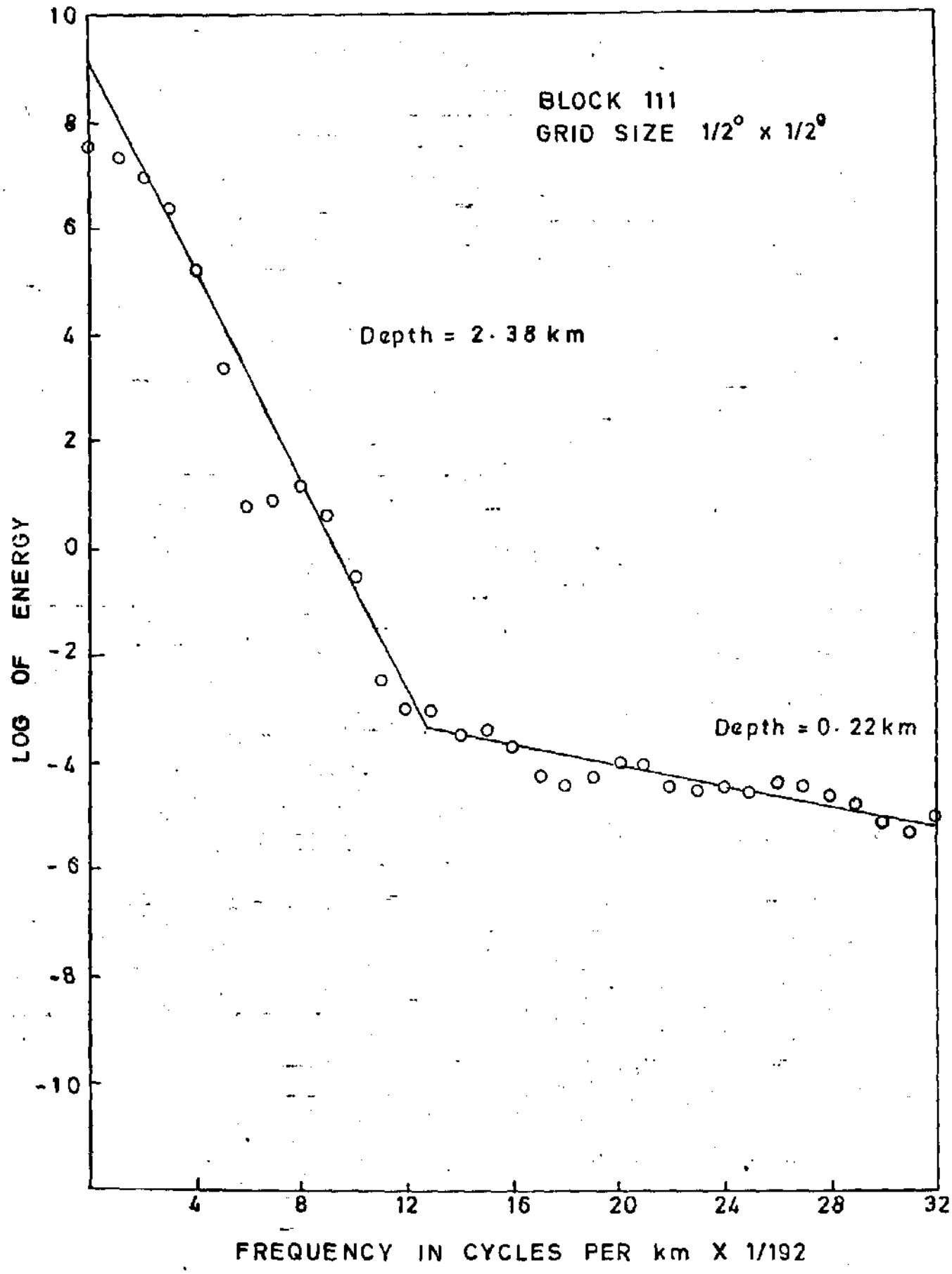

BLOCK 87
GRID SIZE 1/2° x 1/2°
Depth = 2·67 km
Depth = 0·41
LOG OF ENERGY
10
8
6
4
2
0
-2
-4
-6
-8
-10
4
8
12
16
20
24
28
32
FREQUENCY IN CYCLES PER km X 1/192

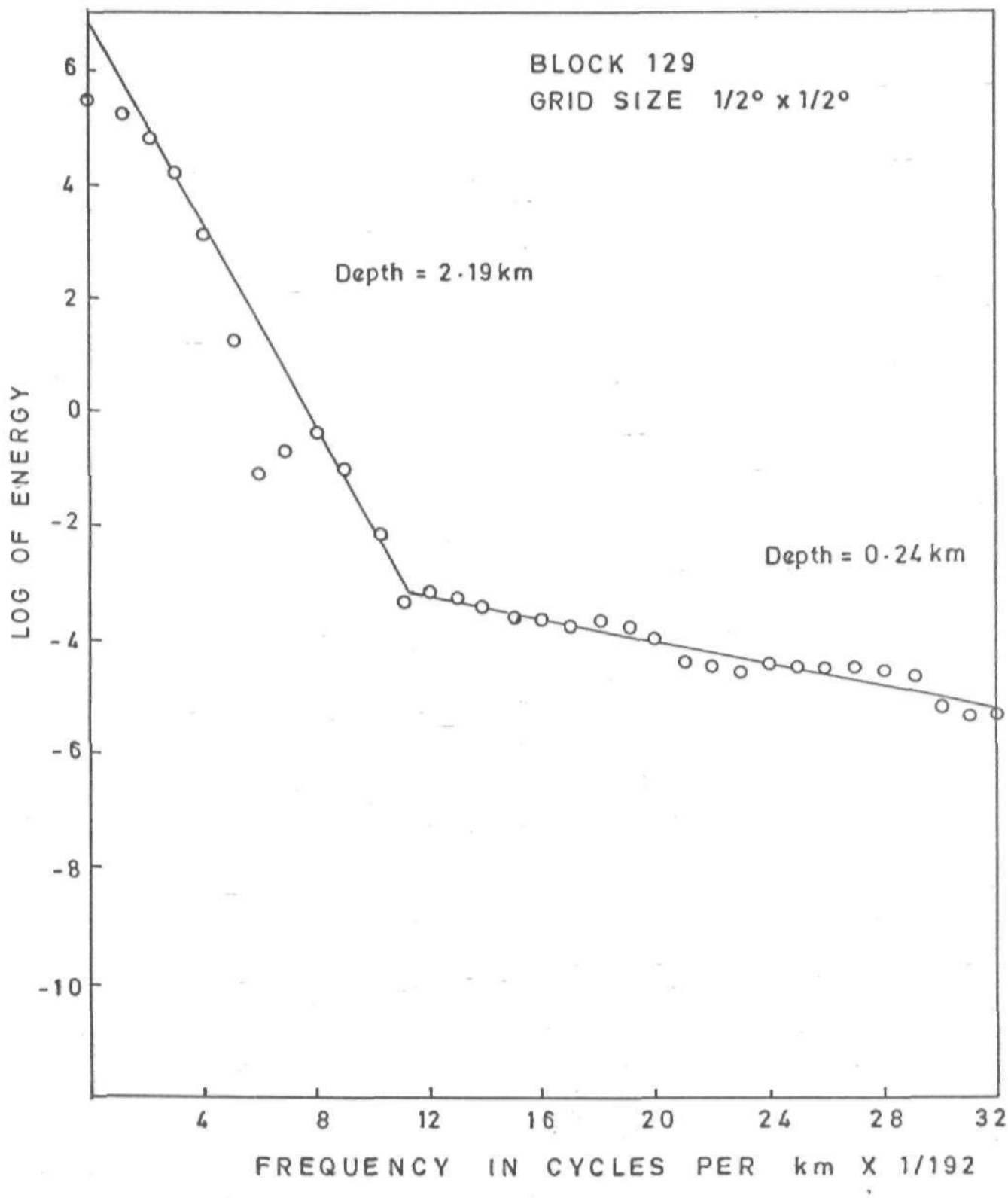

BLOCK 88
GRID SIZE 1/2° x 1/2°
Depth = 2·36 km
Depth = 0·34 km
LOG OF ENERGY
10
8
6
4
2
0
-2
-4
-6
-8
-10
4
8
12
16
20
24
28
3
FREQUENCY CYCLES PER km X 1/192

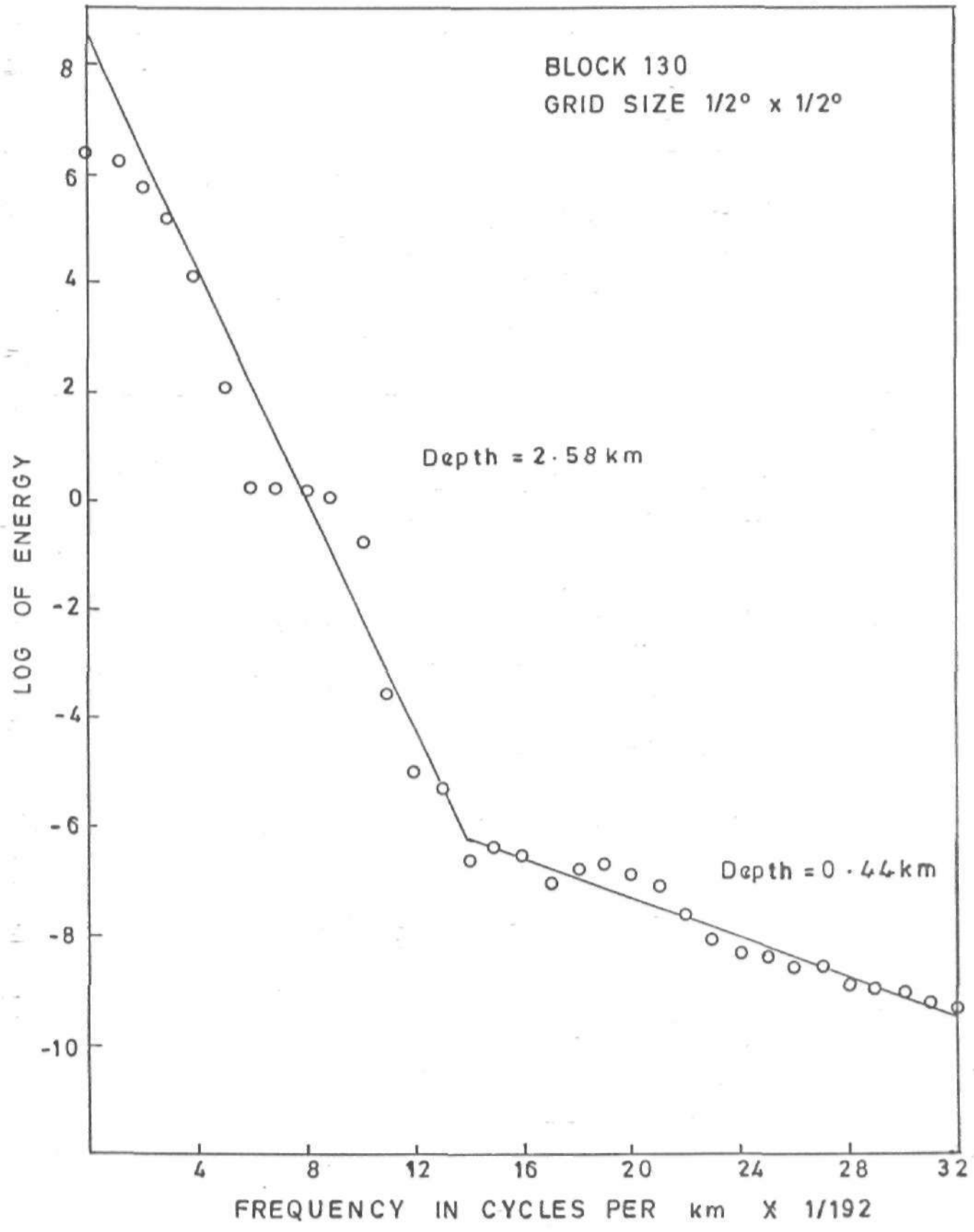

BLOCK 108
GRID SIZE 1/2° x 1/2°
Depth = 2·31 km
Depth = 0·36 km
LOG OF ENERGY
8
6
4
2
0
-2
-4
-6
-8
-10
4
8
12
16
20
24
28
32
FREQUENCY IN CYCLES PER km X 1/192

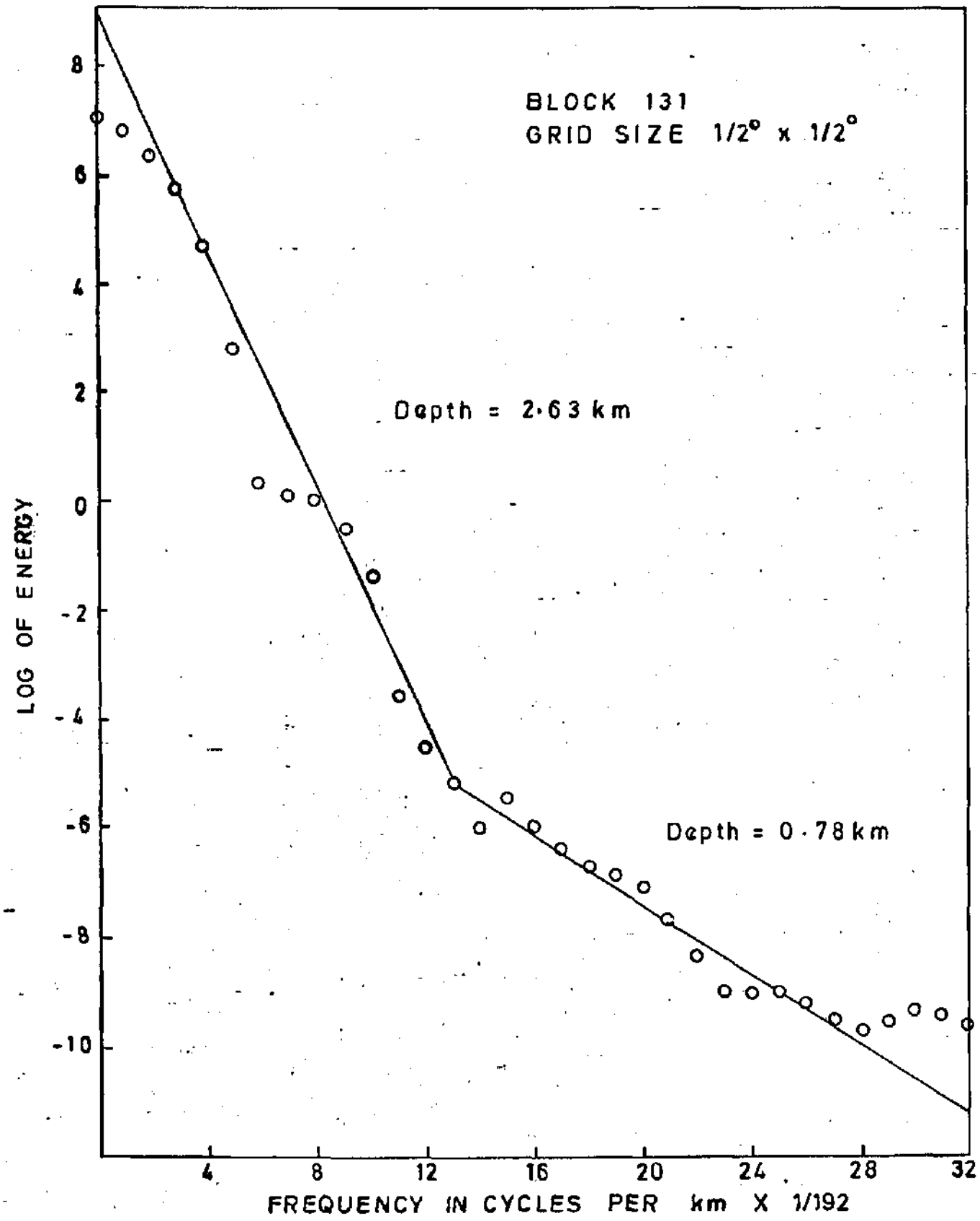

BLOCK 109
GRID SIZE 1/2° x 1/2°
Depth = 2·48 km
Depth = 0·61 km
LOG OF ENERGY
8
6
4
2
0
-2
-4
-6
-8
-10
4
8
12
16
20
24
28
32
FREQUENCY IN CYCLES PER km X 1/192

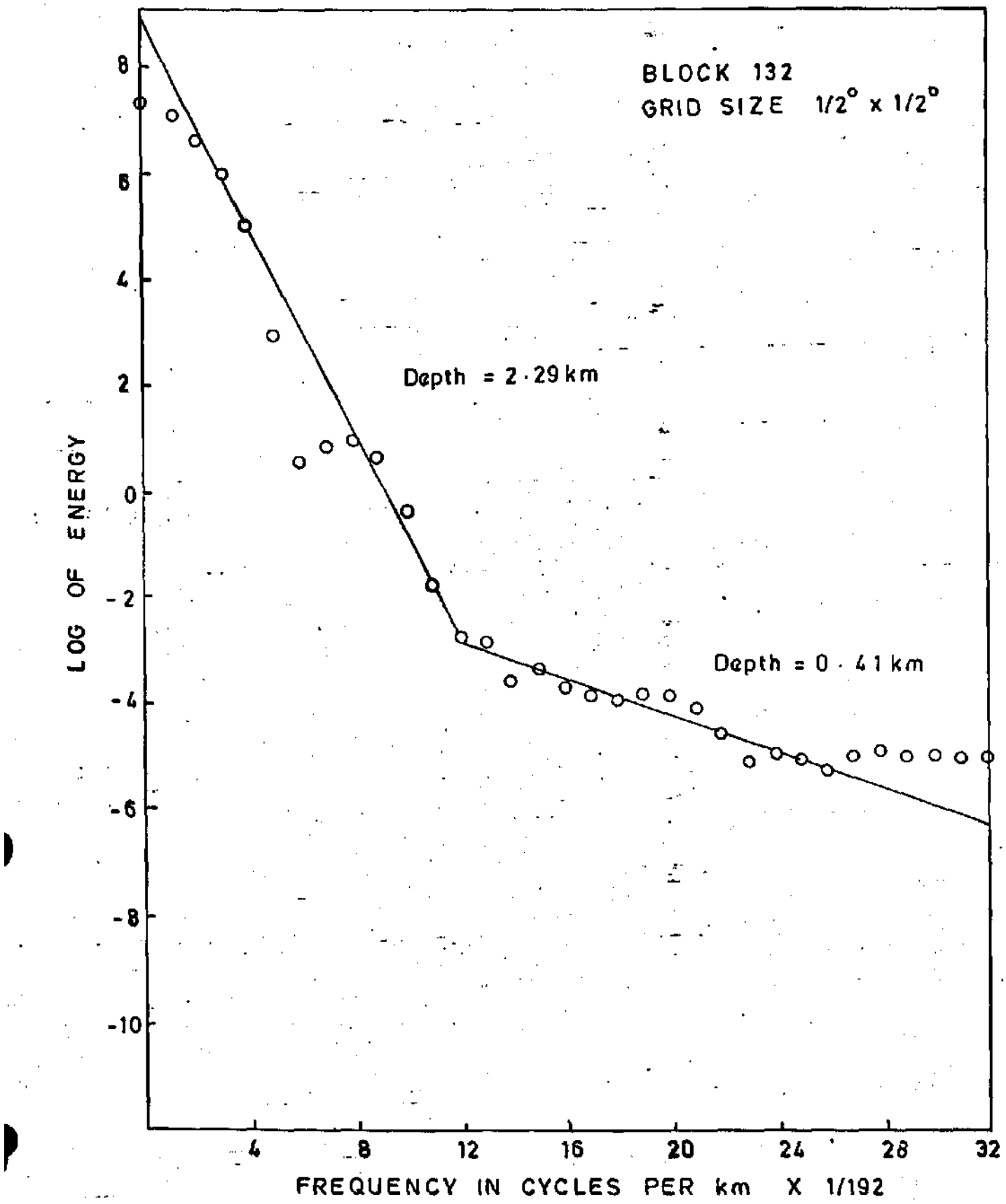

BLOCK 110
GRID SIZE 1/2° x 1/2°
Depth = 2 . 31 km
Depth = 0 - 27 km
LOG OF ENERGY
8
6
4
2
0
-2
-4
-6
-8
-10
4
8
12
16
20
24
28
32
FREQUENCY IN CYCLES PER km X 1/192

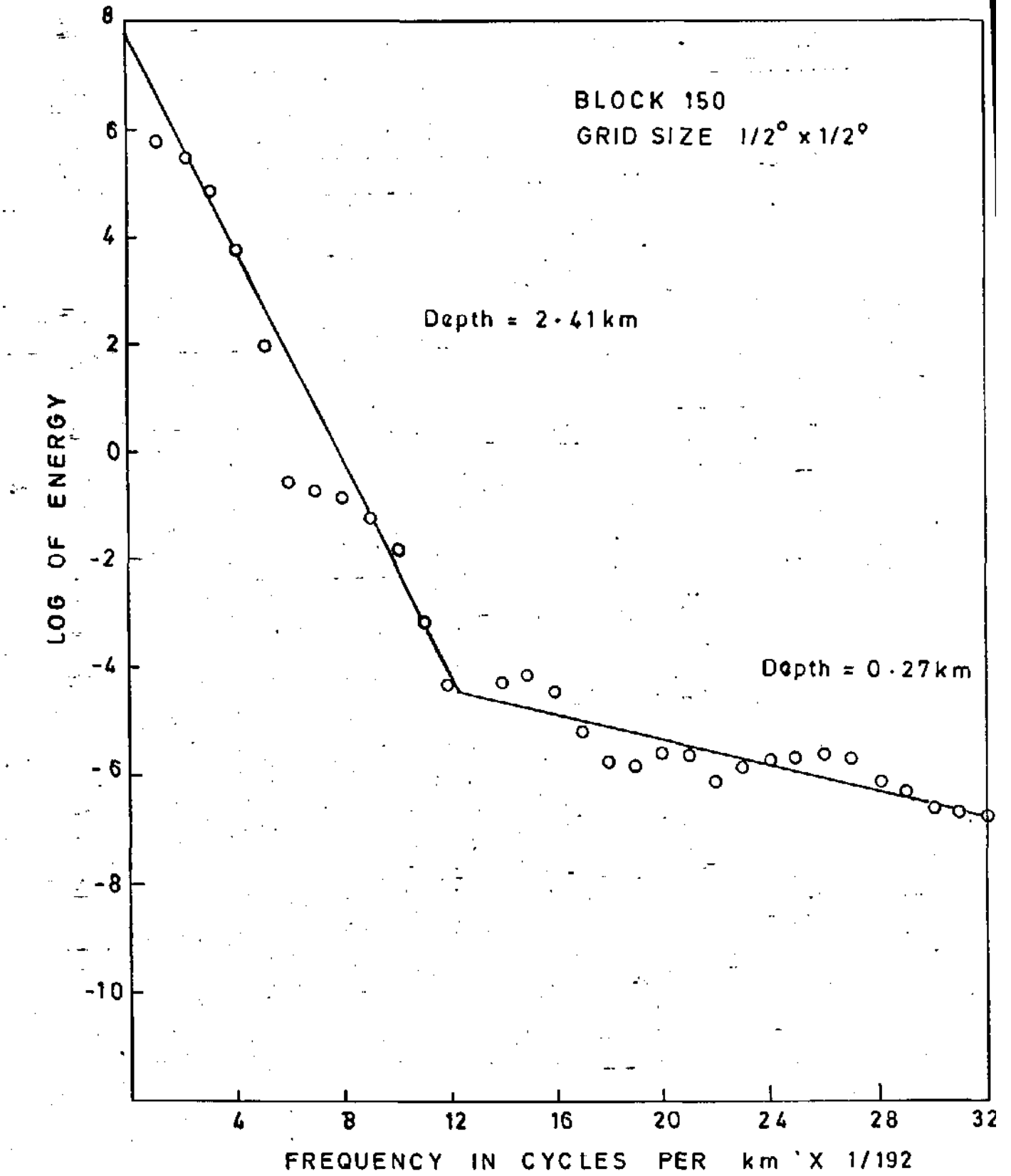

BLOCK 111
GRID SIZE 1/2° x 1/2°
Depth = 2·38 km
Depth = 0·22 km
LOG OF ENERGY
10
8
6
4
2
0
-2
-4
-6
-8
-10
4
8
12
16
20
24
28
32
FREQUENCY IN CYCLES PER km X 1/192

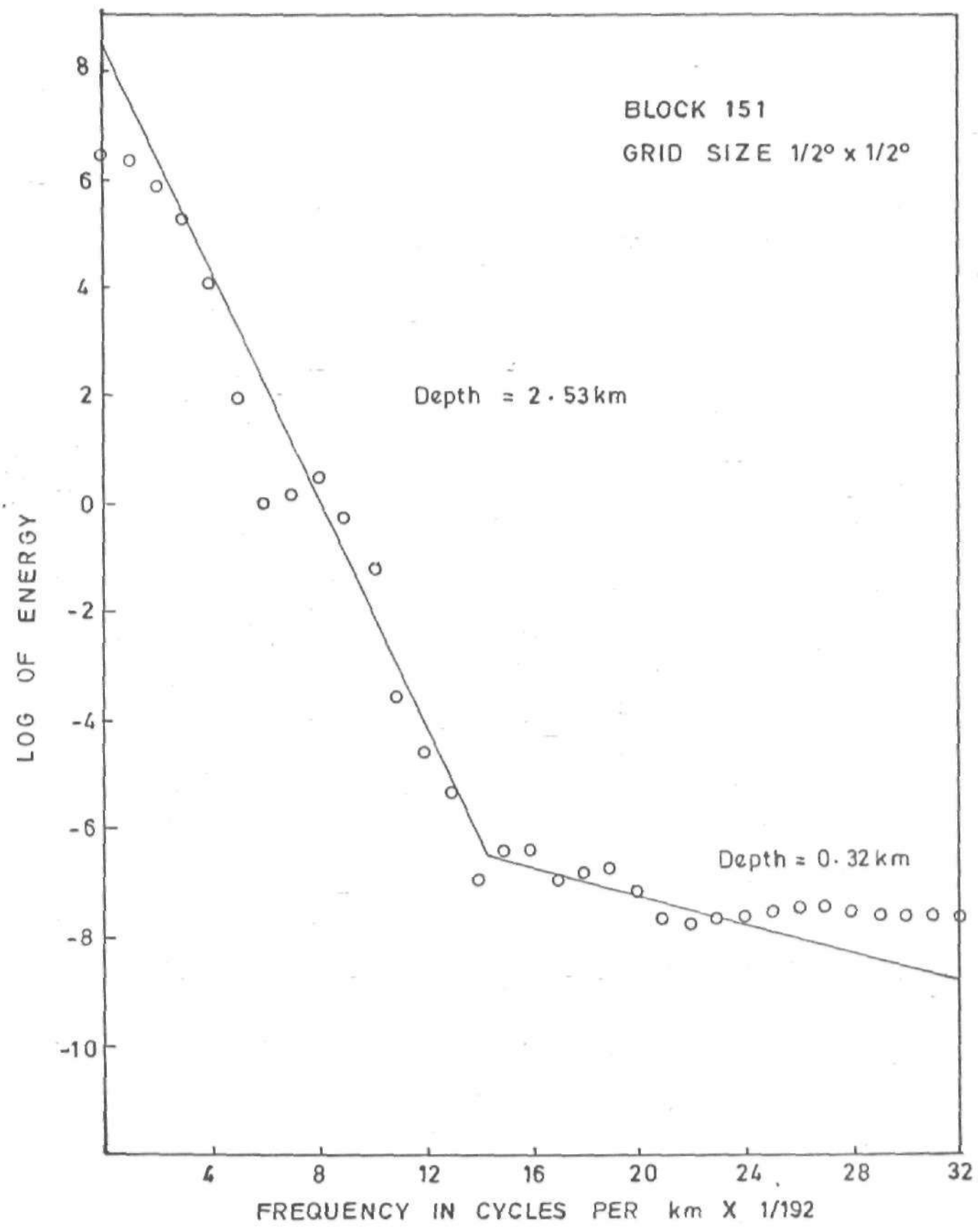

BLOCK 129
GRID SIZE 1/2° x 1/2°
Depth = 2·19 km
Depth = 0·24 km
LOG OF ENERGY
6
4
2
0
-2
-4
-6
-8
-10
4
8
12
16
20
24
28
32
FREQUENCY IN CYCLES PER km X 1/192

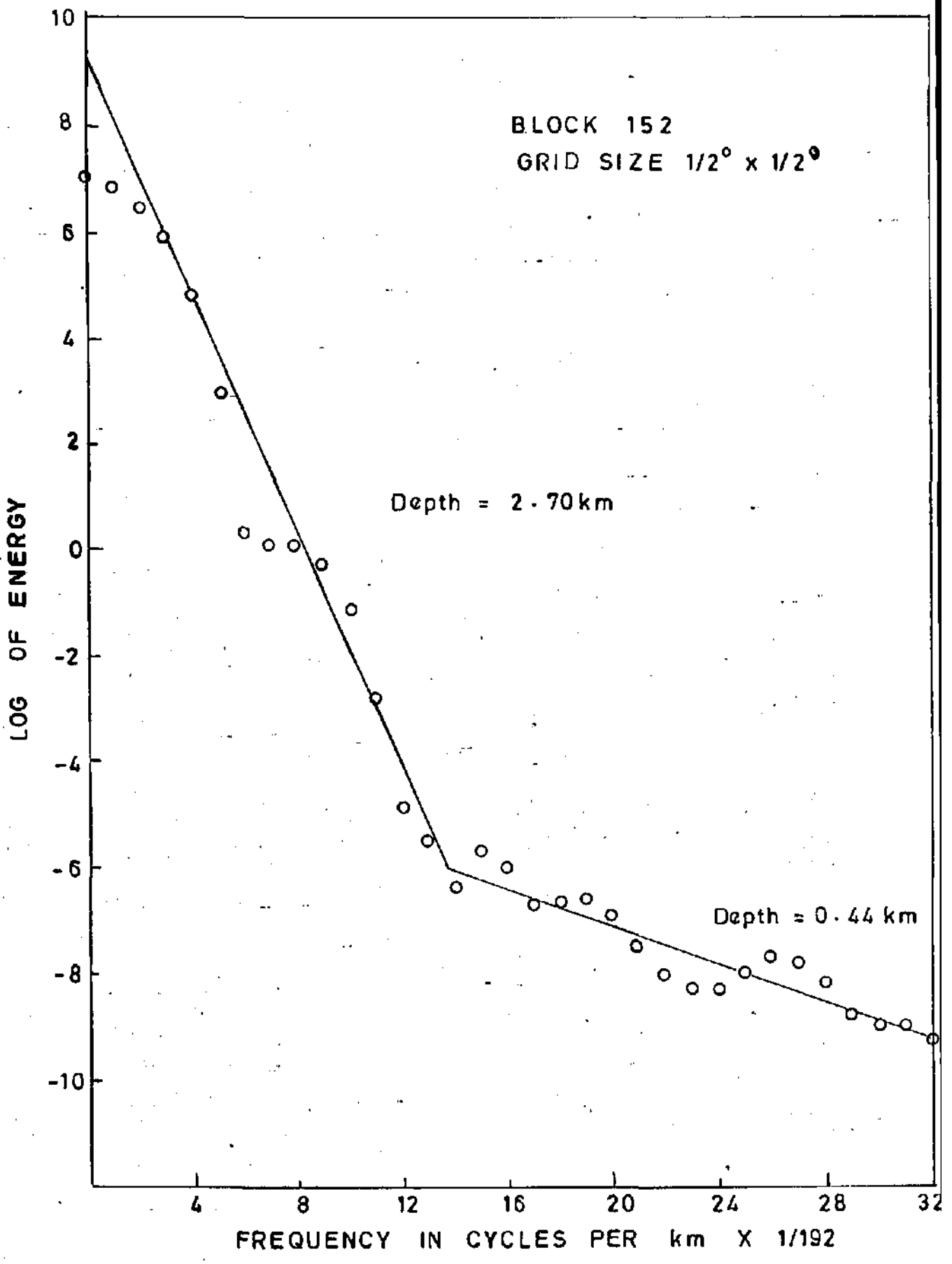

BLOCK 130
GRID SIZE 1/2° x 1/2°
Depth = 2·58 km
Depth = 0·44 km
LOG OF ENERGY
8
6
4
2
0
-2
-4
-6
-8
-10
4
8
12
16
20
24
28
32
FREQUENCY IN CYCLES PER km X 1/192

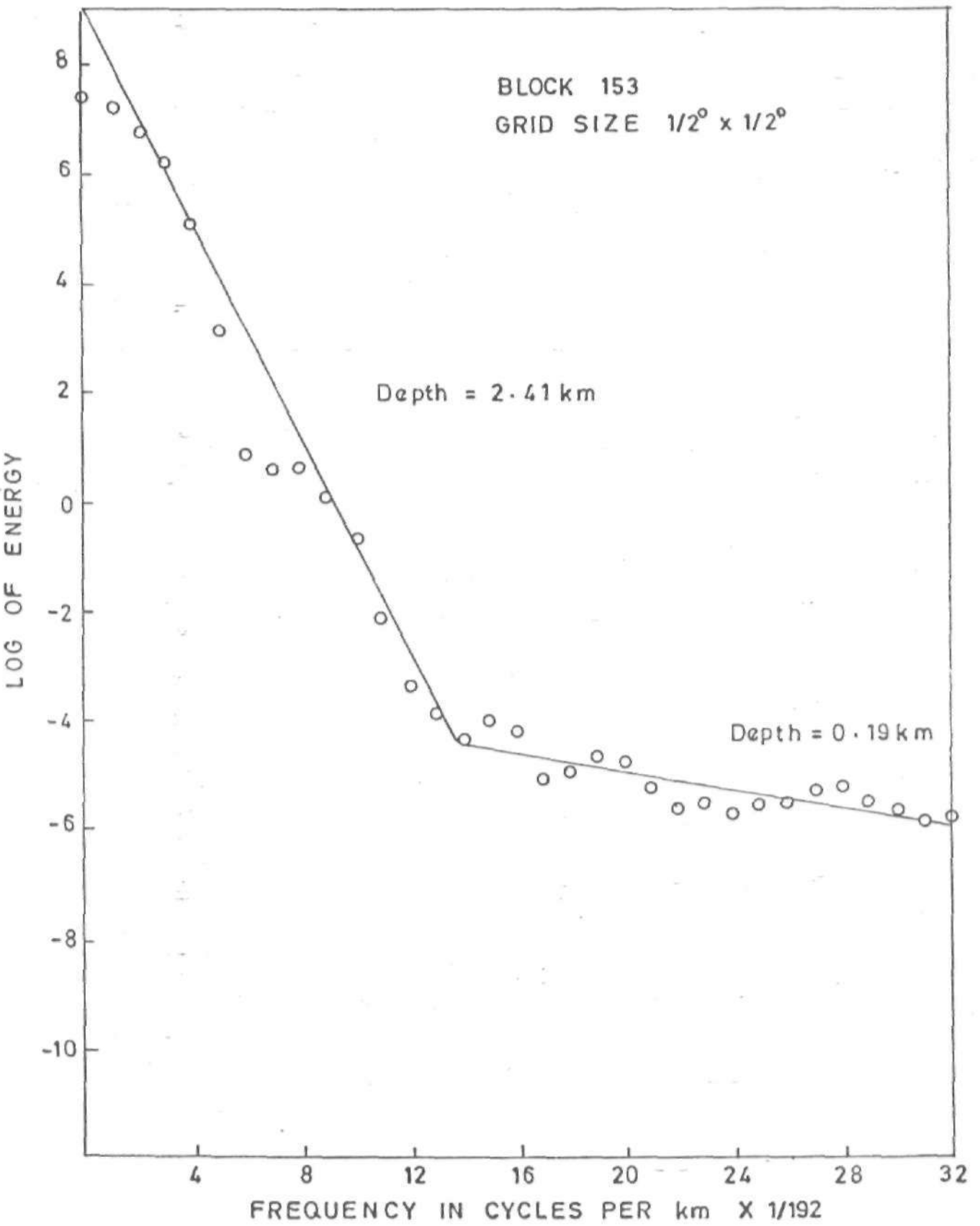

BLOCK 131
GRID SIZE 1/2° x 1/2°
Depth = 2·63 km
Depth = 0·78 km
LOG OF ENERGY
8
6
4
2
0
-2
-4
-6
-8
-10
4
8
12
16
20
24
28
32
FREQUENCY IN CYCLES PER km X 1/192

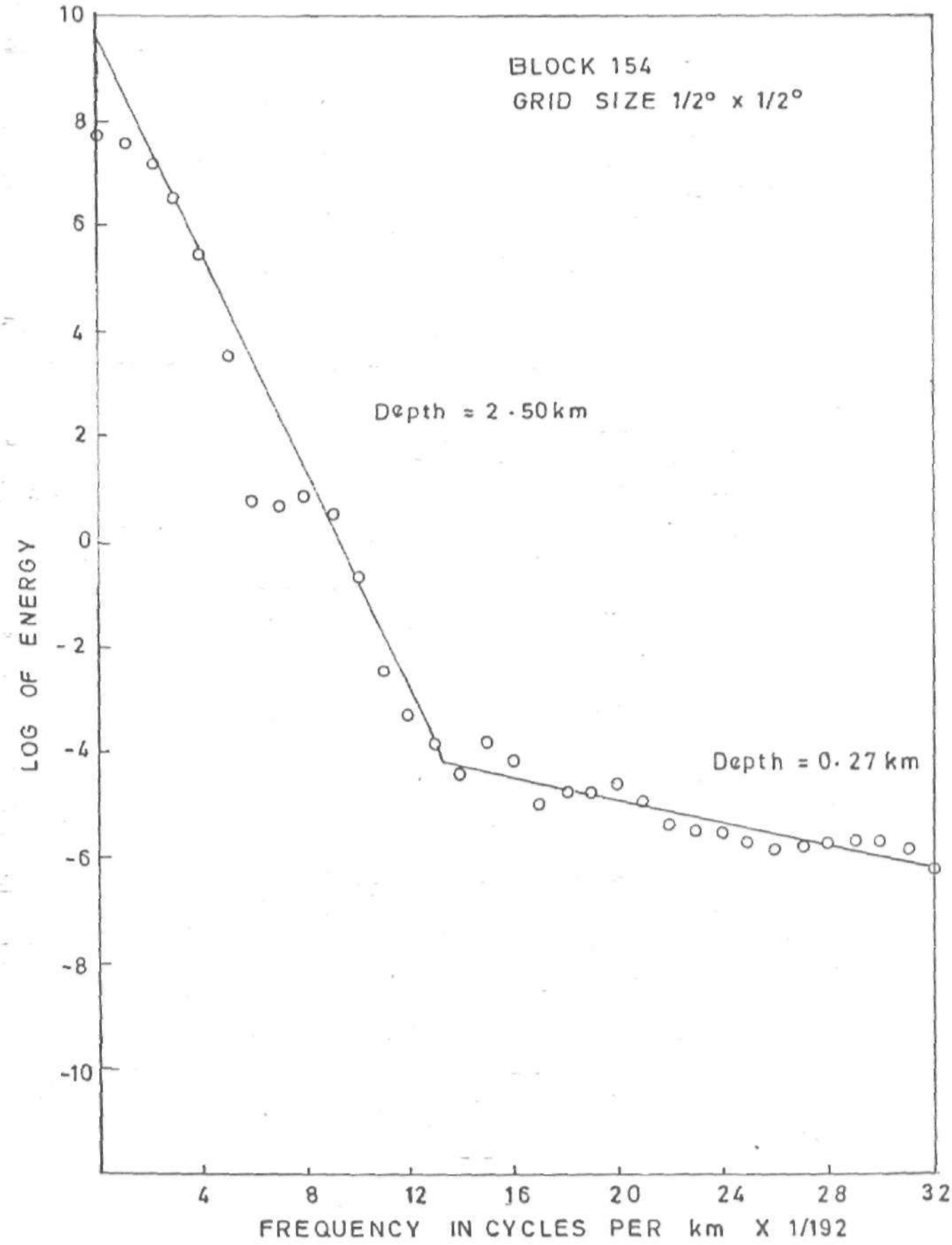

BLOCK 132
GRID SIZE 1/2° x 1/2°
Depth = 2·29 km
Depth = 0·41 km
LOG OF ENERGY
8
6
4
2
0
-2
-4
-6
-8
-10
4
8
12
16
20
24
28
32
FREQUENCY IN CYCLES PER km X 1/192

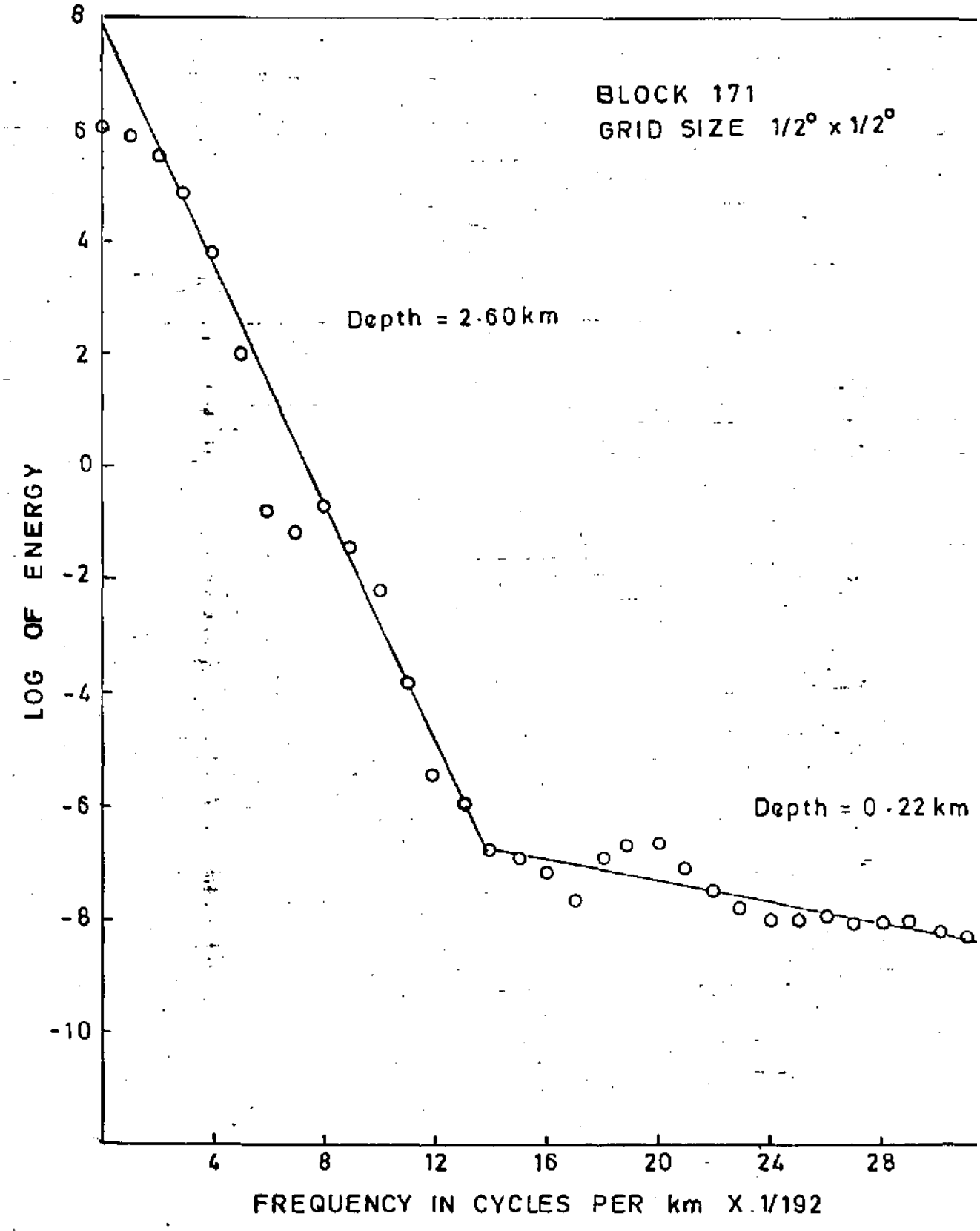

BLOCK 150
GRID SIZE 1/2° x 1/2°
Depth = 2·41 km
Depth = 0·27 km
LOG OF ENERGY
8
6
4
2
0
-2
-4
-6
-8
-10
4
8
12
16
20
24
28
32
FREQUENCY IN CYCLES PER km X 1/192

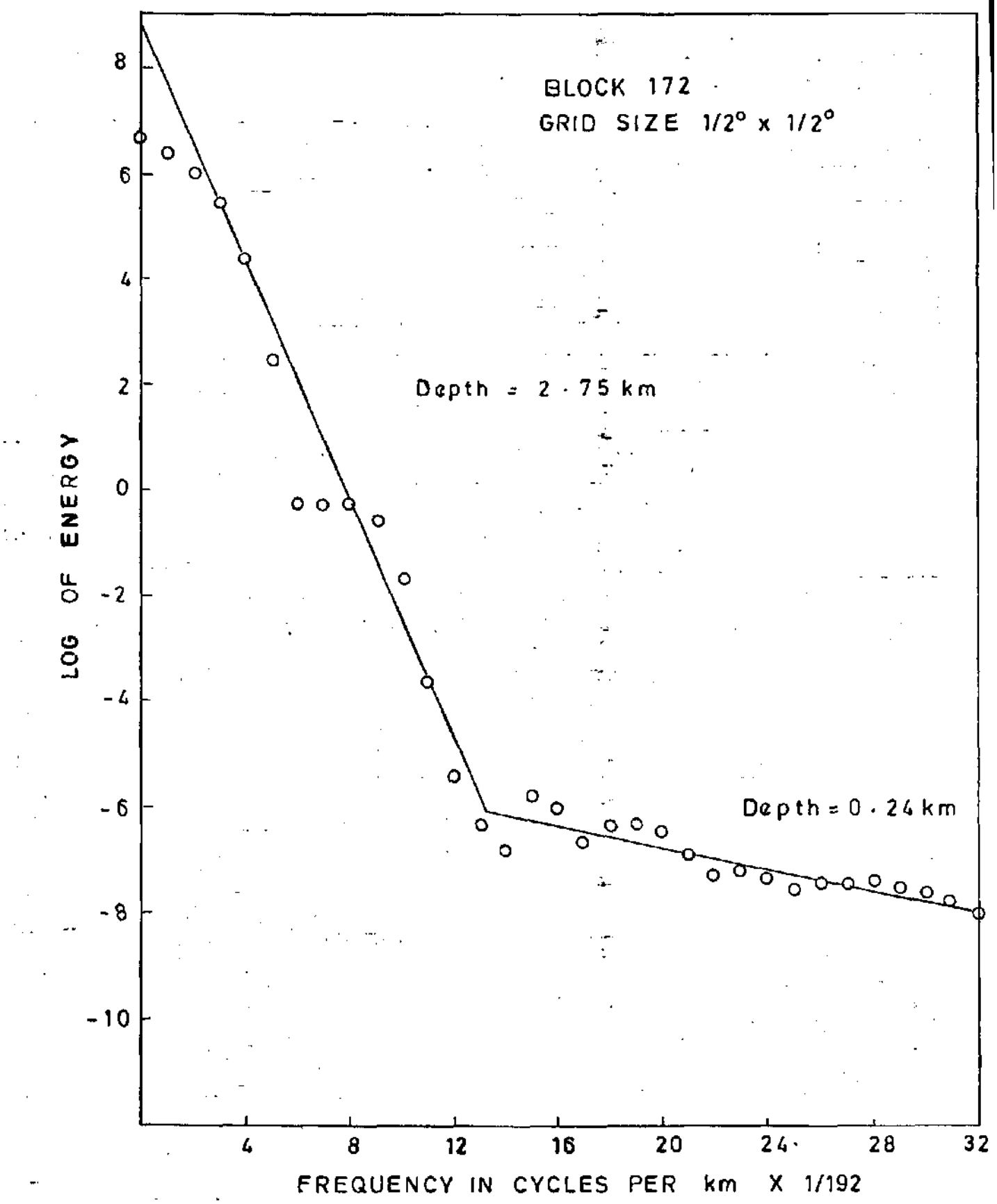

BLOCK 151
GRID SIZE 1/2° x 1/2°
Depth = 2·53km
Depth = 0·32km
LOG OF ENERGY
8
6
4
2
0
-2
-4
-6
-8
-10
4
8
12
16
20
24
28
32
FREQUENCY IN CYCLES PER km X 1/192

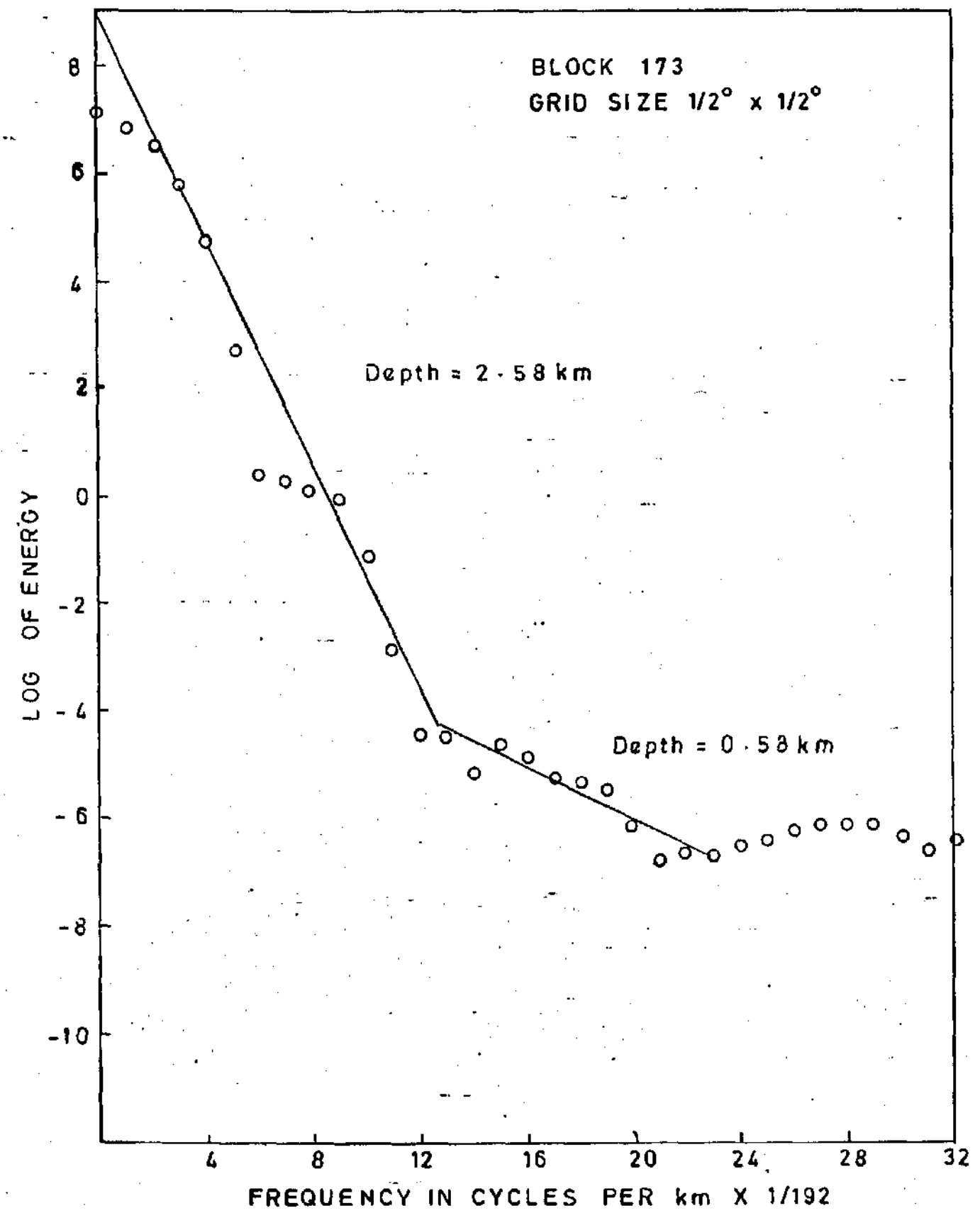

BLOCK 152
GRID SIZE 1/2° x 1/2°
Depth = 2.70 km
Depth = 0.44 km
LOG OF ENERGY
10
8
6
4
2
0
-2
-4
-6
-8
-10
4
8
12
16
20
24
28
32
FREQUENCY IN CYCLES PER km X 1/192

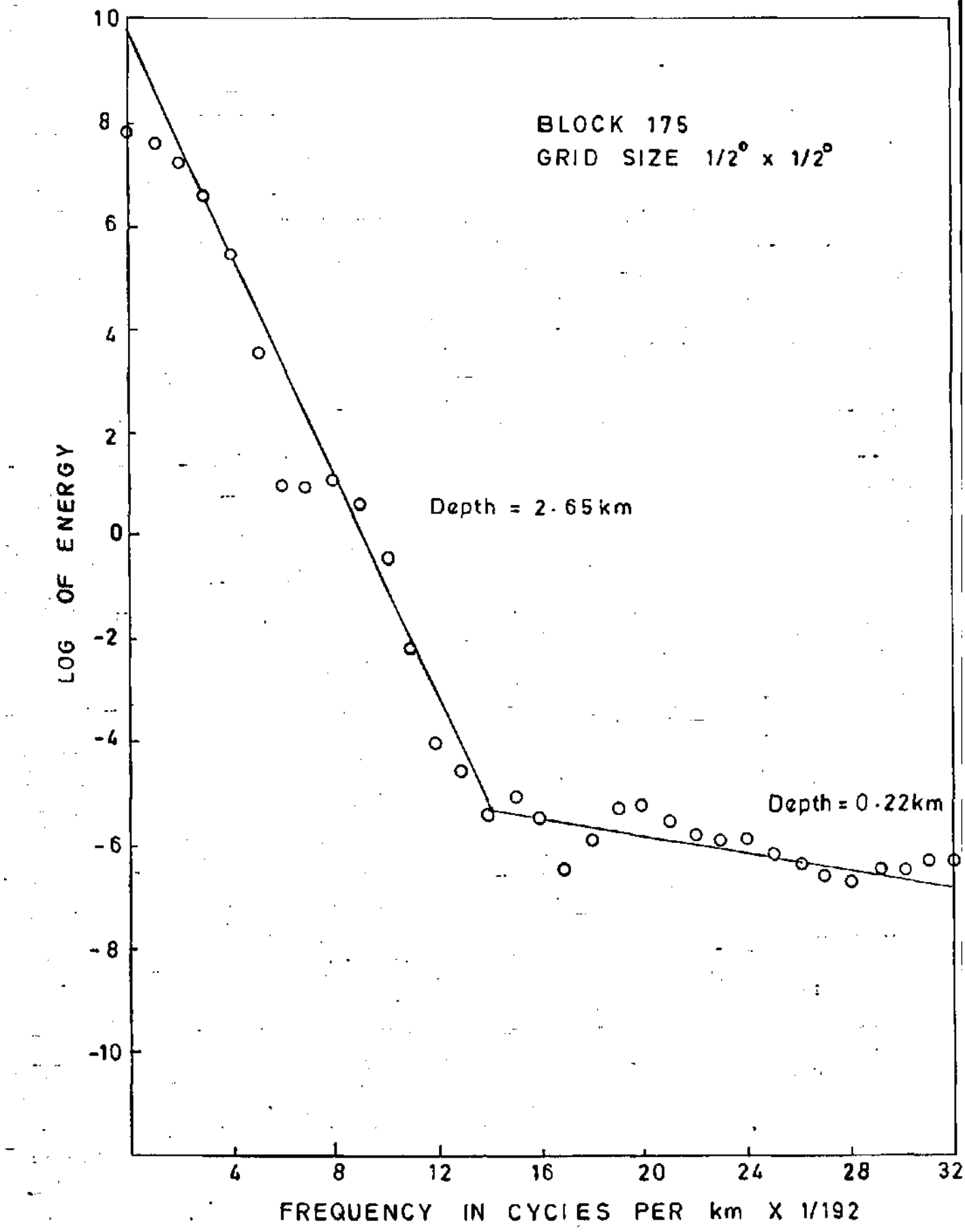

BLOCK 153
GRID SIZE 1/2° x 1/2°
Depth = 2·41 km
Depth = 0·19 km
LOG OF ENERGY
8
6
4
2
0
-2
-4
-6
-8
-10
4
8
12
16
20
24
28
32
FREQUENCY IN CYCLES PER km X 1/192

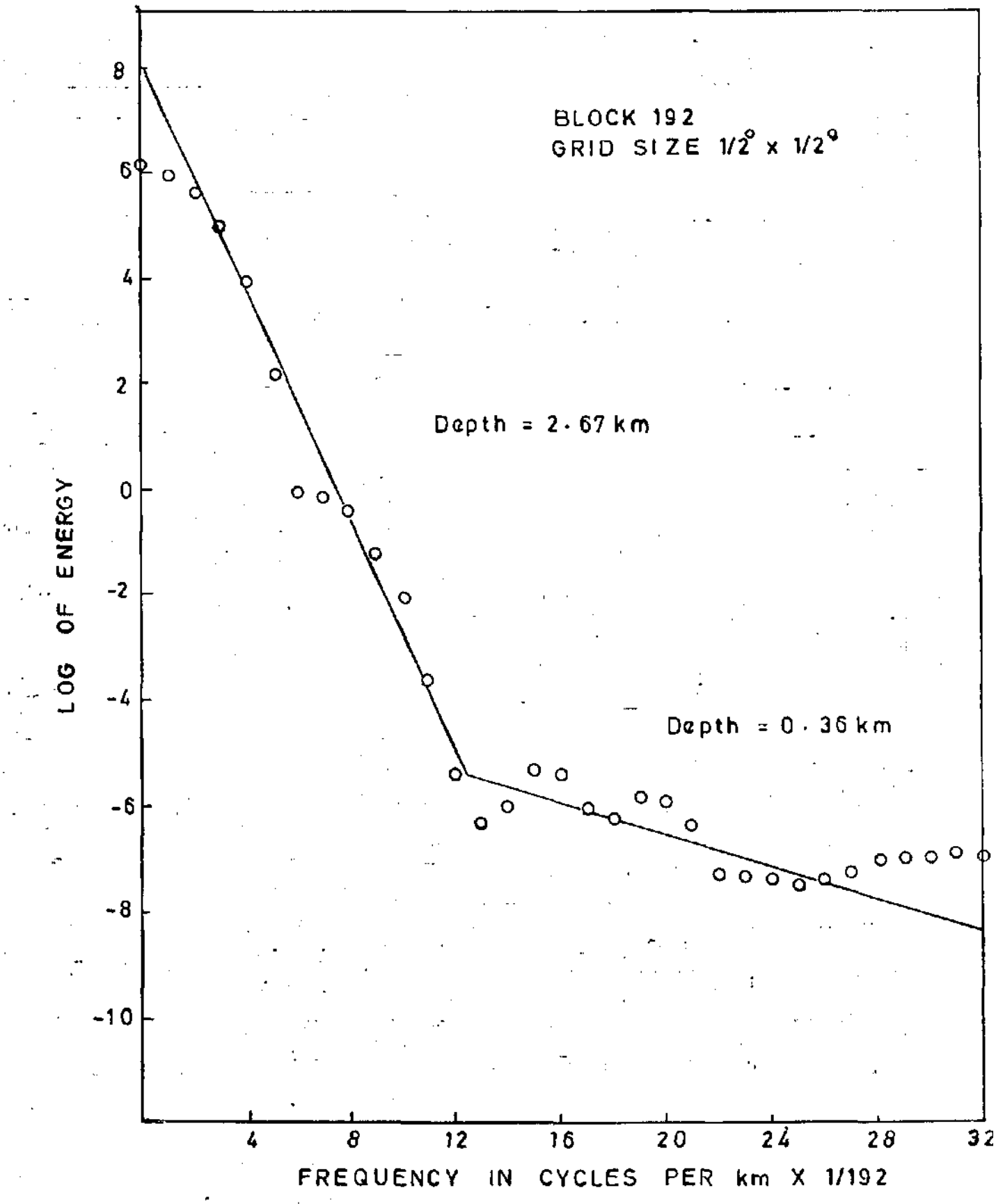

BLOCK 154
GRID SIZE 1/2° x 1/2°
Depth = 2·50 km
Depth = 0·27 km
LOG OF ENERGY
10
8
6
4
2
0
-2
-4
-6
-8
-10
4
8
12
16
20
24
28
32
FREQUENCY IN CYCLES PER km X 1/192

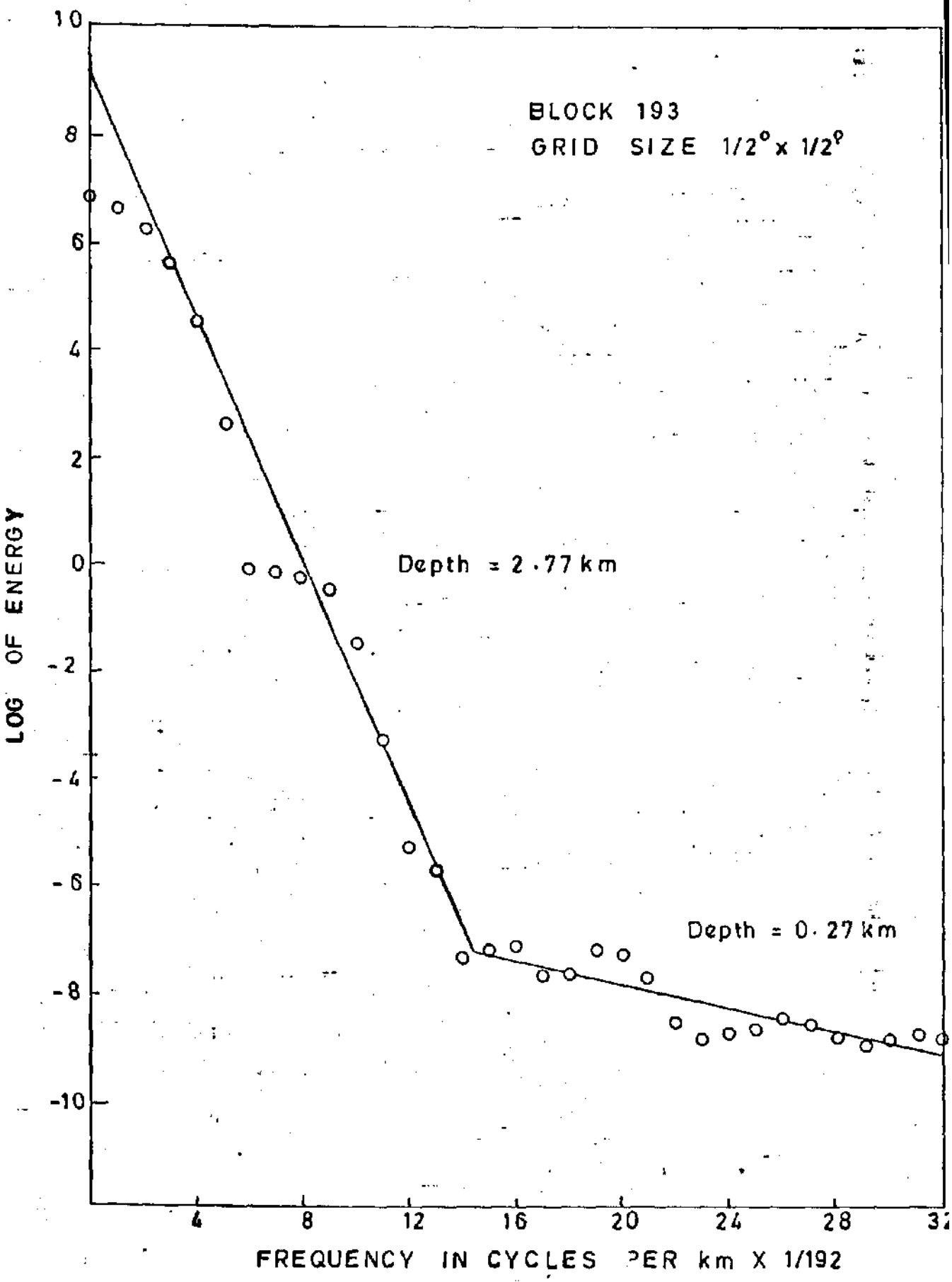

BLOCK 171
GRID SIZE 1/2° x 1/2°
Depth = 2·60km
Depth = 0·22km
LOG OF ENERGY
8
6
4
2
0
-2
-4
-6
-8
-10
4
8
12
16
20
24
28
FREQUENCY IN CYCLES PER km X 1/192

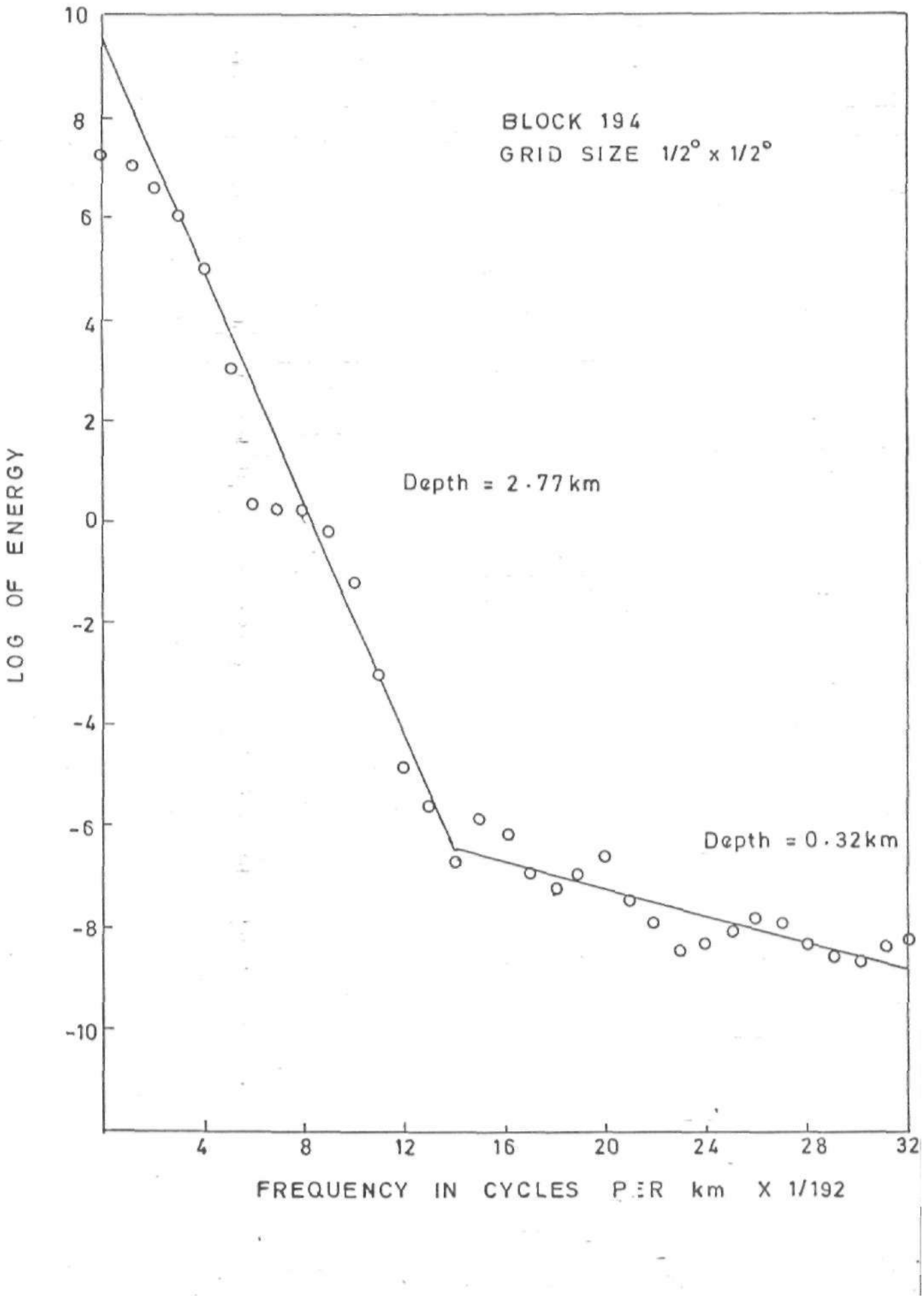

BLOCK 172
GRID SIZE 1/2° x 1/2°
Depth = 2 · 75 km
Depth = 0 · 24 km
LOG OF ENERGY
8
6
4
2
0
-2
-4
-6
-8
-10
4
8
12
16
20
24
28
32
FREQUENCY IN CYCLES PER km X 1/192

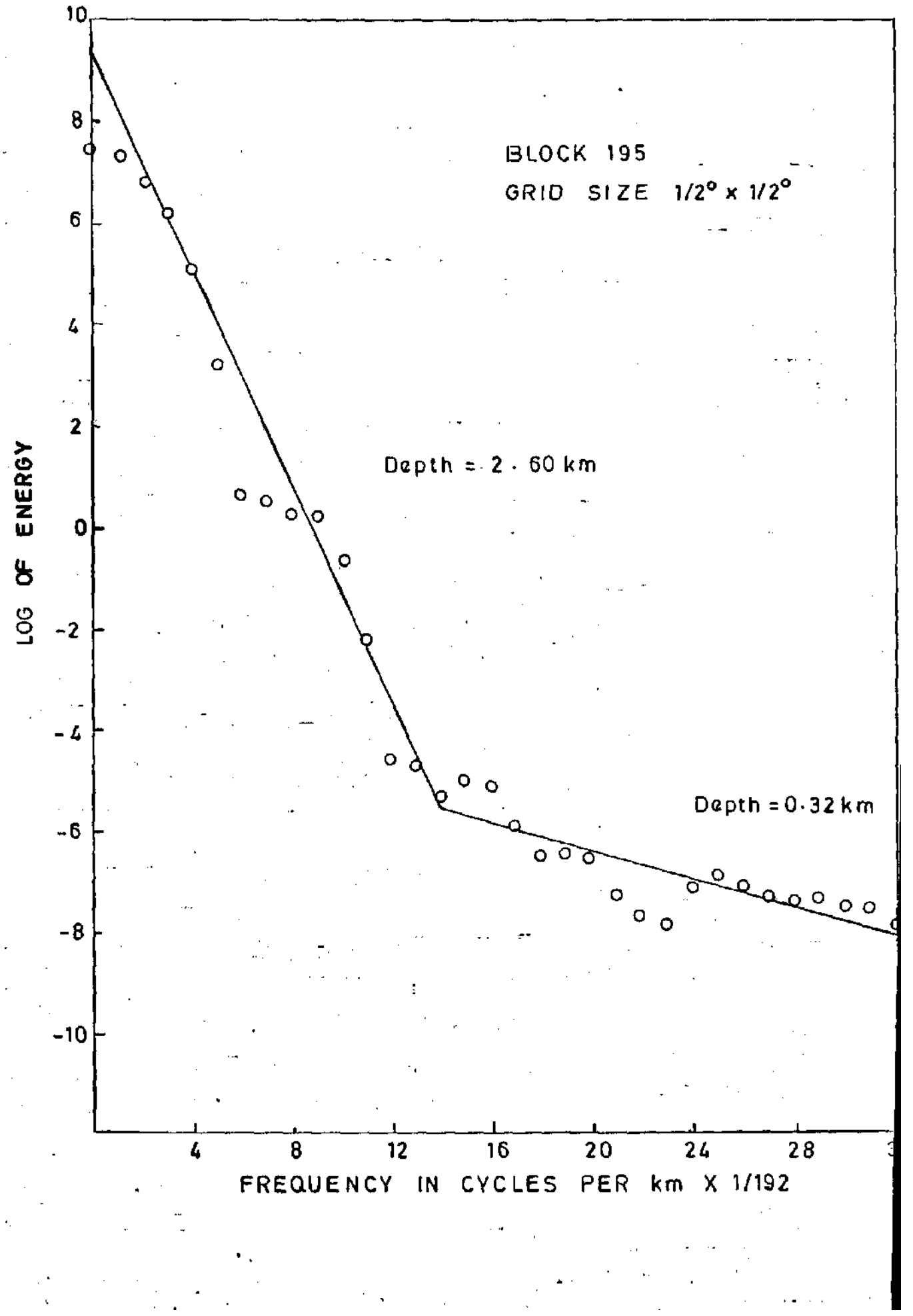

BLOCK 173
GRID SIZE 1/2° x 1/2°
Depth = 2·58 km
Depth = 0·58 km
LOG OF ENERGY
8
6
4
2
0
-2
-4
-6
-8
-10
4
8
12
16
20
24
28
32
FREQUENCY IN CYCLES PER km X 1/192

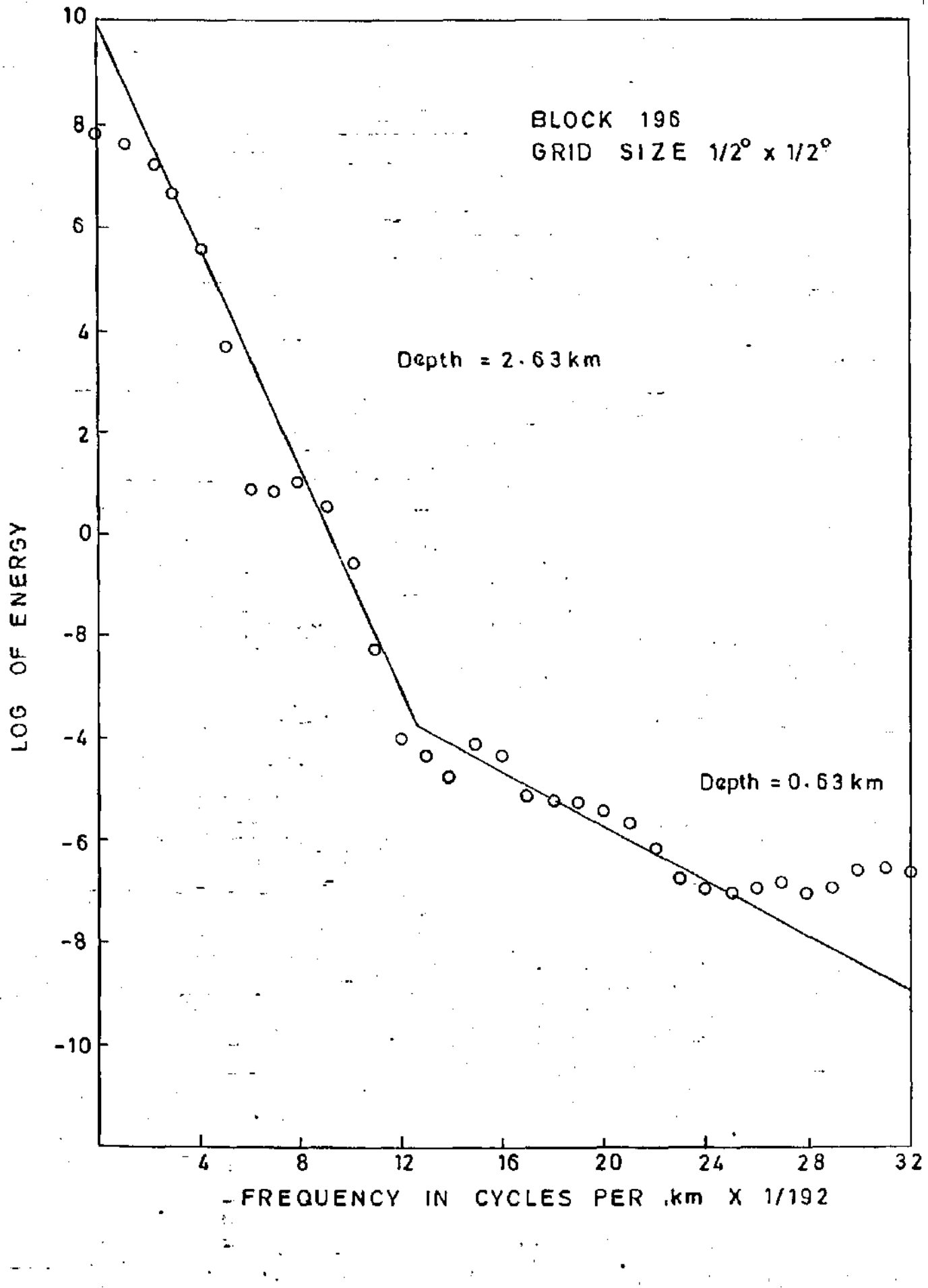

BLOCK 175
GRID SIZE 1/2° x 1/2°
Depth = 2·65 km
Depth = 0·22km
LOG OF ENERGY
10
8
6
4
2
0
-2
-4
-6
-8
-10
4
8
12
16
20
24
28
32
FREQUENCY IN CYCLES PER km X 1/192


BLOCK 192
GRID SIZE 1/2° x 1/2°
Depth = 2·67 km
Depth = 0·36 km
LOG OF ENERGY
8
6
4
2
0
-2
-4
-6
-8
-10
4
8
12
16
20
24
28
32
FREQUENCY IN CYCLES PER km X 1/192


BLOCK 193
GRID SIZE 1/2° x 1/2°
Depth = 2·77 km
Depth = 0·27 km
LOG OF ENERGY
10
8
6
4
2
0
-2
-4
-6
-8
-10
4
8
12
16
20
24
28
FREQUENCY IN CYCLES PER km X 1/192

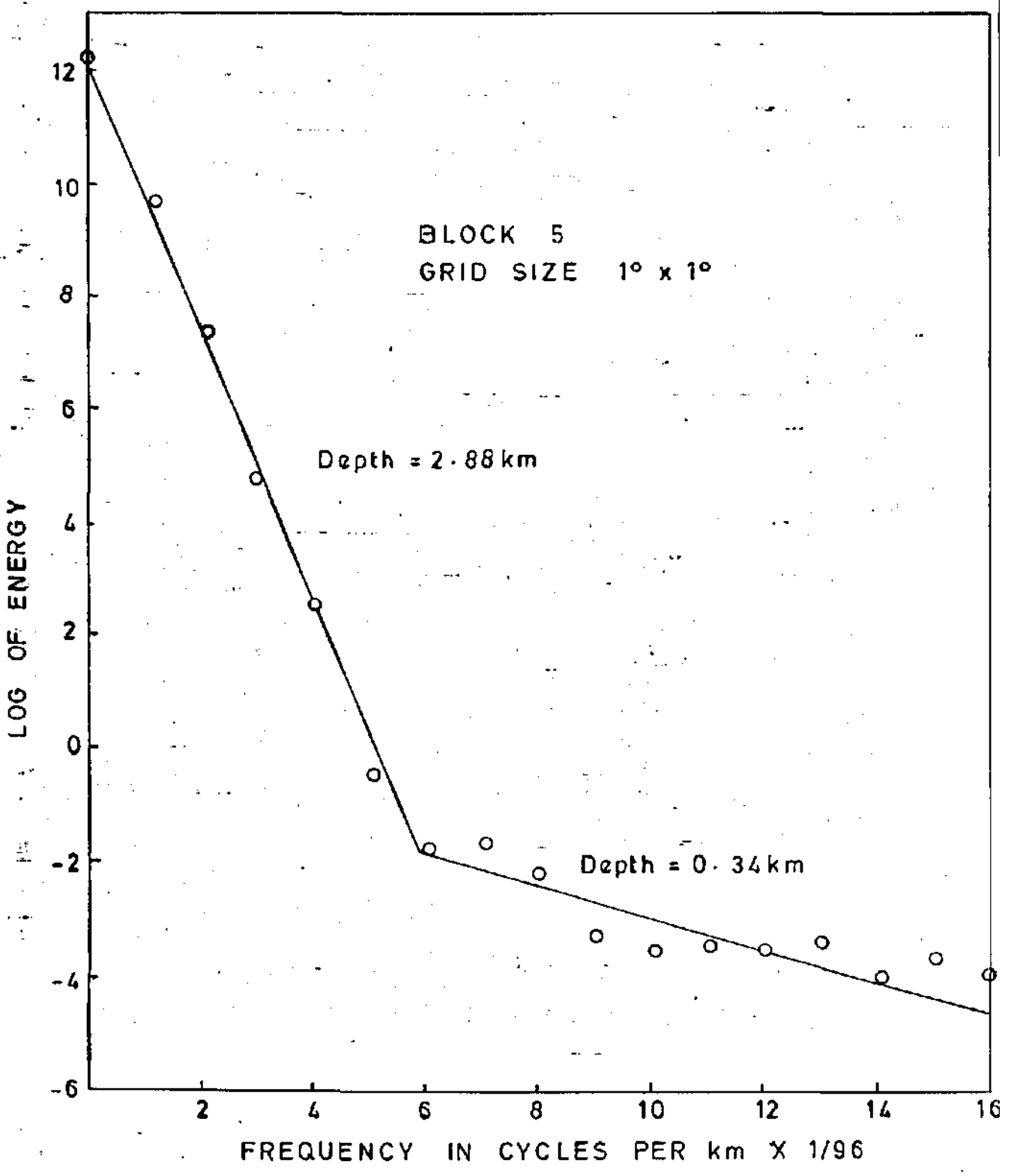

BLOCK 194
GRID SIZE 1/2° x 1/2°
Depth = 2·77 km
Depth = 0·32 km
LOG OF ENERGY
10
8
6
4
2
0
-2
-4
-6
-8
-10
4
8
12
16
20
24
28
32
FREQUENCY IN CYCLES PER km X 1/192

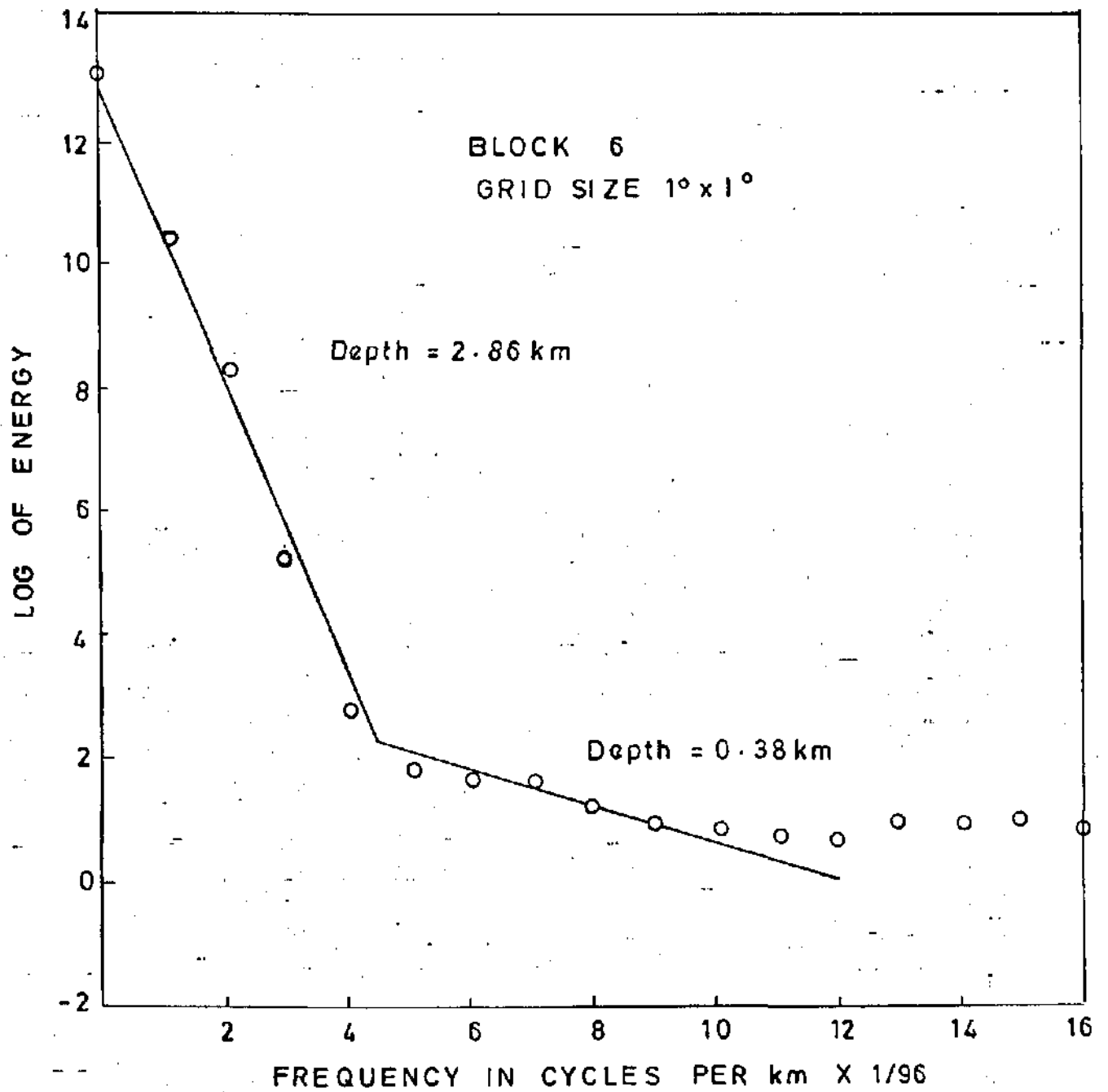

BLOCK 195
GRID SIZE 1/2° x 1/2°
Depth = 2 . 60 km
Depth = 0·32 km
LOG OF ENERGY
10
8
6
4
2
0
-2
-4
-6
-8
-10
4
8
12
16
20
24
28
FREQUENCY IN CYCLES PER km X 1/192

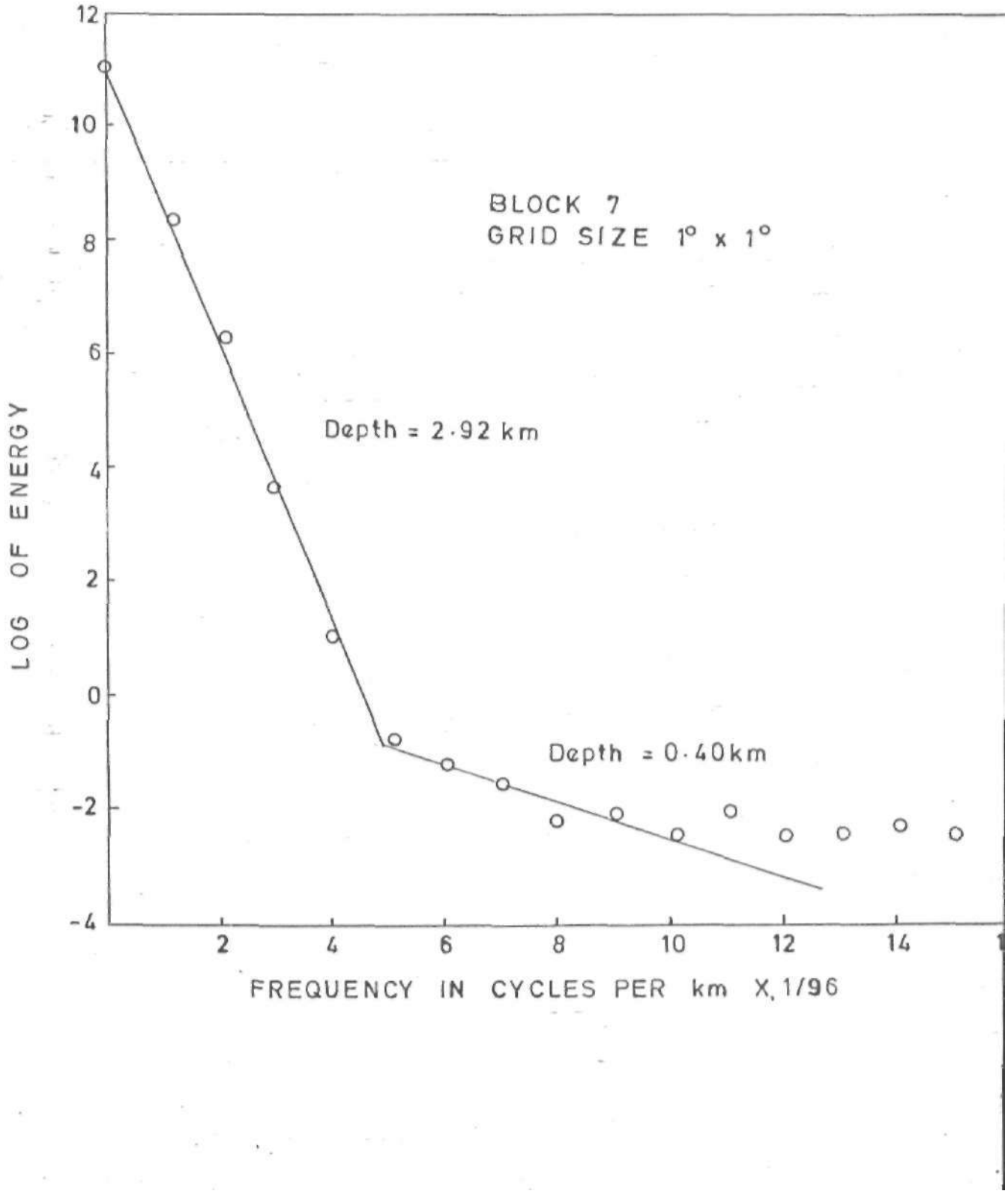

BLOCK 196
GRID SIZE 1/2° x 1/2°
Depth = 2.63 km
Depth = 0.63 km
LOG OF ENERGY
10
8
6
4
2
0
-8
-4
-6
-8
-10
4
8
12
16
20
24
28
32
FREQUENCY IN CYCLES PER .km X 1/192

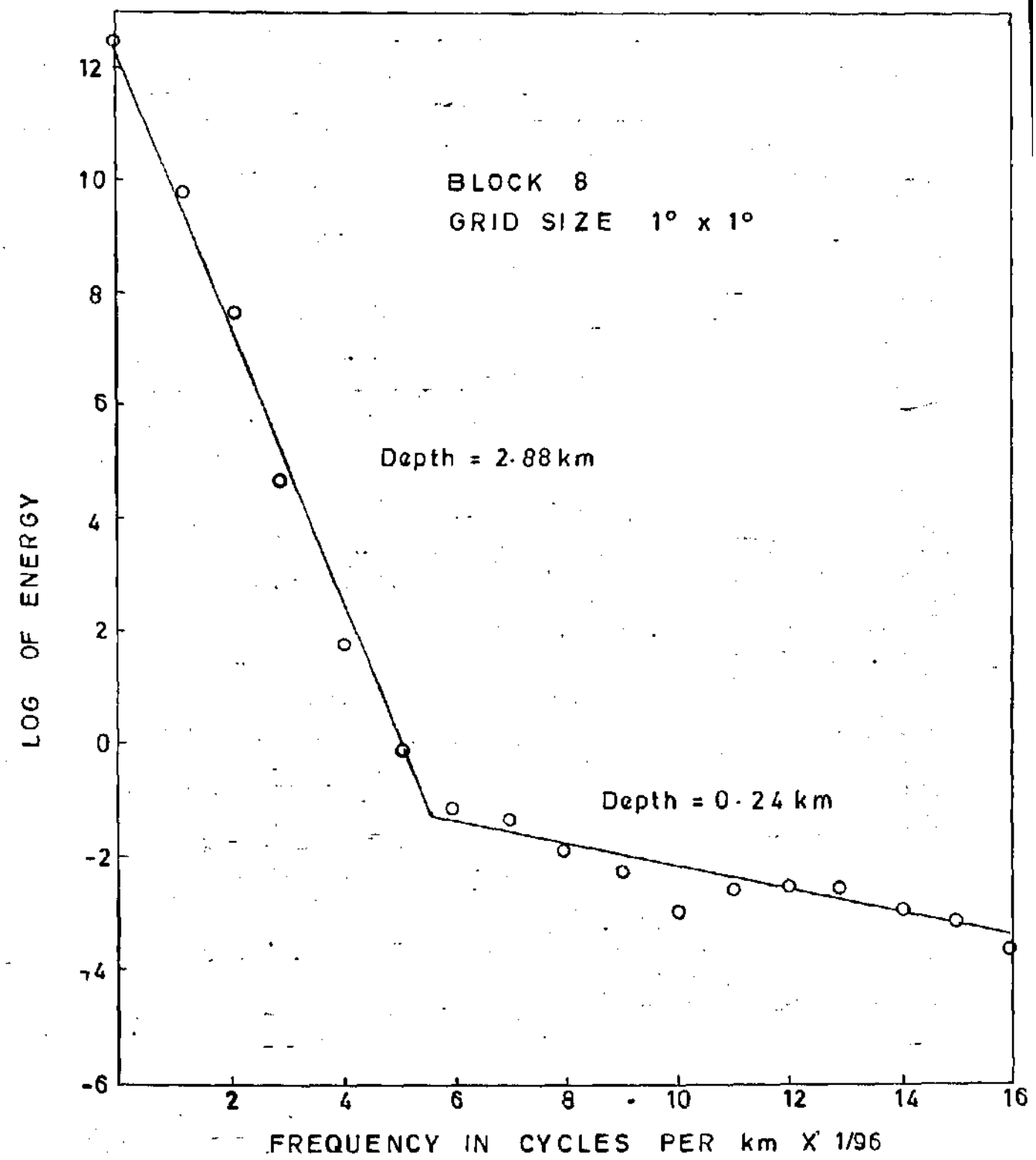
APPENDIX B

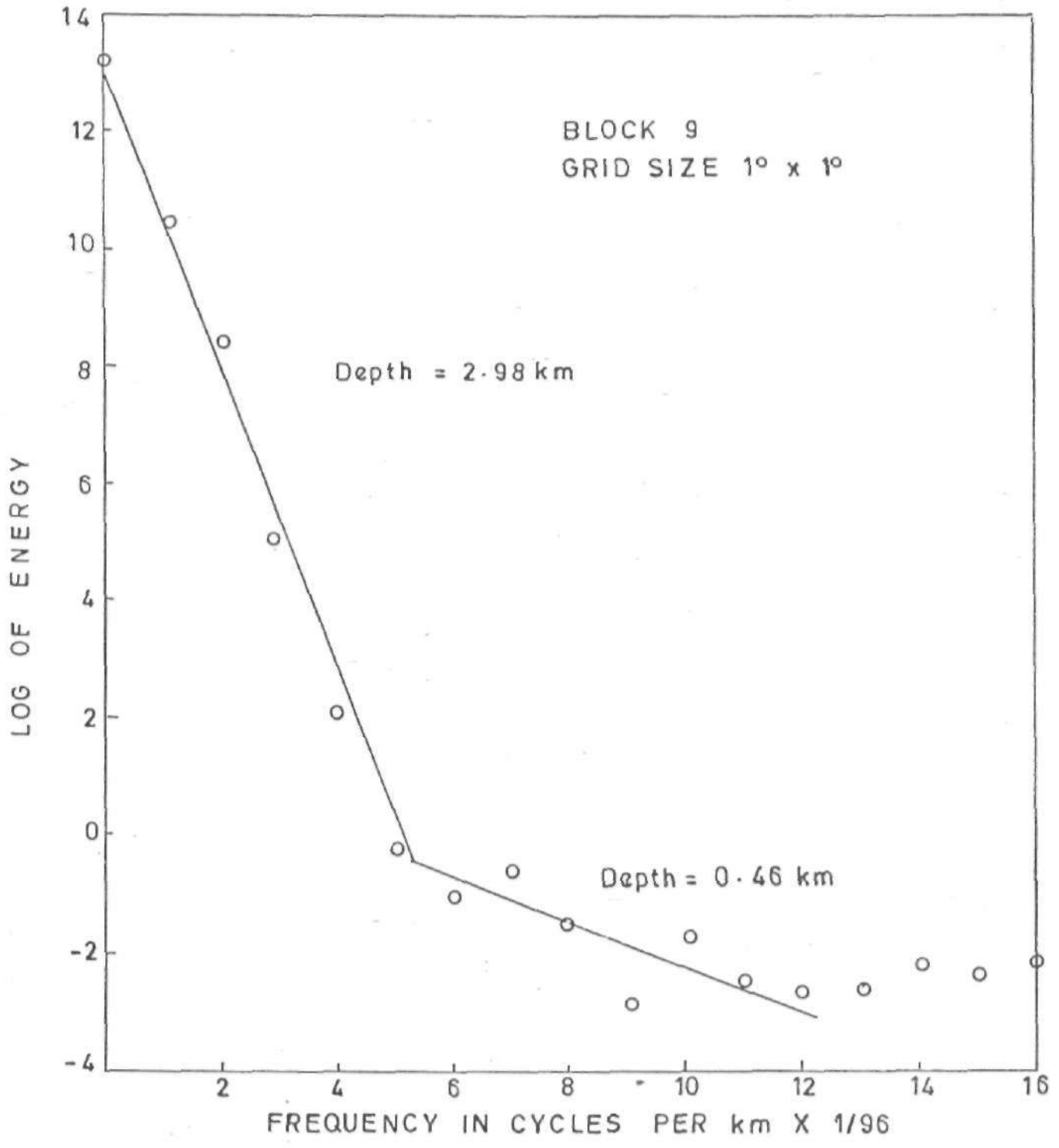
Spectral Plots for the 1^{o} x 1^{o} Blocks


BLOCK 5
GRID SIZE 1° x 1°
Depth = 2·88 km
Depth = 0·34 km
LOG OF ENERGY
12
10
8
6
4
2
0
-2
-4
-6
2
4
6
8
10
12
14
16
FREQUENCY IN CYCLES PER km X 1/96


BLOCK 6
GRID SIZE 1° x 1°
Depth = 2·86 km
Depth = 0·38 km
LOG OF ENERGY
FREQUENCY IN CYCLES PER km X 1/96
14
12
10
8
6
4
2
0
-2
2
4
6
8
10
12
14
16

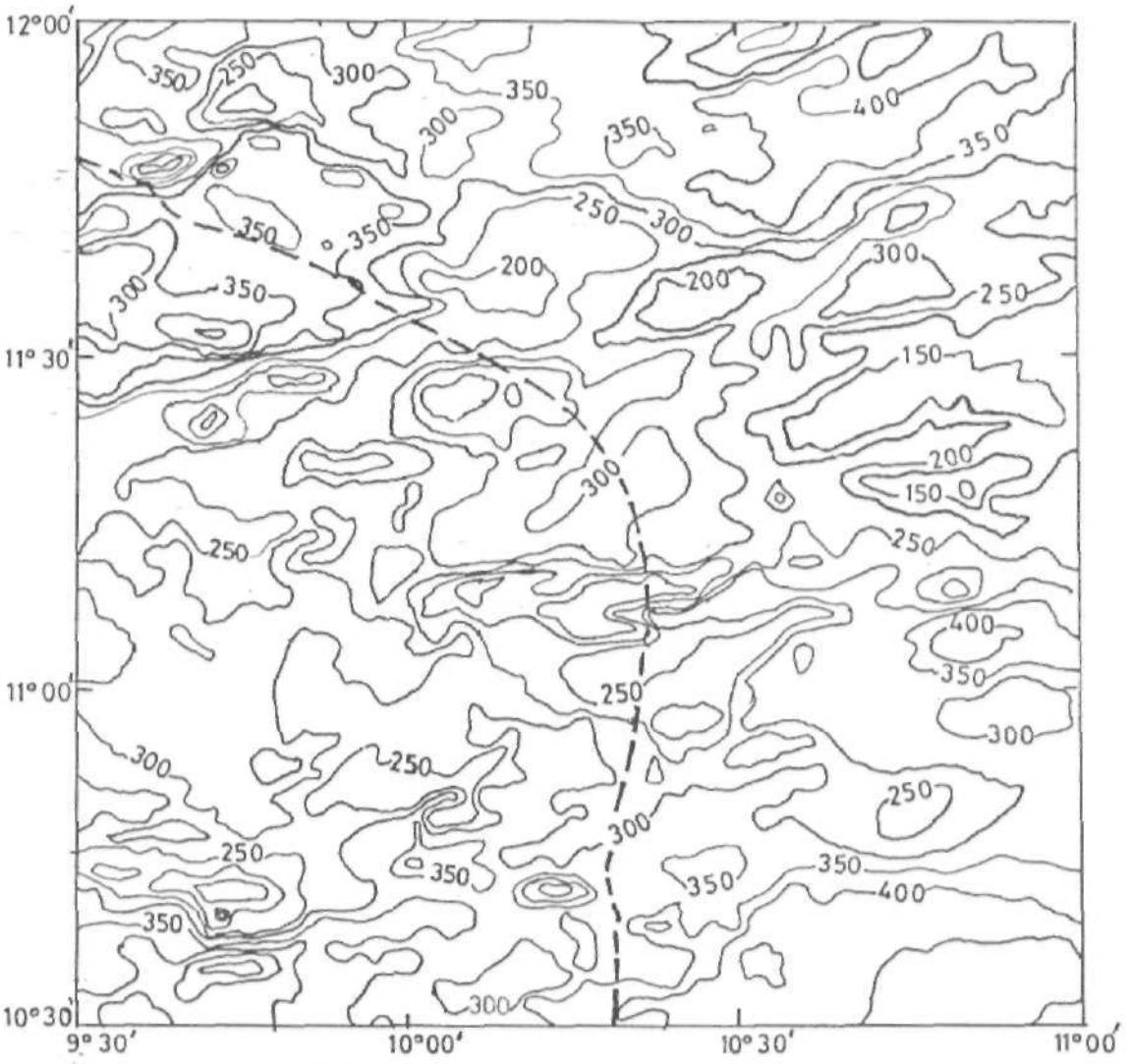

BLOCK 7
GRID SIZE 1° x 1°
Depth = 2·92 km
Depth = 0·40km
LOG OF ENERGY
FREQUENCY IN CYCLES PER km X 1/96
12
10
8
6
4
2
0
-2
-4
2
4
6
8
10
12
14


BLOCK 8
GRID SIZE 1° x 1°
Depth = 2·88 km
Depth = 0·24 km
LOG OF ENERGY
12
10
8
6
4
2
0
-2
-4
-6
2
4
6
8
10
12
14
16
FREQUENCY IN CYCLES PER km X 1/96

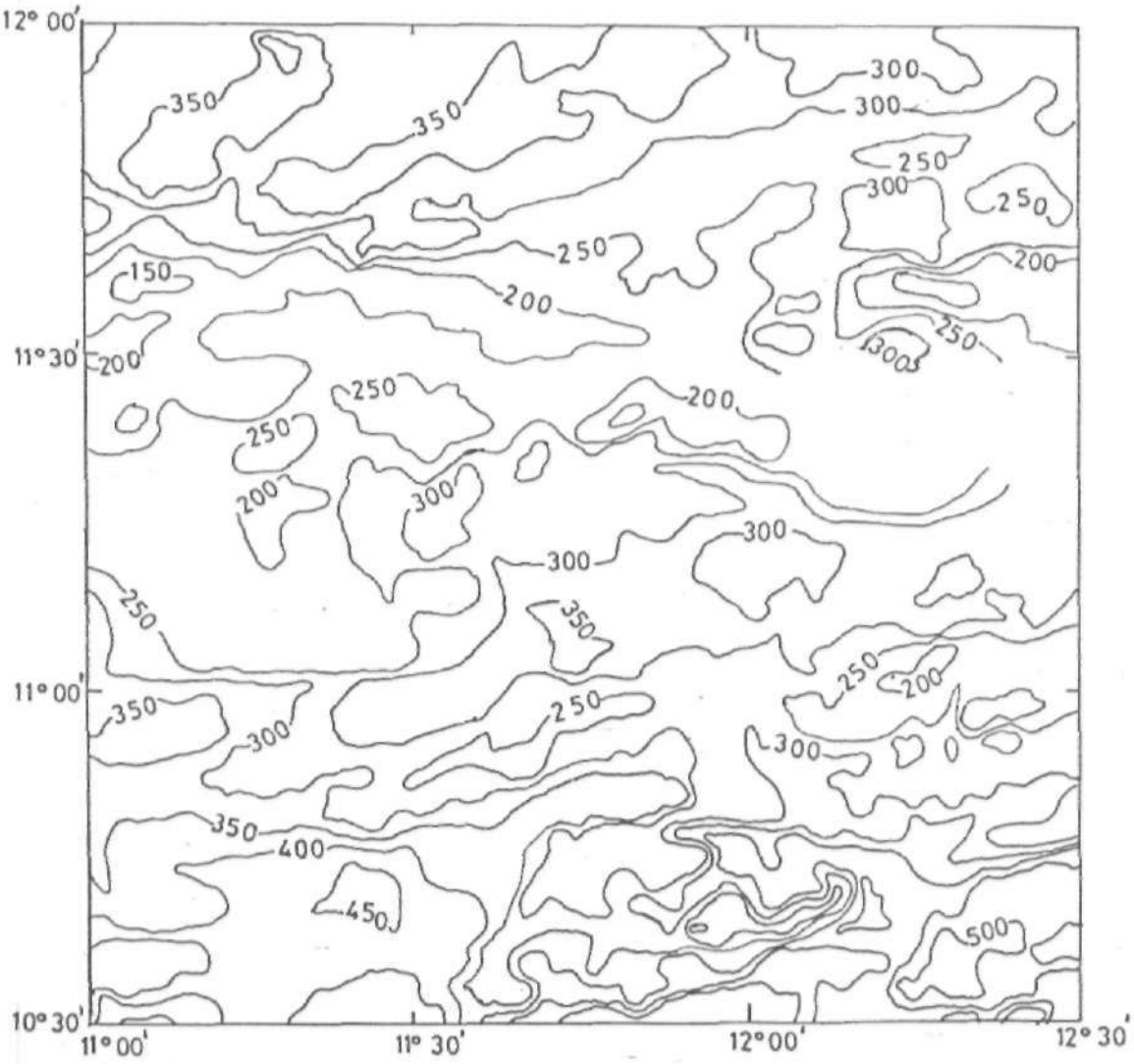

BLOCK 9
GRID SIZE 1° x 1°
Depth = 2·98 km
Depth = 0·46 km
LOG OF ENERGY
FREQUENCY IN CYCLES PER km X 1/96
14
12
10
8
6
4
2
0
-2
-4
2
4
6
8
10
12
14
16

APPENDIX C

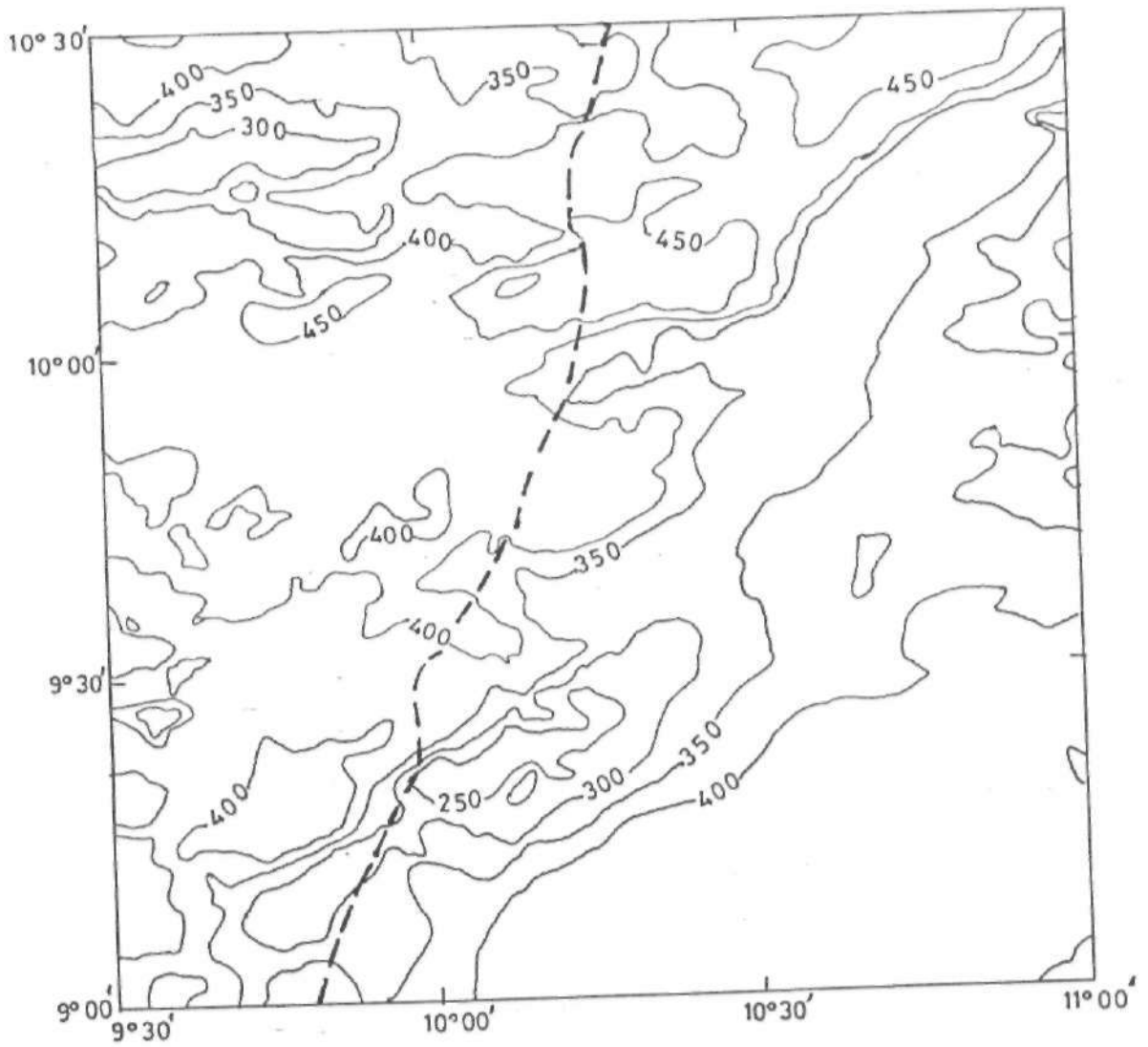
Total field anomaly maps of the 4 Blocks of $1\frac{1}{2}^{O}$ x $1\frac{1}{2}^{O}$ map window.



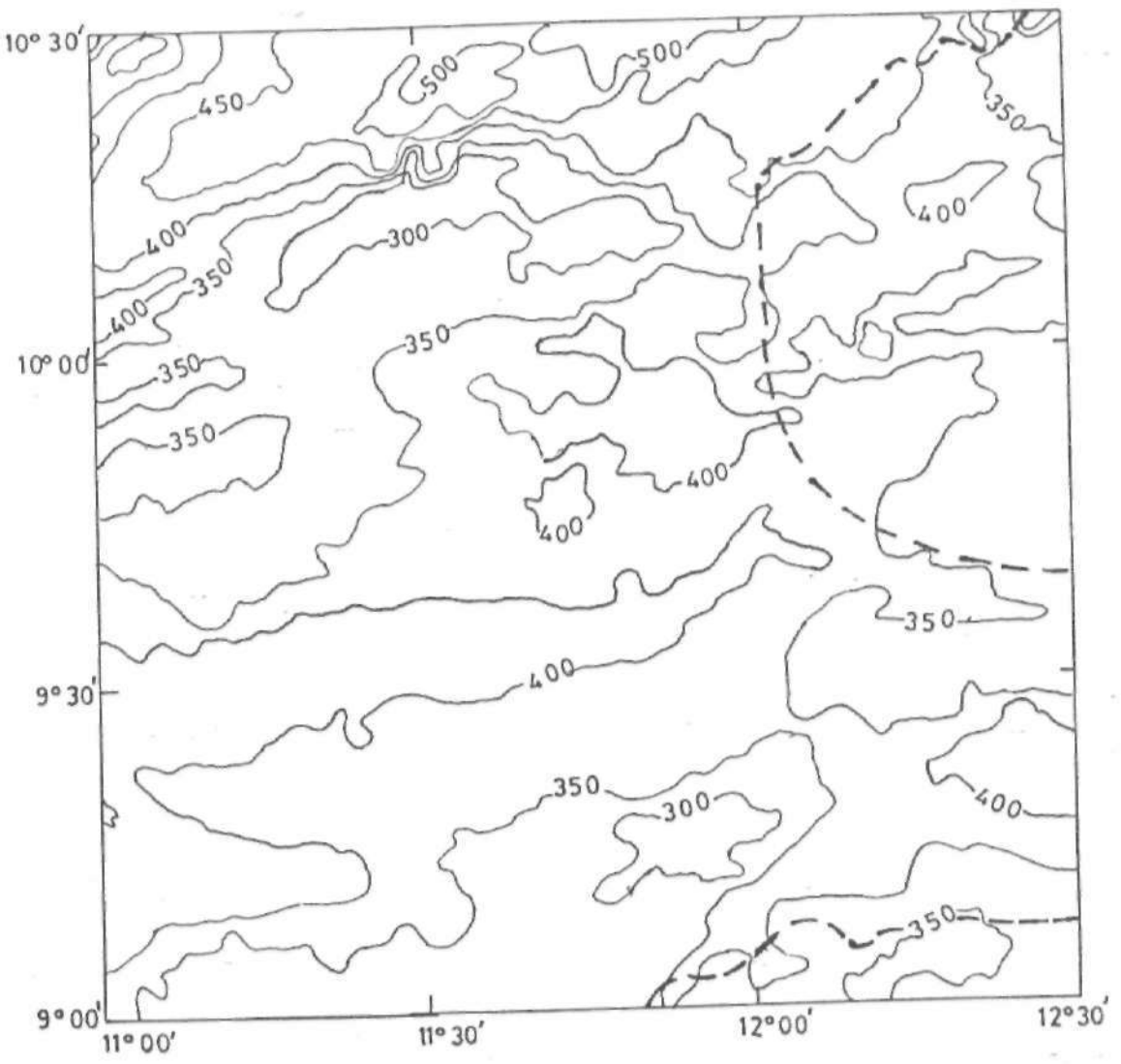
TOTAL FIELD ANOMALY MAP OF BLOCK 1



TOTAL FIELD ANOMALY MAP OF BLOCK 2



TOTAL FIELD ANOMALY MAP OF BLOCK 3



TOTAL FIELD ANOMALY MAP OF BLOCK 4